Modeling an SI engine with WEDACS for control purposes

van de Sanden, Michiel C.W.

Award date:
2012

Modeling an SI engine with WEDACS for control purposes

M.C.W. van de Sanden

CST 2012.013

Master's thesis

Coaches: ir. R.H.L. Eichhorn
dr.ir. M.D. Boot

Supervisor: dr.ir. F.P.T. Willems

Committee: dr.ir. A.G. de Jager
dr.ir. H. Ouwerkerk
prof.dr.ir M. Steinbuch
dr.ir. F.P.T. Willems

Eindhoven University of Technology
Department Mechanical Engineering
Dynamics and Control Technology Group

Eindhoven, February, 2012

Acknowledgements

This research has been performed at the Eindhoven University of Technology in order to obtain the degree of Master of Science at the Mechanical Engineering department within the Control Systems Technology group. During my Masters I coincidentally came across the WEDACS project of dr.ir. Michael Boot. His unlimited enthusiasm motivated me to participate in this innovative project. Also during my research I was encouraged by his out-of-the-box ideas.

I would like to express my gratitude to ir. Ruud Eichhorn for his valuable support. His advise regarding the experiments provided a solid base for my research. Furthermore, I would like to thank dr.ir. Frank Willems for his constructive suggestions and thorough feedback during my research. I also would like to thank prof.dr.ir. Maarten Steinbuch for providing the resources and opportunity to graduate on this project.

On a more practical level, I would like to thank Toon van Gils, Gerard van Hout, Wietse Loor and Jan de Vries for helping me in realizing the WEDACS prototype and upgrading the test setup. I would like to thank Erwin Meinders and my colleagues of the famous Automotive Engineering Science laboratory for their suggestions, many fruitful discussions and in particular for providing a pleasant working atmosphere.
Finally, I would like to thank my friends and family for their non-technical support during my entire study.

Michiel van de Sanden
Eindhoven, February 2012

Abstract

The efficiency of a spark ignition combustion engine is highly dependent on the throttle valve. Under most driving conditions the engine power output is small compared to its maximum potential power. To retain the engine from producing its maximum power a throttle valve is used to restrict the air mass flow to the engine. Restricting the air flow causes significant losses, referred to as throttling losses.
An innovative system called WEDACS is proposed as a throttling device which is able to recover part of the throttling losses. WEDACS uses a variable geometry turbine to drive an alternator thereby generating electric power. The variable geometry turbine is equipped with adjustable stator vanes enabling a variable air flow restriction. While extracting energy from the air mass flow the temperature drops significantly behind the turbine. Cold air could be utilized for improving the volumetric efficiency or to cool the airconditioning fluid. WEDACS could reduce fuel consumption by assisting the engine in delivering power for auxiliaries such as the airconditioning pump and charging the car battery.
The research as described in this report is focussed on modeling and control of the WEDACS system. The goal is to maximize the fuel consumption reduction while maintaining the engine response with respect to the performance/comfort experience by the vehicle driver.
A WEDACS prototype is built and installed on an engine in an experimental setup. Experiments have been conducted in order to gain insight in the potential of the system. The experimental data is analyzed with respect to throttle loss recovery and potential turbine power generation. A model for the complete engine in combination with WEDACS is designed using the mean value modeling approach. The model is validated using obtained measurement datasets.
Based on the results during the research a control strategy is proposed to actuate WEDACS properly with respect to the vehicle's throttle pedal position. WEDACS consists of a throttle valve and a variable geometry turbine in parallel, thereby introducing two control inputs: the throttle valve position and the turbine vanes position. Important considerations to determine the control strategy of WEDACS is the fuel consumption reduction in the standardized NEDC drive cycle and at common engine operating points. The control strategy also accounts for dynamic transients (e.g. during vehicle accelerations), where the engine response must be equal to the standard throttle valve reference situations.
In the end, conclusions and recommendations are drawn based on the presented research results.

Contents

Chapter 1

Introduction

The current issues regarding pollutant emission levels of internal combustion engines and the declining amount of available fossil fuels are well known hot topics. Although increasing knowledge may lead to a more efficient combustion process, efficiency limitations are caused by a very essential part in the spark ignition (SI) engine: the throttle valve.
In SI engines the throttle valve is used to control the air mass flow into the engine which, together with the fuel amount and spark timing, determines the produced engine power. However, the throttling process is an inefficient way of reducing the air mass flow since it wastes energy (pumping loss) which the engine has to produce. In fact, most of the time the engine runs at part load which means that the average efficiency is substantially below the optimal Brake Specific Fuel Consumption (BSFC) value. Studies show that averaged utilization is often less than 10% of the maximum engine power and that averaged measured tank-to-wheel efficiency values even vary between $12 - 18\%$ [Guzzella and Onder, 2010].

In short, the main operating area of the combustion engine does not always include the maximum efficiency region, partially due to pumping losses. The main idea behind the Waste Energy Driven Airconditioning System (WEDACS) is to recover part of the pumping losses during throttling in order to reduce the overall fuel consumption of an SI engine. An innovative way to throttle is to use a variable geometry turbine (VGT) which is typically found in exhaust systems of diesel engines. By changing the position of the guiding vanes in the turbine the air flow is throttled. The difference with a throttle valve however is the potential of recovering energy by using the turbine. The rotating turbineshaft is used to generate electrical power, which can help or maybe even eliminate the alternator. Since the temperature after the turbine drops significantly, an additional heat exchanger could be used to cool the airconditioning fluid. In essence, WEDACS will reduce the engine's auxiliary losses to the alternator and airconditioning, which directly reduces the fuel consumption. Additionally, the higher density of cold air results in more air in the cylinders, thereby increasing the volumetric efficiency and subsequently the maximum engine power output.

WEDACS can be integrated in new cars or installed as aftermarket product. Key to success is the ratio of potential fuel consumption reduction compared to the total costs of an installed WEDACS system. For aftermarket purposes the packaging is important: standardized, compact and easy to install. Both the existing automobile fleet as well as the next generation of SI engines could become more efficient with WEDACS.

1.1 Research objective

The research described in this report is based on a WEDACS consisting of a VGT in parallel with a throttle valve. This parallel setup is necessary because the maximum airflow through the VGT is limited. This is not necessarily a restriction because the pumping losses are high at a specific region where the VGT might have an optimum in efficiency. Another advantage of the parallel system is the response to the throttle pedal since the throttle valve can react fast, where the VGT might have a time delay.

The objective is to develop and validate a dynamic engine model equipped with WEDACS. Furthermore a control strategy has to be designed for WEDACS to maximize the fuel consumption reduction while retaining the engine power output and throttle pedal response compared with the current situation.

1.2 Thesis structure

The concept of WEDACS is explained in more detail in Chapter 2. The theory and previously conducted research on WEDACS is a summarized here. Next, the experimental setup and measurement results are elaborated in Chapter 3. In Chapter 4 an engine model equipped with WEDACS is developed. The model is fitted and validated using experimentally obtained data. The model is used to design a control strategy which is developed in Chapter 5.

Chapter 2

WEDACS system description

2.1 Basic theory

2.1.1 Spark ignition engine

The engine considered in this research is a four-stroke spark ignited gasoline engine. A mixture of air and fuel (gasoline) is fed to the engine cylinders. This mixture is close to a stoichiometric ratio in order to get a proper reaction during combustion. Inside the combustion chamber (cylinder) this mixture is being compressed and ignited, which results in a high pressure peak. The resulting force on the piston is converted to torque at the crankshaft.
The reciprocating motion of the pistons describes four strokes during two crankshaft revolutions. Two strokes are used to pump the fresh air in and exhaust gas out of the cylinders. This action costs energy. During the other two strokes of the cycle the air/fuel mixture is being compressed and ignited, which delivers useful energy at the crankshaft.
An engine is able to produce a variety of torque levels at different speeds. These engine operating points are dependent on the load at the crankshaft and the energy release inside the cylinder. The amount of energy release depends on the air/fuel mixture and spark ignition timing. The on-board Engine Control Unit (ECU) controls the spark timing and the fuel supply. The fuel amount is related to the amount of air which is enters the cylinders. The amount of air is regulated using a throttle valve.

2.1.2 Throttle valve

A throttle valve is a flow restricting device which causes a significant pressure drop in the flow without involving work. This flow exists because the reciprocating pistons create a vacuum in the (throttled) intake manifold. This vacuum is related to the amount of torque produced by the engine.
A pressure drop is often related to a temperature drop which explains the application of throttle valves in refrigeration and air-conditioning systems. The Joule-Thompson coefficient μ_{JT} describes the magnitude of the temperature drop (or rise in some cases) for constant-enthalpy processes [Çengel and Boles, 2002]. However, when considering an ideal gas the Joule-Thompson coefficient becomes zero. A throttling valve is in this case an isenthalpic device, since there is no heat transfer (adiabatic), no work performed and insignificant change in kinetic and potential energy. The sum of the flow energy and the internal energy before and after the restrictor remains

constant during the throttling process and therefore the temperature of the air mass flow will not change.

2.1.3 Variable Geometry Turbine

A turbocharger is commonly used in automotive applications and consists of a turbine and a compressor. Both the turbine and the compressor rotor are mounted on the same shaft. The exhaust gas circuit drives the turbine rotor which drives the compressor. As a result, fresh air is compressed and forced into the intake manifold due to the higher pressure. The VGT differs from an ordinary turbine such that the amount of air flowing through the turbine is influenced by adjustable vanes inside the turbine housing. See Fig. 2.1 for an illustration.

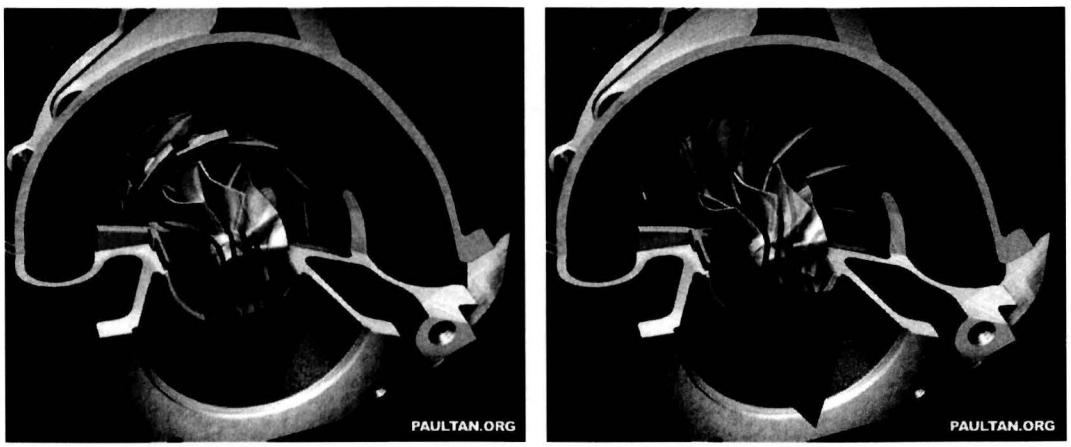

Figure 2.1: Illustration of the influence on the air flow by vanes [Tan, 2006]

In contrast with a throttle valve, a temperature difference exists between the in- en outlet of the turbine since work is performed at the rotating turbine shaft. The temperature drop over a turbine is dependent on the efficiency and the pressured drop. Due to internal kinetic energy change inside the turbine, the isentropic efficiency is considered and stagnation pressures and temperatures are taken into account [Heywood, 1988]. The total turbine efficiency is then defined as:

$$\eta_{turb} = \frac{1 - (T_{04}/T_{03})}{1 - (p_{04}/p_{03})^{\frac{\kappa-1}{\kappa}}} \tag{2.1}$$

with,

$$p_{03},\, T_{03} = \text{turbine inlet stagnation pressure and temperature} \tag{2.2}$$
$$p_{04},\, T_{04} = \text{turbine outlet stagnation pressure and temperature}$$

In general, de turbine efficiency decreases for decreasing pressure ratios (manifold pressure/ambient pressure). This implicates that the turbine efficiency will drop when the turbine is throttling more.
J.R. Serrano [2008] shows that the isentropic efficiency of a VGT is lowest at closed or fully opened vanes positions. Experimental results show that this holds for various turbine speeds.

The efficiency of the turbine determines the amount of potential energy recovery, not the throttling quality in terms of reducing the mass flow.

2.2 Principle of operation

WEDACS is an intake flow restricting device and replaces the original throttle valve in the reference situation. The concept of WEDACS consists of a throttle valve in parallel to a turbine with a variable geometry of the vanes (VGT). It is chosen to apply the VGT in parallel with the throttle valve for various reasons. First of all, the throttling losses decrease exponentially with an increasing throttle valve angle. Also the turbine flow range is limited due to the turbine dimensions, so a throttle valve bypass is needed for higher speed-load conditions.
The turbine shaft is connected to an alternator and also a heat exchanger is located between WEDACS and the intake manifold. The system partly recovers throttling losses in two ways [R.H.L. Eichhorn, 2009]:

Electrical power The WEDACS alternator generates electricity using the rotating turbine shaft. The standard alternator is assisted or even eliminated, resulting in lower auxiliary power provided by the engine. Energy which is not withdrawn by auxiliaries could be used to charge the battery.

Cooling power The expansion of air due to the pressure drop over the turbine causes a drop in temperature. This cold air is used in a heat exchanger to cool the airconditioning (A/C) fluid thereby relieving the engine in auxiliary power for the airconditioning compressor. When the airconditioning is not used, the cold air can be used for power boost since the volumetric efficiency is increased due to higher air density.

In general, fuel consumption is reduced with WEDACS by using recovered throttling losses to relieve the engine from producing auxiliary power. Since the cooling power for A/C fluid will be limited, other forms of utilization of the cold mass should be searched for [R.H.L. Eichhorn, 2009]. Further investigation on this topic is beyond the scope of this research. During this report it is assumed that all generated power by the turbine is converted to electrical power. Throughout this research, a comparison is made between the standard reference situation and the WEDACS equipped setup. Schematic overviews of the reference situation and the WEDACS concept are shown in Fig. 2.2 and Fig. 2.3.

2.2.1 Operating region

Pumping losses due to throttling increase with increasing air mass flow and increasing pressure drop across the throttle valve. The smaller the throttle valve opening angle, the higher the pumping work. In general, the engine is always throttled when the driver is not requesting maximum power output at wide-open throttle. To be more specific a standard New European Driving Cycle (NEDC) is used to determine the location and residence time of the engine operating points as

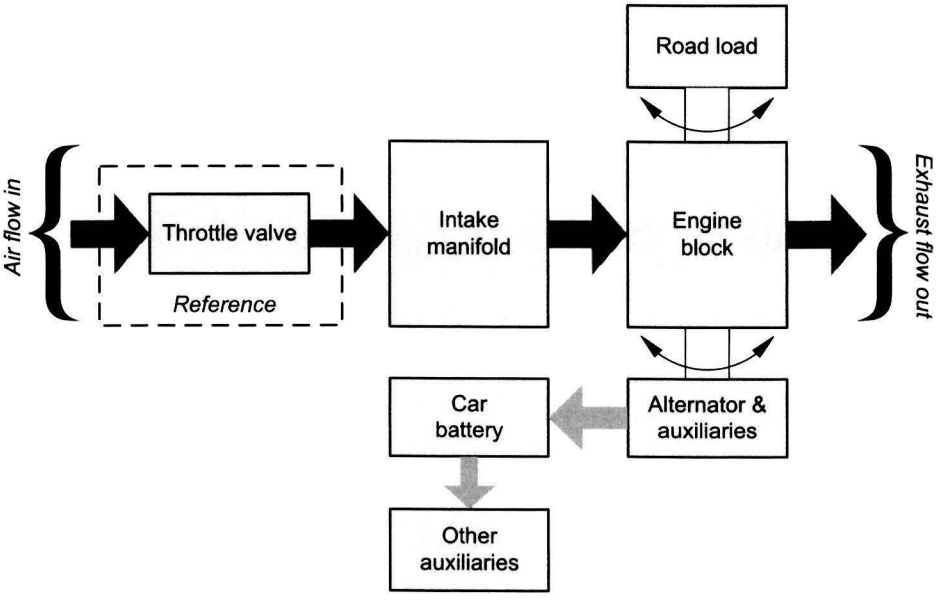

Figure 2.2: Schematic overview of reference situation

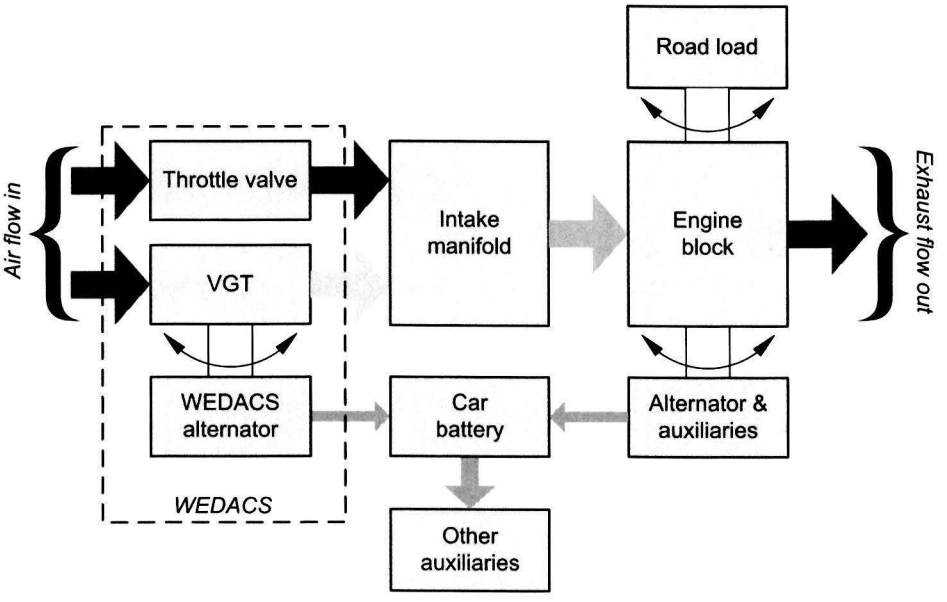

Figure 2.3: Schematic overview of the WEDACS concept

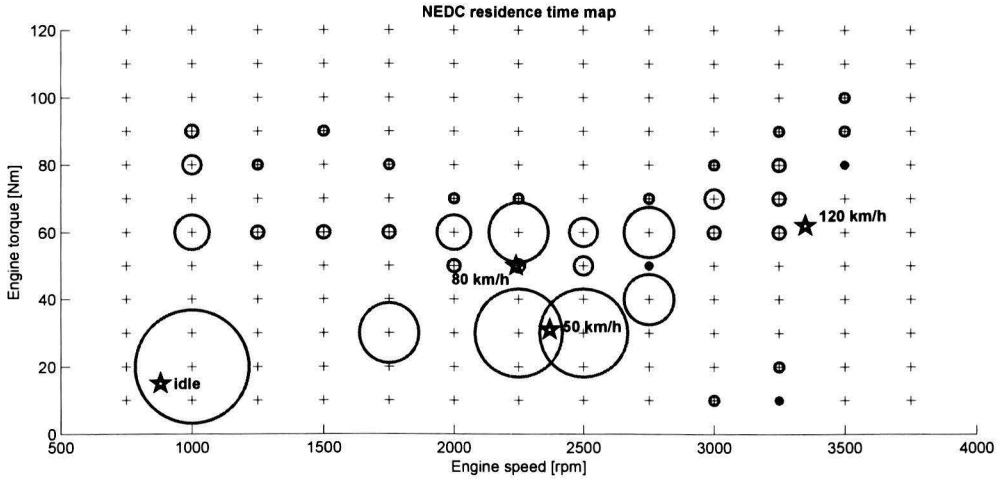

Figure 2.4: Engine operating points density plot for a NEDC cycle

shown in Fig. 2.4. In this graph, the diameter of the encircled engine operating point grid is proportional to the residence time near that point. A high density residence point is at idle speed at vehicle stand-still. There is also a concentration in residence density at 20-40 Nm @ 2300-2500 rpm, which equals a vehicle velocity of $50[km/h]$. The WEDACS system should be optimized for optimal throttle loss recovery at this region. The exact target region must be defined in order to set a research goal. One should realize that the NEDC is a test cycle and represents an averaged statistically determined cycle. The NEDC is considered as a guideline and not the absolute reality. In reality every driver has different drive cycle.
The optimization techniques can be either hard- or software based. One could think of scaling the turbine geometry or change the flow characteristics of the vanes for optimal efficiency in terms of hardware optimization. Software optimization would be an optimal control strategy using an existing VGT, which is the case in this research.

2.2.2 Electrical energy management

The electrical energy recovery using a generator is the main focus of this research, since R.H.L. Eichhorn [2009] showed the limited capacity for effectively assisting the A/C system with WEDACS. Over the last 30 years the battery capacity of an ordinary car has been multiplied 3 times, while the alternator power has been multiplied 6 times [Laurent Bertoni, 2002]. Besides transportation, consumers expect power consuming safety, comfort and entertainment systems (e.g. anti-lock brake system, parking systems, power steering, active cruise control, climate control, multimedia, navigation). Besides this there exists a tendency to electrify current hydraulic auxiliaries such as pumps. It is plausible that the electrical power demand in cars could reach $5kW$ within the next few years. It is therefore necessary that the onboard electric power supply should be increased.
This is a hot topic since manufacturers are forced to reduce energy consumption to propel the car on one hand, while the consumer expects more features on a car besides propulsion alone. Although $5[kW]$ cannot be generated by WEDACS alone, WEDACS could assist in generating additional electric power to fulfil these demands.

However, the actual electric energy generation in this research is limited to potential power recovery. Further research is necessary in order to optimize the use of a generator. More in depth knowledge is needed about specific auxiliary demands in terms of voltage and current flows as well as battery charging management.

2.3 Alternative throttling loss reduction methods

2.3.1 Direct injection (Stratified charge lean burn)

The amount of fuel for the combustion process in a SI engine is controlled using a λ-sensor, where λ indicates the air/fuel equivalence ratio. If $\lambda = 1$ the air/fuel mixture is stoichiometric which is theoretically optimal. Furthermore, for $\lambda > 1$ excess air is present resulting in a lean air/fuel mixture. An excess of fuel is called a rich mixture ($\lambda < 1$).
Fuel is injected either direct or indirect, depending on the injector location. Most common systems are indirect multi port injected fuel systems, with an injector located just in front of the cylinder inlet valve(s). However for direct injection, also known as gasoline direct injection (GDI) engines, the injectors are located inside the combustion chambers. Advantage is the possibility to operate in lean conditions at low to medium loads/speeds. This is possible in a stratified charge mode where fuel is injected late in the compression stroke. With the spark plug located near the fuel injection spray, combustion takes place at the locally richer mixture [Magnus Gäfvert, 2004]. This has several advantages including reduced pumping losses which occur in the unthrottled stratified mode where λ can reach values between 1.6 and 3.4. It is shown that at part-load pumping loss can possibly be reduced by 95%. Another benefit of GDI engines is the reduction in heat loss through the cylinder walls (-42%) and in the exhaust gas (-26%) since the late stratified fuel injection results in lower temperatures [F. Zhao and Harrington, 1999].
Tests on a Mitsubishi GDI engine show a total fuel economy improvement of 30% during a Japanese 10-15 drive cycle, from which 15% is a direct result of reduced pumping loss [T. Kume and Ando, 1996].
Downside however is the higher soot production due to locally very rich air/fuel mixture composition. Also a standard three-way catalyst can only operate close to $\lambda = 1$, so GDI engines need an oxidation catalyst similar to Diesel engines. Besides this a more expensive lean nitrogen oxide catalyst can be used.

2.3.2 Variable valve timing and valve lift

In conventional situations the profiles on the camshaft determine the valve lift and timing which is independent of engine speed or load and synchronized with half de speed of the crankshaft. The Fiat MultiAir technology eliminates the use of a throttle valve by using a variable hydraulic valve actuation system to control the air mass flow in the cylinders. The technology also enables multiple open/close actions within one cycle to optimize the combustion.
Boretti [2010] mentions an increase in maximum power of 10% and 10% fuel consumption reduction due to reduced pumping losses. Also a torque increase of 15% at low speeds is claimed due to minimizing the back flow when closing the inlet valve(s) earlier.
BMW also uses a variable valve system, where a fuel economy improvement of $20 - 25\%$ at idle and $11 - 14\%$ in a NEDC cycle is reached.

A limiting factor using variable valve timing/lift is the higher intake pressure at part load which results in poorer evaporation of the fuel. The potential pump loss reduction is therefore about $5 - 15\%$ compared to conventional (fixed) valve timing/lift, according to Osman Akin Kutlar [2005].

2.3.3 Active turbine throttling (LoRiS)

At the Swiss Federal Institute of Technology in Zurich a concept similar to WEDACS has been developed [Lino Guzzella and Auckenthaler, 2004]. Here a small axial turbine, accompanied by two throttle valves is used to generate electric power using a generator as shown in Fig. 2.5. Two throttle valves are needed to for the high and low engine power, because the air mass flow range of the turbine is too small to cover the whole engine operating area. This limits the energy production. It is chosen to heat the cold air behind the turbine with exhaust gas, instead of using the cold air for other purposes which is the case with WEDACS. The reason for heating the intake air is the possibility of slower burning speeds and increased hydrocarbon emissions.
The prototype is tested on a 2.8L six-cylinder SI engine and a peak turbine power of $600[W]$ was measured. The authors concluded that the turbine size should be halved in order to match the turbine operating region to the most used engine operating area. This means the maximum turbine power would drop to $400[W]$ but the electrical energy produced during an MVEG-95 driving cycle is increased. A measured electrical energy production of 1.6% of a full cycle is shown.

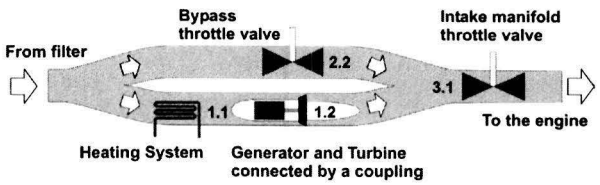

Figure 2.5: LoRiS schematic overview obtained from Lino Guzzella and Auckenthaler [2004]

2.4 Research approach

The net fuel consumption will be the main parameter to specify the objective. The measured fuel consumption without WEDACS during constant engine operating points will be the reference. With WEDACS the additional obtained power with the VGT will be subtracted from the delivered engine power to compare the fuel consumption improvement with the reference situation.

2.5 System description chapter summary & discussion

One of the biggest challenges in order to reduce fuel consumption in an SI engine is to eliminate the throttling losses. By introducing the WEDACS system a new way is found to recover part of the throttling losses by using a VGT as a restrictor. Two ways of energy recovery are possible: use cold air to cool the airconditioning fluid and drive a generator with the rotating turbine shaft. Due to increasing demands in onboard electrical power, the possibility to produce electricity while

throttling is very attractive.

Considering the most frequent occurring operating regions of a combustion engine, the WEDACS has the potential to lower the overall fuel consumption. The focus of this research is based on optimizing this amount of potential energy recovery.
Alternatives in reducing pumping losses are mentioned. Although significant fuel economy improvements are shown, several disadvantages retain these systems from being widely applied in the current automotive fleet.

The research objective of this report focusses on modeling an engine with WEDACS and the development of a control strategy to maximize fuel economy while maintaining the drivability of a car. In the next Chapter a model is proposed in order to predict the WEDACS performance, engine response and fuel economy.

Chapter 3

Experimental setup

3.1 Hardware

The department of Mechanical Engineering facilitates an engine test bed with a multiport-injected 2.0L Nissan SI engine including the Jatco CK2 CVT as found in a 2000 Nissan Primera 2.0 M6 Hypertronic. A flywheel is attached to the driveshaft in order to simulate the total vehicle inertia. A flywheel is connected to an Eddy current dynamometer to apply the road load in terms of angular speed and torque.

3.1.1 Engine: Nissan SR20DE

An overview of the engine specifications is given in Table 3.1. It is important to consider some ECU controlled features, which might affect the implementation of the WEDACS system. These systems are explained below, in Appendix B.1 all ECU functions are given [NissanMotorCoporation].

Multiport fuel injection system

The fuel is injected one time per engine cycle for each cylinder in firing order (cyl $1-3-4-2$) at 30^o before the piston reaches the top dead center ($\theta_{SOI} = -30[^oCA\ \text{TDC}]$). Different control techniques are applied in order to optimize the combustion process, such as lookup tables, feedback control, open loop control and self learning control. The fuel injection duration per injector is initially determined by a programmed lookup table in the ECU memory, as a function of camshaft position sensor (for engine speed) and mass air flow sensor. In addition the amount of injected fuel is increased/decreased for some situations, as shown in Table B.1 in Appendix B. The mixture ratio feedback control system provides the best air-fuel mixture ratio λ for driveability and emission control. This system uses a front heated oxygen sensor (λ-sensor) in the exhaust manifold to monitor the combustion process (rich or lean). The injection pulse width is then adjusted by the ECU according to the sensor voltage signal in a closed loop control sequence. This closed loop control system only applies for steady state engine operating conditions, not during accelerations, decelerations and engine starup/warm up. In those cases the open loop compensated map values are used.
Self-learning control is applied to account for the difference between theoretical and real combustion. Differences in manufactured products (mass air flow sensor), wear and injector clogging

Table 3.1: Engine specifications [Liu, 1998][AutoWeek, 2011]

Name	**Nissan SR20DE**
Type	Straight-4, 4-stroke, spark-ignition, water cooled, normally aspirated
Cylinders	Displacement volume 1998 cc, bore x stroke 86.0 x 86.0 mm, Clearance volume 58.8 cm^3, 9.5:1 compression ratio, Pentroof combustion chamber, centrally located spark plug
Valves	4 Valves/cyl, dual overhead cam (DOHC), roller-rocker cam followers, inlet valve diameter 34.0 mm, exhaust valve diameter 30.0 mm
Fueling	Multiport fuel injection
Timings	Inlet valve opens (IVO) @347[^oCA TDC], Inlet valve closes (IVC) @ – 125[^oCA TDC], Exhaust valve opens (EVO) @123[^oCA TDC], Exhaust valve closes (EVC) @ – 357[^oCA TDC], Injection timing (SOI) @ – 30[^oCA TDC], Spark timing @ – 27[^oCA TDC]
Performance	Max. power 103 kW @ 5800 rpm Max. torque 181 Nm @ 4800 rpm

have influence on the actual combustion process and are compensated for by adjusting the injection pulse duration.

Ignition timing

The ignition timing or spark advance is also an ECU controlled parameter and determines when the sparkplugs ingnite the air/fuel mixture inside the combustion chambers. In general, the timing values are stored in a map in the ECU memory as function of injection pulse width and engine speed. In some cases the ignition timings are adjusted:

- At starting and during warm-up
- At idle
- At low battery voltage
- During acceleration

The ignition timing map is programmed to be within anti-knocking limits. As a safety measure the knock sensor retard system is able to retard the ignition timing when necessary.

Positive crankcase ventilation

To prevent vacuum, the crankcase is ventilated with filtered fresh air, so part of the measured air mass flow in the air filter does not directly reach the combustion chambers. Instead, a system returns blow-by gas to the intake manifold by means of a positive crankcase ventilation (PCV) valve. The pressure level of the crankcase is important to consider when calculating the allocation of intake/exhaust pumping losses of the engine. The pumping losses are determined using the in-cylinder pressure profile integrated over volume profile.

Idle air control valve (IACV) / Auxiliary air control (AAC) valve

To control the engine idle speed a fine adjustable IACV-AAC valve bypasses the throttle valve. The IACV-AAC valve consists of a conical shaped pin which is translated axially by a stepper motor. The IACV-AAC valve is relatively small compared to the throttle valve and is located inside the throttle valve housing. The IACV-AAC valve controls the engine speed during idling and compensates for engine auxiliary loads such as airco, power steering, cooling fan and electrical load. Since the only auxiliary load on the engine at the test bed is the alternator, the effects are expected to be minor during the experiments.

Exhaust gas recirculation (EGR)

The standard engine is equipped with exhaust gas recirculation (EGR). Part of the exhaust gasses are fed back into the intake manifold transported along with fresh air into the combustion chambers. For simplicity the EGR system is blocked in the experimental setup, otherwise there would be an unknown internal feedback system (EGR massflow) which has to be taken into account when calculating the fuel massflow from the air mass flow and the λ signal.

3.1.2 Dynamometer: Schenck E2-330

The engine test bed brake load is supplied by a water cooled Schenck E2-330 Eddy current dynamometer. Eddy current dynamometers provide relative quick controlled braking torque and consist of an electrically conductive core which is rotating in a magnetic field. The strength of the magnetic field and the corresponding brake torque is controlled by a Schenk LSG2010 controller in combination with variable electromagnets. The Schenk E2-330 has two rotors to enable a maximum brake torque of 900 Nm. The power curve is given in Fig. B.1 in Appendix B.3 [W.J. Gorter, 2003].

Table 3.2: Brake load specifications [DynamometerWorld, 2011]

Name	Schenck E2-330
Type	Eddy-current, water cooled dynamometer
Performance	Max. power 330 kW Max. speed 8000 rpm Max. torque 900 Nm

3.1.3 Transmission: Jatco CK2 CVT

On the test bed setup strain gauges are attached to the outgoing engine crankshaft and the outgoing CVT driveshaft to measure torque. Unfortunately, the engine crank shaft sensor system malfunctioned during the performed experiments. In order to validate the modeled engine load torque, a CVT torque transfer function was constructed using measurement data from earlier experiments. These experiments were performed on exactly the same setup including the calibrated sensors. The measured data was averaged over time at constant torque loads and engine speeds. A multiple regression analysis with Statgraphics Centurion was executed to obtain a function for

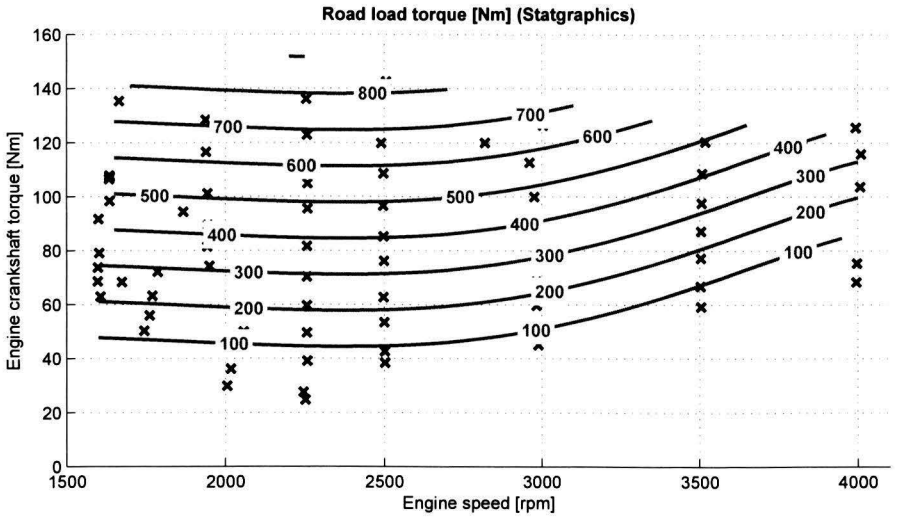

Figure 3.1: Steady state CVT transfer function between engine crankshaft torque and drive shaft road load torque.

engine load torque dependent on CVT output shaft torque (road load) and engine speed, since the CVT efficiency is highly dependent on speed and torque:

$$M_{load} = d_1 + d_2 \cdot M_{road} + d_3 \cdot \omega_{eng} + d_4 \cdot \omega_{eng}^2 + d_5 \cdot \omega_{eng}^3 + d_6 \cdot \omega_{eng}^4 + d_7 \cdot \omega_{eng}^5 \qquad (3.1)$$

with engine crankshaft torque $M_{eng}[Nm]$, driveshaft torque $M_{road}[Nm]$ and engine speed $N_{eng}[rpm]$. Note that the CVT ratio is not taken into account here, since the ratio during the experimentst is fixed. Normally the CVT efficiency is also ratio dependent.
Statgraphics mentions a R-squared of 79.46% the chosen regression fits the data moderately and one should keep in mind that the mean absolute error is $12.66[Nm]$. However, since the CVT torque transfer model is used in both the experimental and the modeled data set, the relative error values resemble an accurate indication of the model performance with respect to the model. In Fig. 3.1 the CVT torque transfer model is shown in a engine operating map.

The torque measurements have been performed during steady state measurements. Transient response of the CVT is not measured and therefore the dynamic CVT effects are ignored throughout this research. This is however not accurate since the presence of a hydrodynamic torque converter which dynamically responses to speed changes. The torque converter acts like a damper at low frequencies and as a low pass filter at higher frequencies [Darrell Robinette and Beikmann, 2011]. At steady state conditions the torque converter has no dynamic influence on the torque transfer. Although various methods exist to model these effects it is chosen to neglect the torque converter since no data exist to validate a model.

3.1.4 WEDACS: Prototype setup

An experimental WEDACS setup is built consisting of an adjusted Nissan throttle valve and a Garrett variable turbine placed in parallel. The original cable operated Nissan throttle valve is adjusted to enable a more accurate and direct control of the throttle position. The hysteresis in the

cable and the throttle valve spring are eliminated since a Woodward L-series rotational actuator is mounted directly on the valve shaft. The Woodward is chosen for its internal fail safe protection and integrated fully adjustable PID controller and friction compensation. When the actuator is malfunctioning or shuts down, the throttle valve will close automatically due to an internal spring in the actuator. Although complete electronic throttle valves modules are available, it is decided that the original Nissan valve is adjusted to keep the ECU functions for IACV/AAC in tact.
The turbine load is in this case a compressor instead of an alternator. The compressor is equipped with a butterfly valve to create a variable pressure drop. However, this valve is not controlled and the load is unknown. Also there is no heat exchanger installed between the VGT and the intake manifold.
The Garrett variable turbine is also adjusted with respect to the vanes position range. To allow the IACV/AAC system full control of the idle speed, the vane orientation must be able to block the air massflow through the turbine. To accomplish this the VGT is adjusted to allow a wider vane position range. Next, a second Woodward actuator is used to control the orientation of the vanes. The concept is based on assisting the engine alternator with power produced by WEDACS. Since the WEDACS prototype is not equipped with an alternator, the power contribution of WEDACS is computed and not physically measured on the test setup.

3.2 Signal processing

To ensure that reliable measurement data is obtained, the signals in the measurement loops have to be qualified and the sensors need to be calibrated. Also, the tolerance with respect to model errors can be put into perspective and feasible control goals can be drawn.

3.2.1 Sensor calibration

Some of the original engine sensors are being monitored by the dSPACE system, for instance the speed at the crankshaft, the throttle position sensor (TPS) signal and the intake air mass flow (MAF). Additionally, various pressure sensors, thermocouples, torque sensors and speed sensors are being installed throughout the engine test bed. Also, a wideband air/fuel ratio λ sensor is mounted in the exhaust manifold. An overview of the sensors and actuators and their location is given in Fig. 3.2.
The calibration results are shown in Appendix B.5 for the pressure sensors, thermocouples and crankshaft torque sensor. In addition, Statgraphics Centurion is used for a regression analysis on the obtained data. A linear model $Y = a + b \cdot X$ results in a $R^2 > 99\%$ and a P-value significantly below 0.05, which indicate a statistically significant relationship between the measured and calibrated data.

3.2.2 Signal conditioning

To gain insight in the signal sensitivity a test is performed with the Woodward actuator for the VGT vanes position. The reference voltage signal is compared with the unconditioned, analog conditioned and digitally conditioned feedback signals from the actuator. In the analog case the feedback signal is fed through a dSPACE-con Analog Signal Conditioning Module. In the digital case, the unconditioned feedback signal is filtered using a strong butterworth low pass filter. The

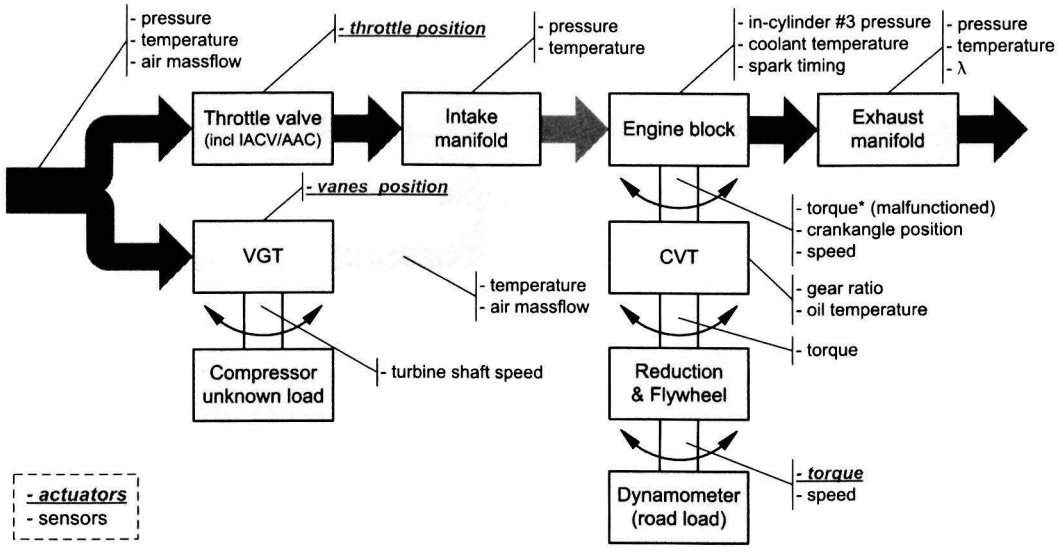

Figure 3.2: Location of the test bed sensors and actuators. The malfunction torque sensor is indicated with an asterix (*).

results show that the analog signal is slightly faster compared to the digital filtered signal, which is more favorable for control purposes. Also considering CPU computation power, analog signal conditioning is more appropriate. In Fig. B.2 the unconditioned, analog conditioned and digitally conditioned feedback signals are compared. Notice the difference in reference and feedback voltage, which is clearly visible in Fig. B.3.

During the in-cylinder pressure measurements, the spark plug cables interfered with the pressure sensor data. The signal noise was periodically in terms of four peaks per engine cycle ($720[^oCA]$), since a four cylinder engine has a cable for each spark plug. Each spark signal caused a peak in the differential pressure signal. The experiments could not be performed again, so the data was post-processed in order to reduce the measurement errors. Please note that since the sensor only registers pressure difference, the post-processing will not be as accurate as a simple filter because the duration of the spark cable interference is estimated. An example of a measured and a post-processed measurement is given in Fig. 3.3. The in-cylinder pressure profile is shifted to match the manifold pressure at IVC (inlet valve closure). This location is marked with a red cross. The graph also shows valve timings (EVC, IVC, IVO, EVO), spark timings and intake/exhaust manifold pressure levels.

3.2.3 Measurement procedure

All tests are performed in steady state engine operating points at constant temperatures. A desired engine operating point (e.g. torque $\times$ speed) is achieved by applying a brake torque load and a throttle valve and turbine vanes position using dSPACE. When the engine operating point becomes stable (e.g. constant pressures, temperatures and engine speed) a measurement is started for $60[sec]$ which is averaged during post processing. These measurements are referred to as *steady state measurements*. The sampling rate is set to $1[kHz]$ for all measurements, in order to gain insight in the dynamic effects during transients.

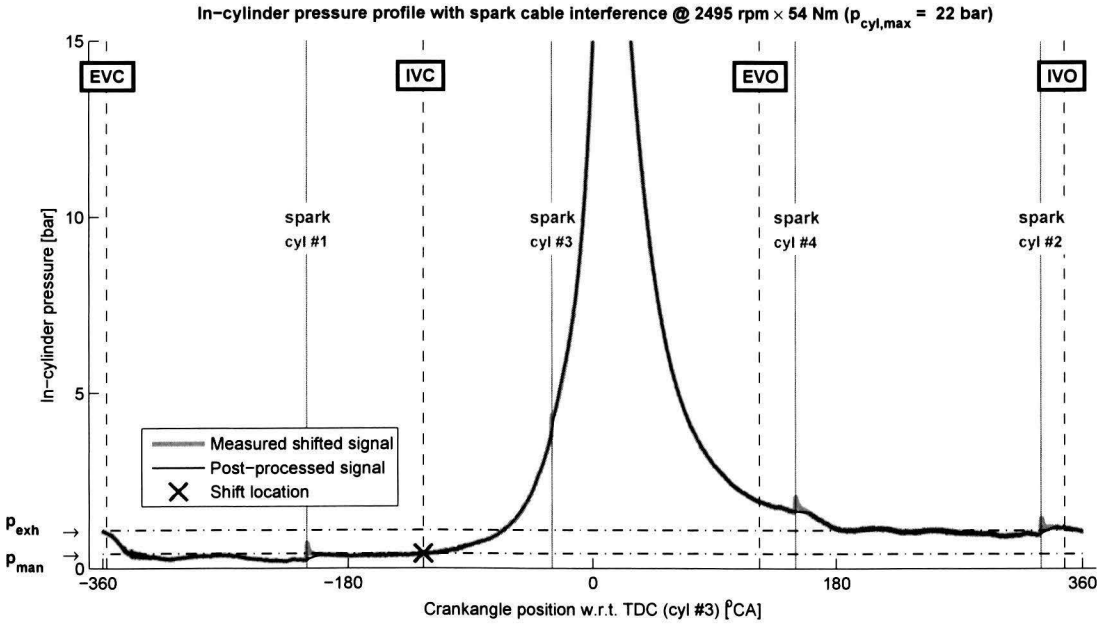

Figure 3.3: Spark plug interference with in-cylinder pressure signal.

Table 3.3: Measured variables during experiments

Category	Variable	Symbol	Sensor type
Mass flow	Total air mass flow	$\dot{m}_{air,tot}[g/s]$	OEM hotfilm
	VGT air mass flow	$\dot{m}_{air,vgt}[g/s]$	Bosch HFM5 hotfilm
Torque	Dyno load torque	$M_{dyno}[Nm]$	Strain gauges
	Road load torque	$M_{road}[Nm]$	Strain guages
Speed	Engine speed	$N_{eng}[rpm]$	OEM sensor
	Dyno load speed	$N_{dyno}[rpm]$	OEM sensor
	VGT shaft speed	$N_{vgt}[rpm]$	ACAM Hall sensor
Pressure	Intake manifold	$p_{man}[bar]$	PTX 1400
	Exhaust manifold	$p_{exh}[bar]$	PTX 7515
	Ambient surroundings	$p_{amb}[bar]$	PTX 1400
	In-cylinder #3*	$p_{cyl}[bar]$	Kistler spark plug sensor 6118B
Temperature	Intake manifold	$T_{man}[^oC]$	Thermocouple Type T
	Exhaust manifold	$T_{exh}[^oC]$	Thermocouple Type K
	Turbine outlet	$T_{vgt}[^oC]$	Thermocouple Type T
	Ambient surroundings	$T_{amb}[^oC]$	Thermocouple Type T
Position	Throttle valve position	$\alpha[\%]$	Woodward L-series 8404
	VGT vanes position	$\beta[\%]$	Woodward L-series 8404
Ratio	CVT pulley ratio	$i_{cvt}[-]$	OEM sensor
	Air/fuel ratio	$\lambda[-]$	Innovate motorsports LC-1
Timing	Spark advance timing*	$\theta[^oCA$ TDC]	Fluke i310s current clamp

* Crankangle resolved variables which are only measured under steady state conditions.

During the experiments the variables as depicted in Table 3.3 are stored in a dataset. However, for the model more variables are needed such as the discharge coefficient of the throttle valve and thermal efficiency and friction/pumping losses for the engine, which have to be determined using the experimental data and physical relations as found in literature.

3.3 Experimental results

3.3.1 Steady state reference experiments

Reference measurements are performed to define the standard engine characteristics with only the standard throttle valve. The reference setup was already depicted in Fig. 2.2. The role for the ECU is to obtain the throttle valve position and use it for engine control, which is graphically indicated in Fig. 3.4. For each engine operating point (i.e. engine torque $\times$ engine speed), the data samples are averaged and statistically assessed (App. C.1). Note that the variation in air mass flow at the maximum engine torque area is significantly larger.

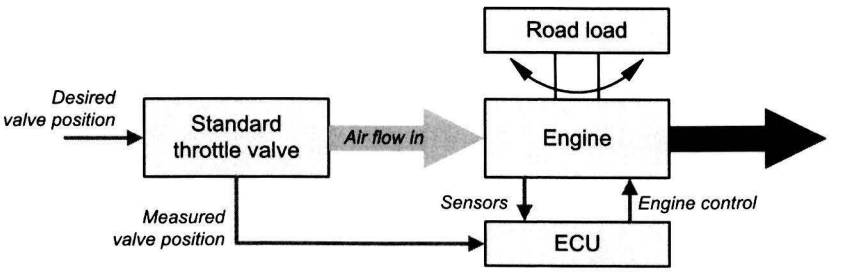

Figure 3.4: Reference measurement setup: standard throttle valve/ECU interaction

The data is then used to build engine maps by constructing trendlines. To value the mapped trends with respect to the measured data, the mean and maximum absolute relative errors (resp. ε_{mean} and ε_{max}) are important parameters:

$$\varepsilon_{mean} = \frac{\sum_{i=1}^{n} |\frac{\check{f}(x_i)-y_i}{y_i}|}{n} \cdot 100\% \tag{3.2}$$

$$\varepsilon_{max} = \max\left(|\frac{\check{f}(x_i)-y_i}{y_i}|\right) \cdot 100\% \tag{3.3}$$

with,

x_i = measured variables at point i

y_i = measured target data at point i

$\check{f}(x_i)$ = function evaluated with measured variables at point i

One of the research goals is to control WEDACS in such a way that the driver does not notice a difference in engine response and drivability. Therefore a graph with trendlines is constructed to gain insight in the air and fuel mass flow at various engine operating points in Fig. 3.5. The black crosses indicate the measured engine operating points and the blue lines are isolines. Also,

the vehicle speeds $50 - 80 - 120[km/h]$ are indicated.

The critical pressure line in the air mass flow graph indicates the level at which the air flow becomes choked. The air flow chokes when the gas velocity reaches sonic conditions. When the pressure decreases beyond the critical level, the gas velocity will stay constant. In Fig. C.12 the air mass flow is shown as function of throttle valve position and manifold pressure. Here, the choking effect is clearly visible.

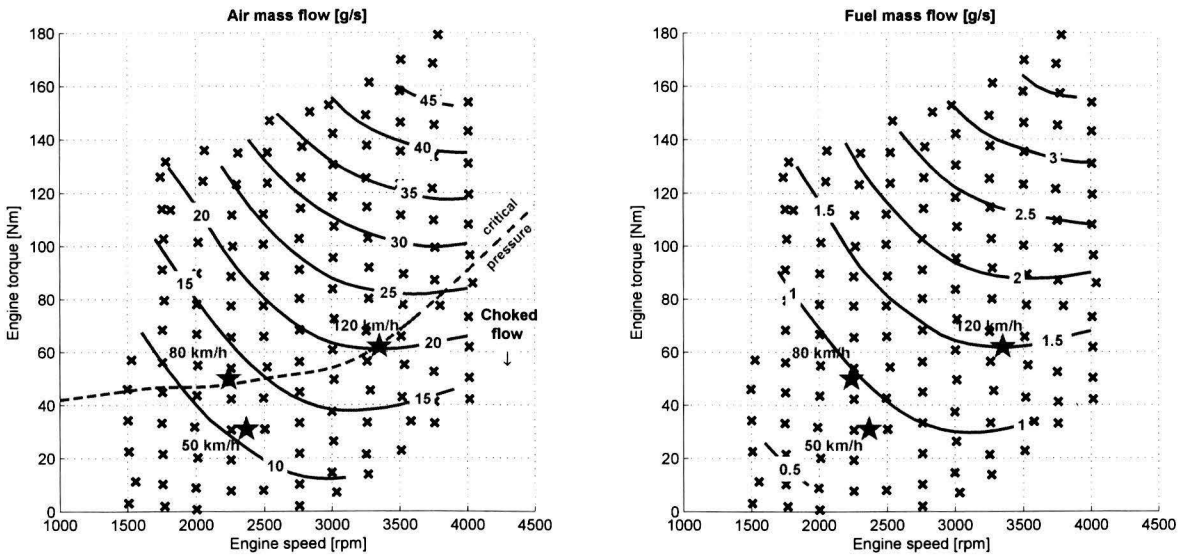

Figure 3.5: Air and fuel mass flow maps.

In the reference situation, the throttle valve position is related to the throttle pedal position via a throttle cable mechanism. Since the throttle valve defines a substantial part of the throttling losses, it is helpful to visualize the throttle valve opening in an engine operating map. The map is shown in Fig. 3.6 together with the throttling losses. The throttling loss is specifically important in this research and determined using:

$$P_{throtl} = \dot{m}_{air,valve} c_p T_{man} \left(\left(\frac{p_{amb}}{p_{man}} \right)^{\frac{\kappa-1}{\kappa}} - 1 \right) \tag{3.4}$$

Fig. 3.6 also shows the engine operating points at 50, 80 and 120 $[km/h]$, at relatively high throttle losses percentages. At $50[km/h]$ there is a throttling loss of $0.9[kW]$, while at $120[km/h]$ $1.2[kW]$ is lost due to throttling. In Fig. C.8 and Fig. C.9, the throttle valve position and throttling loss maps are compared with experimentally obtained values.

The measured in-cylinder signal is used to build p-V diagrams. An additional high-frequency data aquistion system was installed to measure and average the pressure during 70 consecutive engine cycles. The profile of the in-cylinder pressure provides valuable information about the energy transfers during combustion. It is important to consider the crankcase pressure p_{crnk}, which is assumed to be equal or larger than the ambient pressure, depending on the amount of

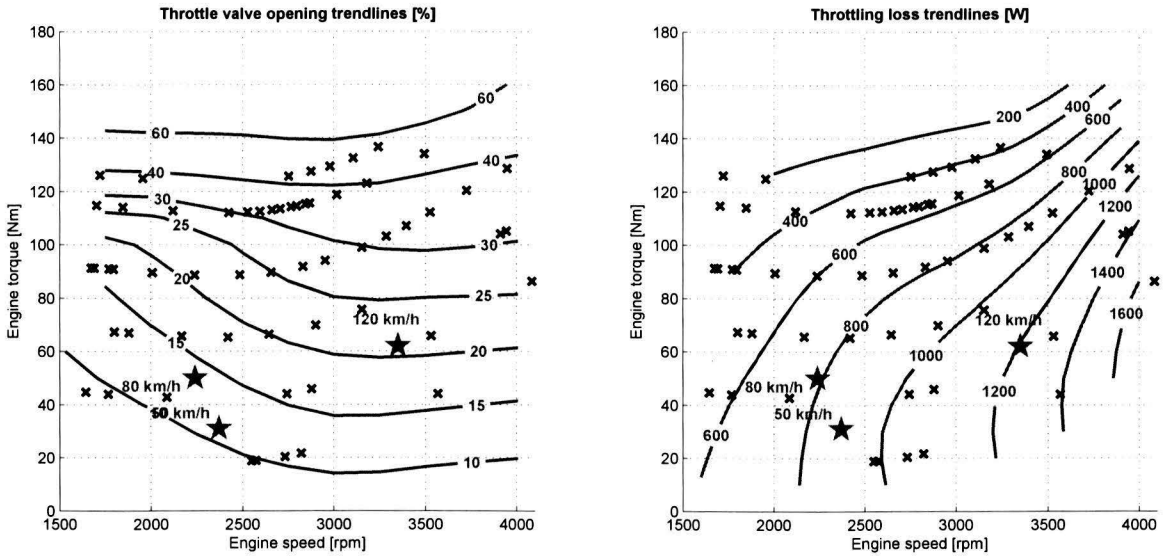

Figure 3.6: Throttle valve opening position map and throttling loss map.

blow-by gasses in the cylinders. However, the pumping loss during the intake stroke is not only caused by the throttle valve itself, but also the valve train introduces pumping losses.
The work per cylinder $W_i[J]$ for each stroke is then computed using:

$$W_{int} = \int_{-360^oCA}^{-180^oCA} (p_{crnk} - p_{cyl}) \frac{\mathrm{d}V_{cyl}}{\mathrm{d}\theta} \mathrm{d}\theta \qquad \text{intake stroke} \qquad (3.5)$$

$$W_{comp} = \int_{-180^oCA}^{0^oCA} p_{cyl} \frac{\mathrm{d}V_{cyl}}{\mathrm{d}\theta} \mathrm{d}\theta \qquad \text{compression stroke} \qquad (3.6)$$

$$W_{pwr} = \int_{0^oCA}^{180^oCA} p_{cyl} \frac{\mathrm{d}V_{cyl}}{\mathrm{d}\theta} \mathrm{d}\theta \qquad \text{power stroke} \qquad (3.7)$$

$$W_{exh} = \int_{180^oCA}^{360^oCA} (p_{cyl} - p_{crnk}) \frac{\mathrm{d}V_{cyl}}{\mathrm{d}\theta} \mathrm{d}\theta \qquad \text{exhaust stroke} \qquad (3.8)$$

$$P_i = n_{cyl} \cdot W_i \frac{N_{eng}}{60 \cdot 2} \qquad (3.9)$$

were the in-cylinder pressure is integrated over the crankangle $\theta[^oCA]$ for the intake, compression, power and exhaust stroke respectively. In Eq. (3.9) the relation between power $P_i[W]$ and work $W_i[J]$ is found.

The cylinder work for each stroke is used to build a Sankey diagram to indicate the losses in the combustion process. Fig. 3.7 shows the specific losses in a common engine operating point. The throttling losses consume 2.8[%] of the potential energy of the air/fuel mixture. In another perspective, the throttling losses account for 13.3[%] compared to the actual engine power.

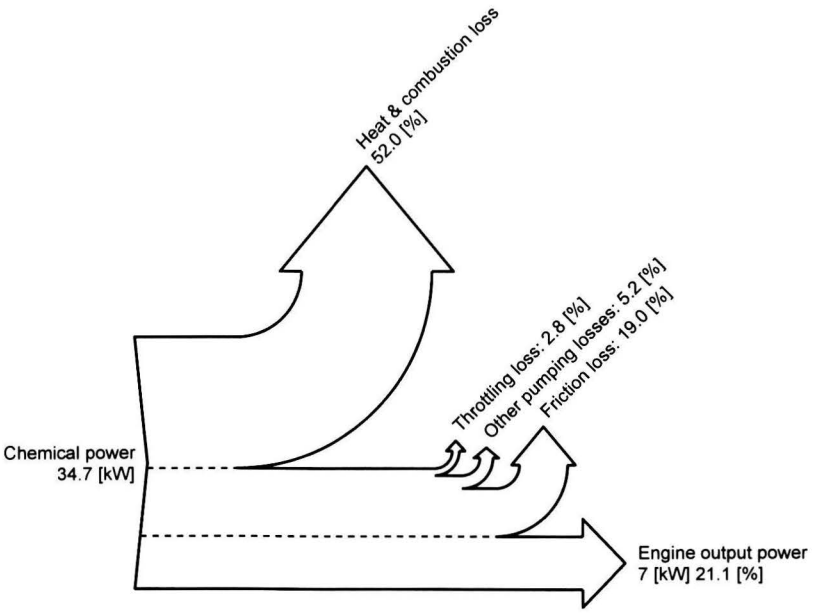

Figure 3.7: Sankey diagram near $50[km/h]$ ($2500[rpm]$ @ $28[Nm]$)

3.3.2 Steady state WEDACS experiments

After the reference experiments the cable operated throttle valve is replaced by the WEDACS system as shown in the WEDACS system description, Fig. 2.3. The original throttle valve is now used as a dummy throttle valve to provide a correct throttle position signal (TPS) and the fully opened/fully closed throttle switch signal for the ECU. This is done to ensure correct feedforward signals for engine control, see the scheme in Fig. 3.8. The WEDACS system has two control inputs: throttle valve position $\alpha[\%]$ and turbine vanes position $\beta[\%]$. Both positions are based on the angular rotation of their actuator shaft and indicate the opening percentage from 0 to $100[\%]$. The load of the turbine is a compressor with a valve to create a pressure drop. This valve is however not actuated and the load amount is unknown.

The air mass flow curves through the VGT and the throttle valve is given in Fig. 3.9 at various brake load torques. Please note that the presence of a CVT gearbox causes that a constant brake load torque does not signify a constant engine (crankshaft) torque since the CVT efficiency is speed dependent. The vertical blue line indicates the point where the vanes position is at maximum. Beyond this line the throttle valve opens to increase the air mass flow (i.e. 'reference position' 120% means fully opened VGT $+20\%$ opened throttle valve). Notice that from this point, the air mass flow through the turbine slightly decreases.
It is striking that the flow through the closed throttle valve is not completely zero, especially at low loads. The flow leakage through the throttle valve when it is supposed to be fully closed is significant with respect to the VGT flow. Here, the IACV/AAC valve might be active, since both air mass flow sensors are calibrated simultaneously. Disabling the IACV/AAC valve could not resolve this leakage, since the engine then operates in save mode.
The temperatures during these experiments are shown in App. C.3. The temperature drop over

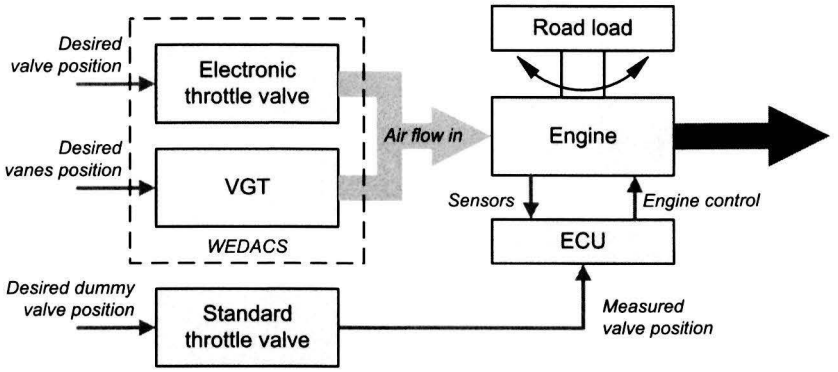

Figure 3.8: WEDACS measurement setup: dummy throttle valve/ECU interaction and WEDACS

the turbine is significant, especially at low loads. Notice a turbo-lag likewise behavior: the temperature drops very sudden at some point.

The map in Fig. 3.10 show the region where the turbine can act alone (black dots) and where the throttle valve needs to assist (red encircled points). The map indicates that the turbine needs throttle valve assistance at ($\Pi > 0.8[bar]$), which limits the turbine operating region in terms of maximum delivered engine torque when using the turbine only. Here the maximum air mass flow of the turbine is reached. In Fig. 3.11 the turbine vanes opening position map is shown. Details about this map are found in Fig. C.15.

To determine the turbine power recovery an ideal cycle of an isentropic process is considered [H.I.H. Saravanamuttoo, 2009]. The turbine power is then calculated using Eq (3.10):

$$P_{vgt}(t) = \dot{m}_{air}(t)c_p(T_{amb}(t) - T_{vgt}(t)) \tag{3.10}$$

with $T_{vgt}[K]$ the temperature downstream of the turbine.
However, the significant temperature drop affects the humidity of the air. In fact, due to condensation the measured temperature is slightly higher [R.H.L. Eichhorn, 2009]. The upstream turbine temperature is the ambient temperature, while temperatures downstream of the turbine could drop below $0[^oC]$, resulting in condensation inside the manifold. This is therefore compensated for by adding the condensation energy $P_{cond}[W]$ to the calculated turbine power:

$$P_{cond}(t) = \dot{m}_{air}(t)(\zeta_i - \zeta(t))L_v \tag{3.11}$$

$$P_{vgt}(t) = \dot{m}_{air}(t)c_p(T_{amb}(t) - T_{vgt}(t)) + \dot{m}_{air}(t)(\zeta_i - \zeta(t))L_v \tag{3.12}$$

With ζ_i the initial specific humidity and $\zeta(T)$ the instantaneous (temperature dependent) specific humidity and L_v the latent heat of condensation which is $2257kJ/kg$ [Çengel and Boles, 2002].

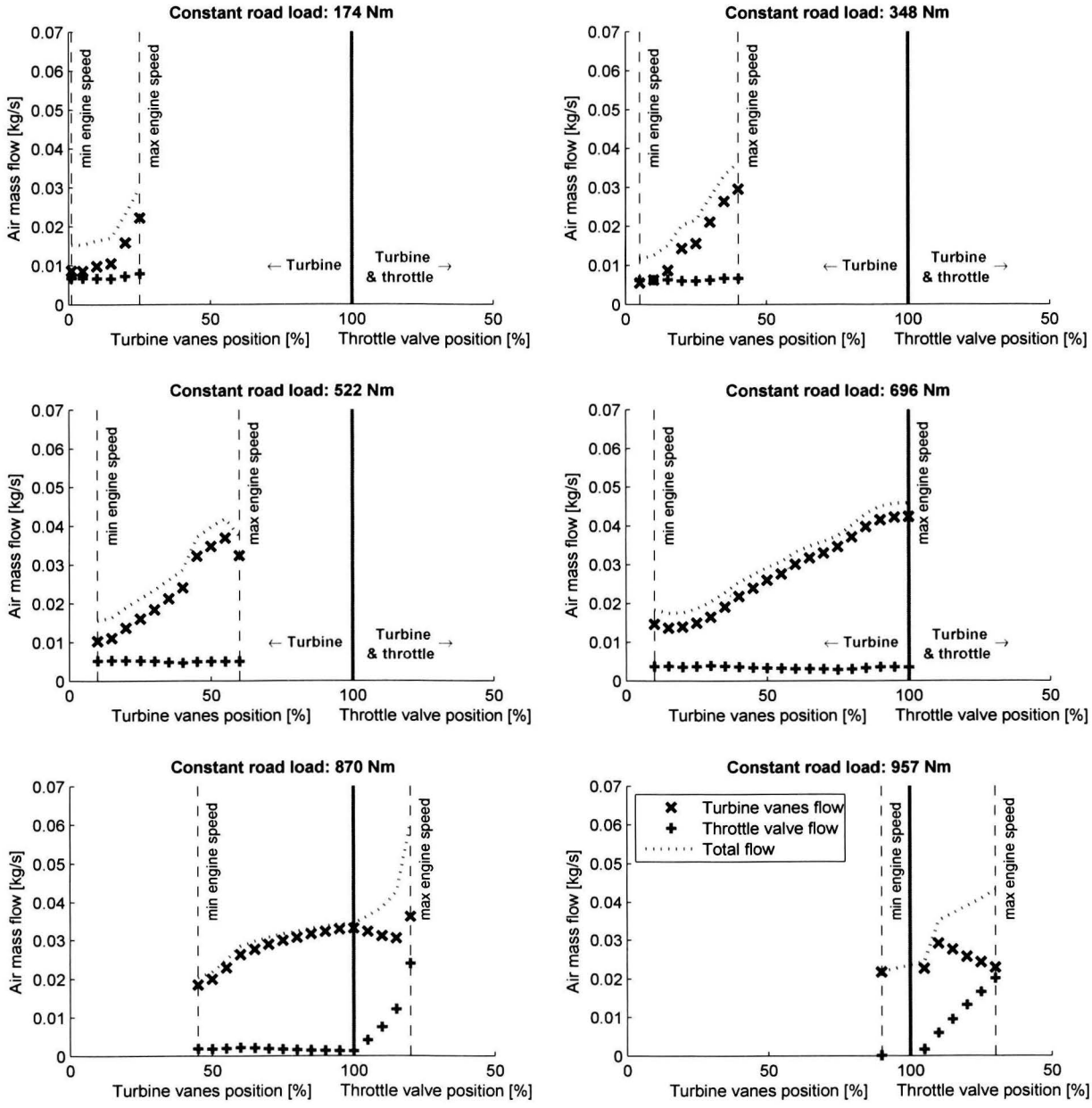

Figure 3.9: Air massflow curves as function of vane positions (0−100%) and additional throttle positions (> 100%) for different road loads.

The potential turbine power is shown in Fig. C.14 per fixed brake load torque as function of vanes/valve position. The turbine power is also visualized with trendlines for different engine operating points in Fig. 3.11. In Fig. C.16 the accuracy with respect to the experimental data is shown.

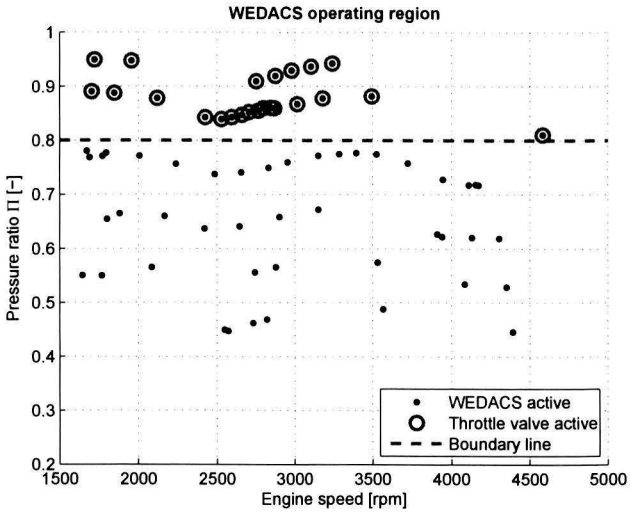

Figure 3.10: WEDACS operating region in terms of pressure ratio ($\frac{p_{man}}{p_{amb}}$) and engine speed

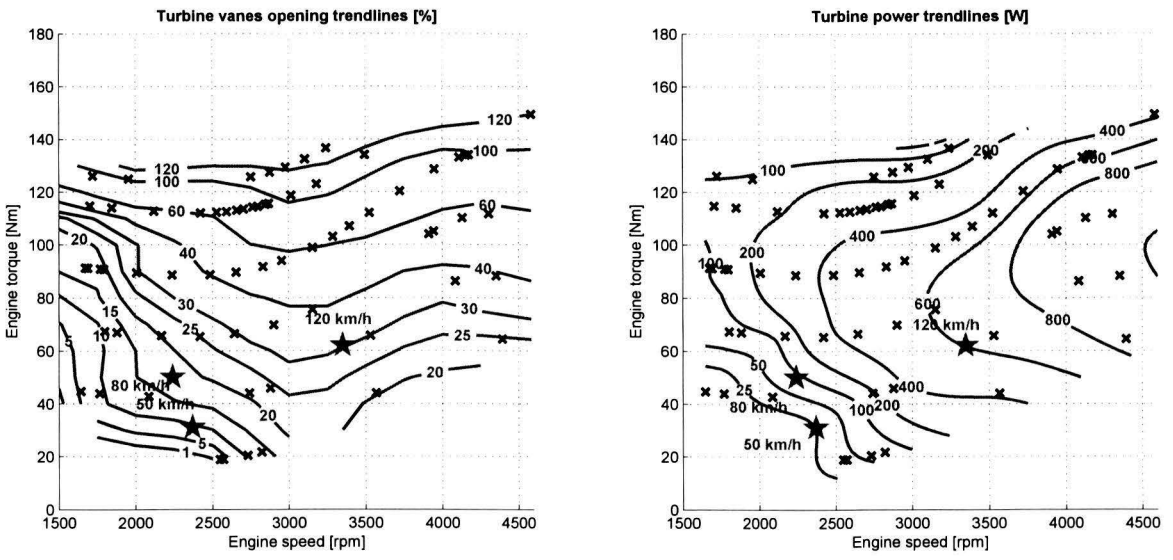

Figure 3.11: WEDACS vanes opening position (left graph) and power recovery trendlines.

Fig. 3.12 shows the throttling losses with the potential power by WEDACS. The potential power loss and gain at $50/80/120[km/h]$ is shown in Table 3.4. It is shown that between 2 and $40[\%]$ of throttling losses could be recovered. In perspective to the engine power, this results in a gain of $0.34[\%]$ in total power output at $50[km/h]$ to $2.8[\%]$ engine power increase at $120[km/h]$.

In Fig. 3.13 the opening position of the WEDACS system is compared with the throttle valve opening at various engine operating points. Again, WEDACS vanes position $\beta > 100\%$ indicates support by the throttle valve. In the region below the $\beta = 100\%$ isoline the turbine can act alone.

Table 3.4: Throttle loss compared to potential WEDACS power recovery under steady state conditions

	Engine power $P_{eng}[W]$	**Throttle loss** $P_{throtl}[W]$	**WEDACS power** $P_{vgt}[W]$	**Percentage throttle loss** $\frac{P_{throtl}}{P_{eng}}[\%]$	**Percentage recovered loss** $\frac{P_{vgt}}{P_{throtl}}[\%]$
$50[km/h]$	7700	900	25	11.7	2.9
$80[km/h]$	11700	785	85	6.7	11.0
$120[km/h]$	19800	1210	605	5.6	50.0

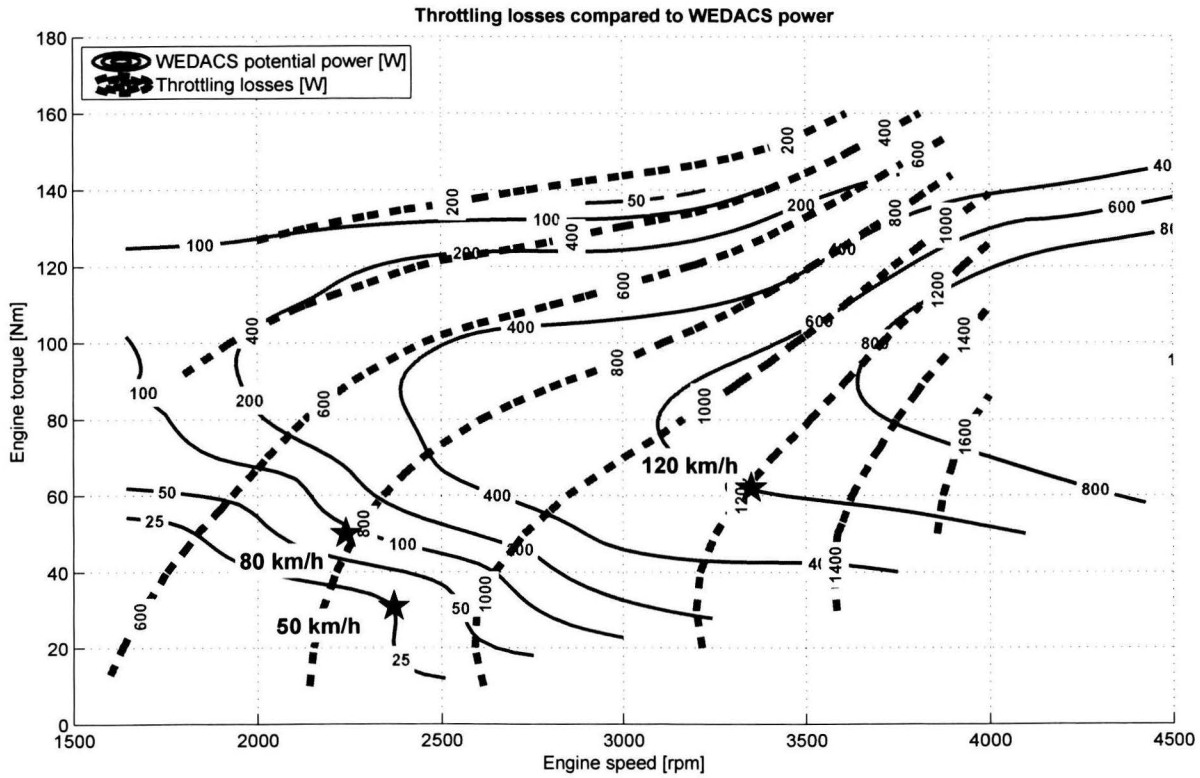

Figure 3.12: Trendlines of throttling loss (thick dotted red lines) compared with potential turbine power by WEDACS (blue lines)

The graph shows that with WEDACS the engine is able to provide at least $120[Nm]$ of torque at the crankshaft. However, considering the residence during a NEDC drive cycle, the turbine vanes opening position does not exceed $40[\%]$ under steady state driving. In fact, at $50[km/h]$ the turbine vanes are opened at only $10[\%]$.

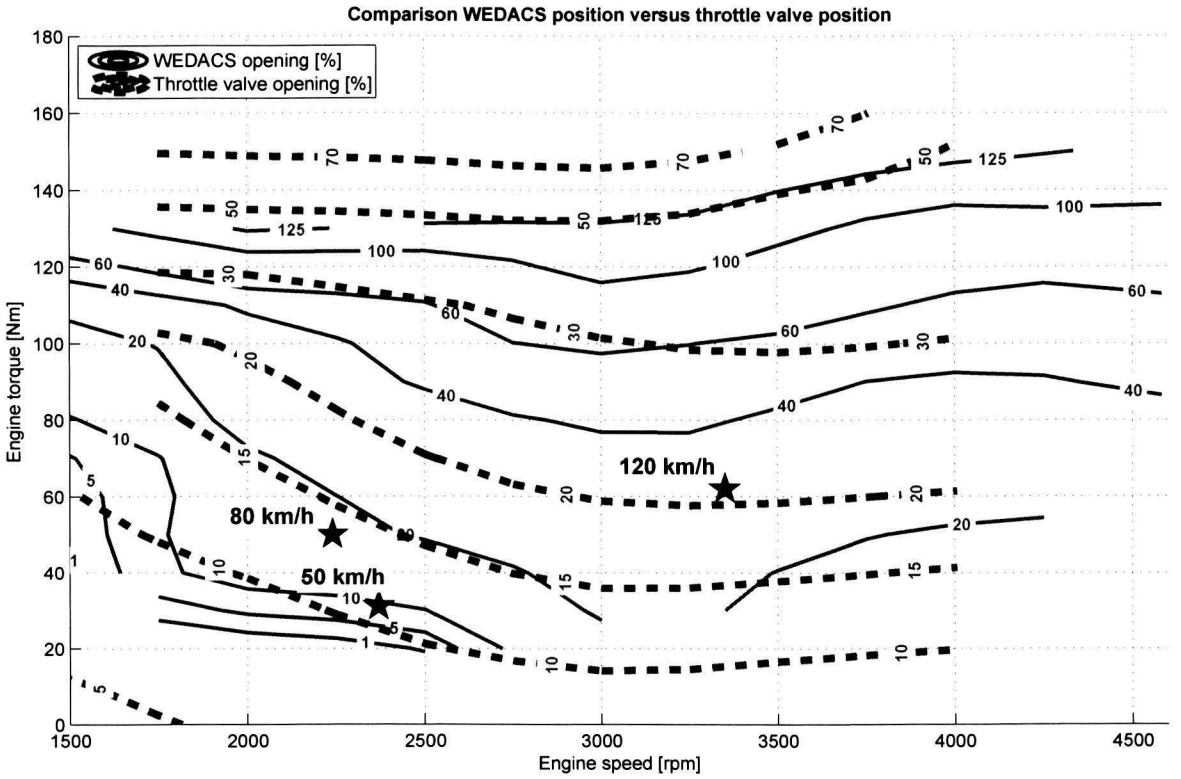

Figure 3.13: WEDACS vanes opening percentage β versus throttle valve opening percentage α. Blue lines are isolines from the WEDACS steady state experiment. Red (thick dotted) lines are the trendlines as found in Fig. C.8 during the reference measurements.

As described by J.R. Serrano [2008] the turbine efficiency is lowest at near closed vanes positions. However, the turbine is used at different pressure levels then its designed application. Therefore an efficiency map is constructed using:

$$\eta_{vgt} = \frac{1 - (T_{man}/T_{amb})}{1 - (p_{man}/p_{amb})^{\frac{\kappa-1}{\kappa}}} \tag{3.13}$$

The efficiency map in Fig. 3.14 shows a maximum efficiency of $\eta_{vgt} = 0.45[-]$. The map shows indeed that the turbine efficiency decreases near fully opened and fully closed vanes positions. In general, the efficiency also decreases with an increasing intake manifold pressure. The map fitting results are shown in Fig. C.17.

The turbine speed trendlines are indicated in Fig. 3.14. The turbine speed is independent of manifold pressure at low turbine vanes positions ($\beta < 30[\%]$), but increases with the turbine vanes position. At higher vanes opening positions an opposite behavior is noticed where the speed becomes mainly pressure dependent and independent of turbine vanes position. When the vanes are fully opened and the throttle valve assists, the turbine speed stays approximately constant. In Fig. C.18 the speed map is compared to the measured data.

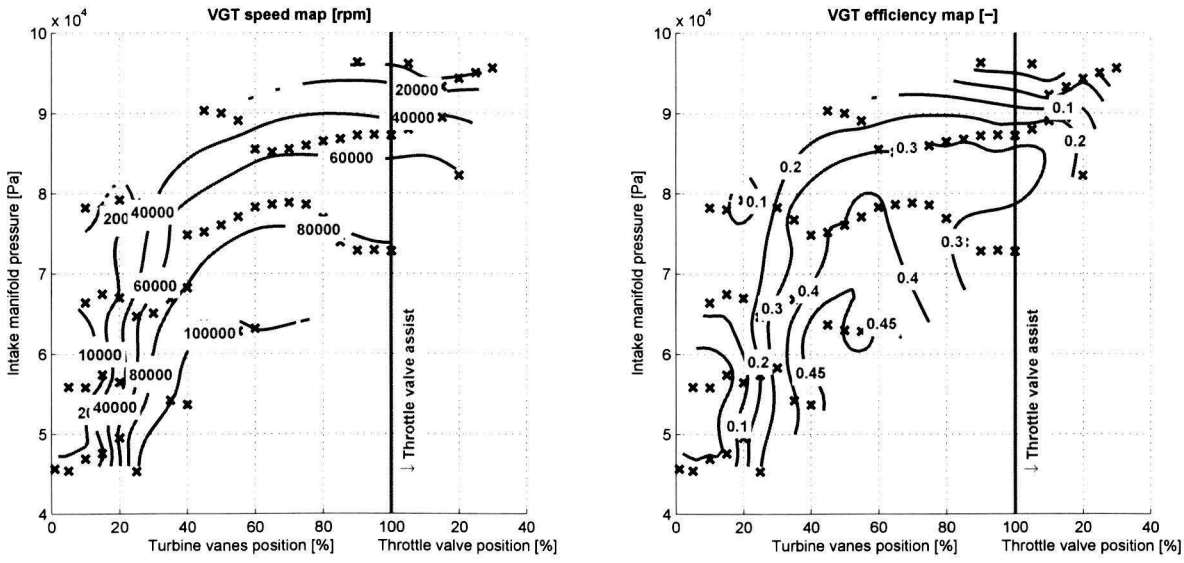

Figure 3.14: VGT efficiency and speed trendlines as function of WEDACS opening position and intake manifold pressure

3.3.3 Dynamic response experiments

Dynamic step response measurements are performed to determine the transient engine speed response to a throttle valve/turbine vanes position step input under constant road load conditions. The test bed dynamometer is able to apply a constant torque at varying speeds. Two types of experiments have been performed: throttle valve position step responses and turbine vanes position step responses. A combination of both the valve and the vanes together was not performed. The transient engine speed and manifold pressure results are used to fit some variables of the model. This is discussed in detail in Chapter 4.

3.4 Experimental setup chapter summary & discussion

The experimental setup is explained in terms of the engine hardware, actuator and sensor locations, data signal processing, engine control systems and the WEDACS prototype. Especially the signal conditioning in combination with sensor calibration was found to be an essential, time consuming part of the measurement procedure in order to obtain reliable results.
The engine is externally controlled using dSPACE and actuators to prescribe the throttle valve positions, turbine vanes position and the brake load torque supplied by the Eddy current dynamometer. The engine ECU controls the fuel supply and ignition timing. A second actuated dummy throttle valve is used to generate signals for this ECU in order to maintain proper functioning fuel and ignition control loops.
The malfunctioning engine torque sensor introduced an additional uncertainty since a CVT transmission transfer function had to be obtained in order to calculate the torque at the engine crankshaft. The CVT efficiency had shown to be speed and torque dependent. The transfer function introduces a mean absolute error of $13[Nm]$ which equals at least 7%.

Two types of measurements sequences have been performed: steady state and transient experiments. During a steady state experiment all temperatures and pressures, engine speed and brake load torque are constant. The data is averaged over $60[s]$ and collected at a wide range of engine operating points. The data is used to construct trendlines and maps. The trendlines indicate the trends roughly over a typical engine speed $\times$ engine torque map.
Both the reference (standard throttle valve) and the WEDACS system are measured under steady state conditions. Trendlines give an indication where most throttle losses occur and what potential turbine power could be generated. Common used engine operating points ($50 - 80 - 120[km/h]$) are shown as a benchmark. Between 3 and $50[\%]$ of the throttle losses could be recovered when assuming a $100[\%]$ turbine efficiency. In total, this is a gain between $0.34[\%]$ and $2.8[\%]$ in addition to the engine power. Comparing the throttling loss map with the turbine power map, the highest absolute gain in power is found at $120[km/h]$. When taking the NEDC drive cycle residence plot into account it is advised to optimize the turbine at a lower speed/torque operating point ($50[km/h]$). Also considering the opening percentage of the vanes under steady driving at $50[km/h]$ ($\beta = 10[\%]$) and $80[km/h]$ ($\beta = 15[\%]$), it is wise to investigate downsizing of the turbine.

In the next Chapter a model for the engine equipped with WEDACS is constructed. This model will be validated using the experimental data from this Chapter.

Chapter 4

Modeling

4.1 Model objective

The goal of the model is to predict the engine response as a function of the engine control inputs, the ambient conditions and the engine load. The model includes WEDACS and could be used to validate different control strategies for WEDACS in order to maximize fuel consumption reduction while maintaining or even improving the dynamic engine responses.
This Chapter describes the model step by step. First, the model equations are elaborated and parameters are fitted on experimental data. At the end of this Chapter the results of the complete model are shown.

4.2 Modeling approach

Engine modeling is a challenging topic. The main purpose of the combustion engine is to convert available chemical energy (air and fuel) into useful mechanical energy at the crankshaft. The engine is considered an open system which is influenced by ambient conditions and incoming and outgoing mass flows. Various perspectives could be used to model the behavior of engine (sub-)systems, since a wide range of dynamic processes occur simultaneous in a running engine. One could think of modeling the air path in terms of turbulence, the fueling process in terms of chemical mixture composition and transport delays, combustion processes in terms of emissions and flame geometry, the reciprocating behavior and the accompanying torque production and the transient behavior of the engine as a complete system. Depending on the research topic, a suitable control oriented model is chosen. In this case, a mean value engine model (MVM) is sufficient to predict the gross engine values such as crankshaft speed, manifold pressure/temperature and efficiencies. The MVM approach neglects discrete events and considers slow time varying processes as constants. The engine is considered a continuously working volumetric pump and the reciprocating behavior is captured using time delays for gas exchange and torque production which are crank angle dependent.

An overview of the model is presented in Fig. 4.1. The MVM model is subdivided into submodels based on known physical and thermodynamic relations. The subsystems are categorized in an air system, a fuel system and a mechanical system as depicted in Table 4.1.

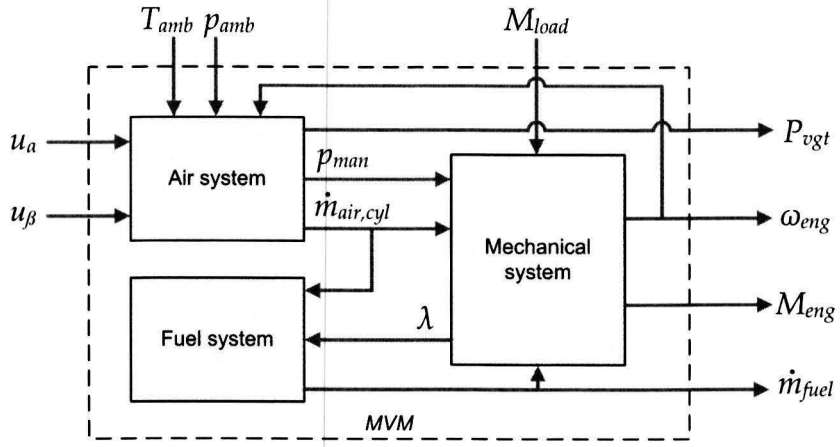

Figure 4.1: Interrelationships between the air, fuel and mechanical system in the engine model. ECU fuel injection control is included in the fuel subsystem and ignition control is embedded in the mechanical subsystem.

Table 4.1: Submodel categories

Air system	**Fuel system**	**Mechanical system**
Throttle valve	Fuel supply	Crankshaft
VGT	(ECU fuel injection control)	Cylinder block
Intake manifold		(ECU ignition timing)

The total model has two control inputs, three uncontrolled inputs and four outputs:

Control inputs

- throttle valve position control signal $u_\alpha[V]$
- turbine vanes position control signal $u_\beta[V]$

Uncontrolled inputs

- ambient temperature $T_{amb}[K]$
- ambient pressure $p_{amb}[Pa]$
- crankshaft load torque $M_{load}[Nm]$

Outputs

- engine speed $\omega_{eng}[rad/s]$
- engine torque $M_{eng}[Nm]$
- potential turbine power $P_{vgt}[W]$
- fuel mass flow $\dot{m}_{fuel}[kg/s]$

The ECU control signals for fuel injection and ignition timing are included in the model and therefore not treated as inputs for the model. The crankshaft load torque is uncontrolled in both

the real world and the controlled test environment. In reality the road slope, rolling friction and aerodynamic drag influence the torque needed to propel the vehicle. During the experiments however, this wheel torque is an input provided by the dynamometer. But then the speed and torque dependent CVT is influencing the torque transfer to the engine crankshaft.

In the following sections each system with the corresponding submodels is presented. The model parameters are fitted by minimizing the objective function Eq. (4.2) based on the absolute relative error ε_{rel}:

$$\varepsilon_{rel,i} = |\frac{y_{model,i} - y_{meas,i}}{y_{meas,i}}| \cdot 100\% \tag{4.1}$$

$$\min_{a_1 \ldots a_N \in \Re^N} \left(\sum_{j=1}^{k} \left(\sum_{i=1}^{n} \varepsilon_{rel,i} \right)_j \right)^2 \tag{4.2}$$

with,

i = model and measurement sample 1 to n

j = model output variables 1 to k

$y_{model,i}$ = modeled output variables value at sample i

$y_{meas,i}$ = measured output variables value at sample i

$a_1 \ldots a_N$ = model parameters 1 to N

The mean absolute relative error ε_{mean} is an important criterium to qualify the model results. The target is to maintain $\varepsilon_{mean} < 10\%$ during transients.

$$\varepsilon_{mean} = \frac{1}{n} \sum_{i=1}^{n} \varepsilon_{rel,i} \cdot 100\% \tag{4.3}$$

4.3 Air system

The air system describes the air delivery path from WEDACS to the engine cylinders. The throttle valve, VGT and intake manifold are all included.
When modeling the system a distinction is made between reservoirs and flows. Reservoirs are objects where mass or energy is stored, such as the intake manifold but also the ambient surrounding is accounted for as a reservoir. The level of a reservoir is described using state variables (e.g. pressure, temperature). The mass flows between the reservoirs are then dependent on these reservoir levels and restrictors in between such as valves.
The non-linear flow between two reservoirs is dependent on the difference between up- and downstream pressure levels. Flows are modeled assuming that there is no friction and no inertial effects in the flow. Also no spatial effects are considered and the flow is completely isolated. The air system and its submodels are schematically shown in Fig. 4.2.

4.3.1 Throttle valve submodel

A throttle valve is a isothermal orifice. For compressible fluids through isothermal orifices two important assumptions are made:

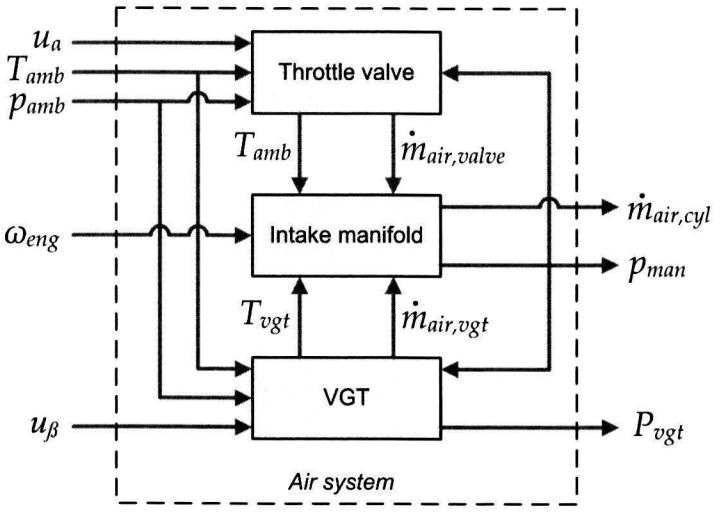

Figure 4.2: Air system with throttle valve, VGT and intake manifold submodels.

- No losses occur during the acceleration of the flow up to the narrowest point. All potential energy in the flow is converted isentropically into kinetic energy.
- Behind the narrowest point the flow is fully turbulent and all resulting kinetic energy is dissipated in thermal energy.

This last point is exactly what the WEDACS system wants to prevent: that kinetic energy is lost due to dissipation into thermal energy. By enabling utilization of the kinetic energy in the flow, this loss is (partly) recovered using WEDACS.

The throttle valve system acts as a variable flow restriction since it determines the air mass flow $\dot{m}_{air,valve}[kg/s]$ into the intake manifold as function of pressure ratio $\Pi[-]$ and throttle valve position $\alpha[rad]$:

$$\dot{m}_{air,valve}(t) = c_d A_{valve}(p_{man}, \alpha) \frac{p_{amb}(t)}{\sqrt{R T_{amb}(t)}} \cdot \Psi\left(\Pi(t)\right) \tag{4.4}$$

with $c_d[-]$ the discharge coefficient, $A_{valve}[m^2]$ the throttle valve opening area and $\Psi\left(\Pi(t)\right)$ the non linear flow function as function of pressure ratio $\Pi(t) = \frac{p_{man}}{p_{amb}}$:

$$\Psi(\Pi(t)) = \begin{cases} \sqrt{\kappa \left[\frac{2}{\kappa+1}\right]^{\frac{\kappa+1}{\kappa-1}}} & \text{for } p_{man} < p_{cr} \\ \Pi(t)^{\frac{1}{\kappa}} \sqrt{\frac{2\kappa}{\kappa-1}\left[1 - \Pi(t)^{\frac{\kappa-1}{\kappa}}\right]} & \text{for } p_{man} \geq p_{cr} \end{cases} \tag{4.5}$$

$$\Pi(t) = \frac{p_{man}(t)}{p_{amb}(t)} \tag{4.6}$$

$$p_{cr} = \left[\frac{2}{\kappa+1}\right]^{\frac{\kappa}{\kappa-1}} \cdot p_{amb} \tag{4.7}$$

At the critical pressure $p_{cr}[Pa]$ the flow reaches sonic conditions in the narrowest part of the valve or orifice.

The flow function as given in (4.5) introduces a problem when modeling near $p_{man} = p_{amb}$ since the gradient becomes infinite here. In practice the intake manifold pressure will be smaller than the ambient pressure, however the model will become more robust when this situation is considered. Guzzella and Onder [2010] suggest to define a threshold pressure ratio $\Pi_{tr}[-]$ close to 1 where a laminar flow condition is assumed to avoid singularity.

The discharge coefficient c_d is not constant but varies over throttle valve position $\alpha[^o]$ and pressure ratio $\Pi[-]$. The throttle valve area $A_{valve}[\alpha]$ is dependent on the throttle valve position only. Although Moskwa [1988] suggests a detailed function for the throttle valve area, it is decided to combine the discharge coefficient with the valve area to minimize the error since both are dependent on throttle valve position. Therefore it is chosen to build a map for the complete term. The map fitting is discussed later in Section 4.3.4.

The IACV/AAC valve is not separately modeled since the exact distribution between throttle valve and IACV/AAC air mass flow is unknown. Also the IACV/AAC position is unknown. Instead, it is assumed that the IACV/AAC flow is accounted for by the throttle valve.

4.3.2 VGT submodel

The VGT submodel predicts the air mass flow, the temperature drop and the potential turbine power. The VGT submodel signals are shown in Fig. 4.2. The turbine has a variable flow area, dependent on the position of its vanes. Since the geometrical parameters are unknown a transfer function between actuator position and vanes position is built. The vanes control input signal $u_\beta[-]$ is described as function of the desired vanes position $\beta[\%]$ in Eq. (4.8):

$$u_\beta(t) = b_1\beta^2(t) + b_2\beta(t) \tag{4.8}$$

The air mass flow through the turbine is a function of pressure drop over the turbine and the vanes position. The VGT model from Wahlström and Eriksson [2006] is used here:

$$\dot{m}_{air,vgt}(t) = A_{vgt,max}\frac{p_{amb}(t)}{\sqrt{T_{amb}(t)}} f_\Pi(\Pi(t)) f_{vanes}(u_\beta(t)) \tag{4.9}$$

$$f_\Pi(\Pi(t)) = \sqrt{1 - \Pi(t)^\kappa} \tag{4.10}$$

$$f_{vanes}(u_\beta(t)) = c_1 + c_2\sqrt{1 - \left(\frac{u_\beta(t) - c_3}{c_4}\right)^2} \tag{4.11}$$

with the choke exponent κ and maximum turbine area $A_{vgt,max}[m^2]$. Experimental data should be used to fit the parameters c_1, c_2, c_3, c_4, κ and $A_{vgt,max}$.

Turbine characteristics are often presented in performance maps supplied by the turbine manufacturer. These maps are usually provided for medium to higher speeds ($> 90000[rpm]$), because at low speeds/air mass flows the heat exchange with the turbine housing affects the measurements of the efficiencies. These low speed/air mass flow ratios are not within the designed operating region for normal turbine use in exhaust systems. For mean value modeling the turbine performance maps are parameterized and extrapolated which results in poor models at the

low speed-load regions [Merten Jung and Watts, 2002]. For the throttling application in this research combined with energy recovery at the turbine shaft, the operating region of the turbine will cover low to medium speed-load points ($< 100000[rpm]$). However, the turbocharger will not encounter the high temperatures from exhaust gas (up to 850^oC). The turbine efficiency heat effects are therefore less dominant when extrapolating in low speed-load regions.

Part of the control objective will be the power recovery using the turbine. The power recovered by the turbine is not measured, since the turbine is not loaded with an alternator. Instead a compressor is mounted to apply an unknown load. To indicate the amount of recovered power $P_{vgt}[W]$ by the turbine Eq. (4.12) is used as proposed by R.H.L. Eichhorn [2009]:

$$P_{vgt} = \dot{m}_{air} c_p (T_{amb} - T_{vgt}) + \dot{m}_{air}(\zeta_i - \zeta) L_v \tag{4.12}$$

However this function does not incorporate the dynamic effects such as turbine shaft inertia.

The temperature downstream the turbine is estimated using the map of Fig. 4.5. It is chosen to use a map instead of a thermodynamic relation due to the relative low sensitivity to temperature in the total model. The map is build using the polynomial:

$$\begin{aligned} f_{vgt}(p_{man}, \dot{m}_{vgt}) = {} & g_1 p_{man}^3 + g_2 p_{man}^2 + g_3 p_{man} + g_4 \dot{m}_{vgt}^3 + g_5 \dot{m}_{vgt}^2 + g_6 \dot{m}_{vgt} \dots \\ & \dots + g_7 (p_{man} \dot{m}_{vgt})^2 + g_8 (p_{man} \dot{m}_{vgt}) + g_9 \end{aligned} \tag{4.13}$$

$$T_{vgt} = \begin{cases} f_{vgt}(p_{man}, \dot{m}_{vgt}) & \text{if } f_{vgt}(p_{man}, \dot{m}_{vgt}) < (T_{amb} - g_{10}) \\ T_{amb} - g_{10} & \text{if } f_{vgt}(p_{man}, \dot{m}_{vgt}) \geq (T_{amb} - g_{10}) \end{cases} \tag{4.14}$$

Note the constraint in Eq. (F.8) for the maximum turbine temperature. The turbine temperature map described by this function are shown in Fig. 4.5. The model is based upon this map, with a time delay to model the transient behavior.

Although the turbine speed has influence on the turbine efficiency, it chosen not to model turbine efficiency and speed within this research. The control objective is qualified by the energy potential and therefore control of turbine load or speed is not investigated here.

4.3.3 Intake manifold submodel

The intake manifold is a buffer between the total flow into the manifold $\dot{m}_{air,in}[kg/s]$ and the flow to the engine block $\dot{m}_{air,cyl}[kg/s]$. There exists a difference in these two flows since the reciprocating motion of the pistons and the corresponding intake valve behavior. These effects are only noticeable over a short timescale in the order of one revolution. Although mean value models do not account for the reciprocating motion of the pistons, this difference in mass flows is necessary to calculate the manifold pressure derivative. Model inputs are the VGT temperature $T_{vgt}[K]$, the air mass flow into the manifold $\dot{m}_{air,in}[kg/s]$ and the engine speed $\omega_{eng}[rad/s]$. Outputs are the air mass flow to the engine cylinders $\dot{m}_{air,cyl}[kg/s]$ and the manifold pressure $p_{man}[bar]$. An overview was already depicted in Fig. 4.2.

The intake manifold is considered a receiver with a fixed volume and modeled as a lumped parameter system. The thermodynamic states (pressure, temperature, mixture composition) of

the mass in the reservoir are considered constant over the entire volume, but not constant over time.
The mass and energy balances apply here, assuming no heat or mass transfers through the walls and no significant energy changes in the flow occur. Also no work is performed by the receiver. These balance equations could be coupled assuming the gas/liquid mixture behaves as an ideal gas at all times. This results in the following set of adiabatic equations. The mathematical operations to obtain these equations are elaborated in App. D.1.

$$\frac{d}{dt}p(t) = \frac{\kappa R}{V}\left[\dot{m}_{in}(t)T_{in}(t) - \dot{m}_{out}(t)T(t)\right] \tag{4.15}$$

$$\frac{d}{dt}T_{man}(t) = \frac{T(t)R}{p(t)Vc_v} \cdot \ldots$$
$$\ldots \left[c_p\dot{m}_{in}(t)T_{in}(t) - c_p\dot{m}_{out}(t)T(t) - c_v(\dot{m}_{in}(t) - \dot{m}_{out}(t))T(t)\right] \tag{4.16}$$

However, this can be simplified if one assumes a relatively large dwell-time of the mass in the receiver and a relatively large surface-to-volume ratio. It is assumed that the temperature derivative is zero over the complete reservoir which leads to an isothermal equation as commonly found in literature:

$$\frac{d}{dt}p_{man}(t) = \frac{R \cdot T_{man}(t)}{V_{man}}\left(\dot{m}_{in}(t) - \dot{m}_{out}(t)\right) \tag{4.17}$$

$$\dot{m}_{in}(t) = \dot{m}_{air,valve}(t) + \dot{m}_{air,vgt}(t) \tag{4.18}$$

$$\dot{m}_{out}(t) = \dot{m}_{air,cyl}(t) \tag{4.19}$$

$$T_{man}(t) = T_{in}(t) = T_{out}(t) \tag{4.20}$$

In Hendricks [2001] both adiabatic and isothermal models are compared for an SI engine with EGR. The effective time constant on the manifold pressure state is found to be mainly dependent on engine speed and not on pressure itself. The order of the time constant is found to be typically between $120[msec]$ for idle speed and $5[msec]$ at full load, while the throttle valve is typically actuated in the order of $50[msec]$. This results in a significant transient error between isothermal and adiabatic models. Hendricks suggests to use an adiabatic model in transient models due to the instantaneous manifold temperature jumps caused by adiabatic expansion/compression effects. Hendricks also shows that this only applies when using exhaust gas recirculation (EGR). EGR is defined as the percentage of recycled exhaust gas in the intake mixture [Heywood, 1988]. Although the EGR will be disregarded in this research, the use of WEDACS will introduce a significant temperature drop behind the turbine. It is therefore necessary to investigate the use of an adiabatic intake manifold model.

Although the flow from intake manifold to cylinder is also controlled by valves, this flow is typically described using the engine speed and volumetric efficiency. The engine is approximated as a volumetric pump where the volumetric efficiency determines the ratio between the actual and theoretically ideal aspiration of the cylinders.

$$\dot{m}_{air,cyl} = \frac{p_{man}}{R_{air}T_{man}}\eta_{vol}\frac{V_d}{2}\frac{\omega_{eng}}{2\pi} \tag{4.21}$$

In general, volumetric efficiency is defined in steady state operations using Eq. (4.22) [Heywood,

1988]:

$$\eta_{vol} = \frac{2\dot{m}_{air,in}}{\rho_{air,in} V_d N_{eng}} \tag{4.22}$$

with $\dot{m}_{air,in}[kg/s]$ and $\rho_{air,in}[kg/m^3]$ respectively the entering air mass flow and air density in the intake manifold.
Jurado [2007] suggests a polynomial function to predict the volumetric efficiency using the mass of air in the manifold $m_{air,man}[kg]$ and the engine speed:

$$\begin{aligned}\eta_{vol} = &\left(b_1\omega_{eng}^2 + b_2\omega_{eng} + b_3\right) m_{air,man}^2 + \left(b_4\omega_{eng}^2 + b_5\omega_{eng} + b_6\right) m_{air,man} + ... \\ &... \left(b_7\omega_{eng}^2 + b_8\omega_{eng} + b_9\right)\end{aligned} \tag{4.23}$$

$$m_{air,man} = \frac{p_{man} V_{man}}{R_{air} T_{man}} \tag{4.24}$$

In L.A. Smith and Osborne [1999] the validity of steady state determined volumetric efficiency under transient operations is investigated. Although differences are found during step changes in engine speed, they conclude that the steady state volumetric efficiencies are valid in transient engine operations. During a engine speed ramp test, there is no difference between transient and steady state efficiency. Therefore, a lookup table or efficiency map is applicable in transient models.

The manifold temperature is calculated by assuming ideal mixing of the VGT and the throttle valve air mass flows. Although thermodynamic mixing relations exist, it is chosen to use a simplified approximation of the manifold temperature which fits the experimental data accurately:

$$T_{man} = T_{amb} - j_1(T_{amb} - T_{vgt}) + j_2 \tag{4.25}$$

4.3.4 Air system parameter fit results

Throttle valve discharge coefficient and flow area

The model for the air mass flow through the throttle valve is based on a map for the term $c_d A_{valve}(p_{man}, \alpha)$. This map is fitted by smoothing a generated surface consisting of triangular cells on the steady state obtained experimental data. The map is then used in the model by interpolation between the mapped values. When comparing the mapped values with the measured values, the map is accurate enough to provide a mean absolute relative error ε_{mean} of 0.5% and a maximum absolute relative error ε_{max} of 3.4% as shown in Fig. 4.3.
The map could also be described using this polynomial:

$$\begin{aligned}c_d A_{valve} = &\, a_1 p_{man}^4 + a_2 p_{man}^3 + a_3 p_{man}^2 + a_4 p_{man} + a_5\alpha^4 + a_6\alpha^3 + a_7\alpha^2 ... \\ &... + a_8(p_{man}\cdot\alpha)^4 + a_9(p_{man}\cdot\alpha)^3 + a_{10}(p_{man}\cdot\alpha)^2 + a_{12}(p_{man}\cdot\alpha) + a_{13} \\ \alpha(t) = &\, u_\alpha(t)\end{aligned} \tag{4.26}$$

The modeled values using this polynomial are also shown in Fig. 4.3 next to the mapped data. The fitted model has a ε_{max} of 6.4% and a ε_{mean} of 1.6%. The fit results for both the map and the model could be found in the Appendix F.2.

The critical pressure limit is also indicated in the figure. Below this limit, the air mass flow function in Eq. (4.4) becomes only dependent on the term $c_d A_{valve}$. The value of $c_d A_{valve}$ to the left of this line should then be constant when decreasing the manifold pressure at a fixed throttle valve position. However, the map indicates a slight increase in air mass flow for decreasing pressures. This is not significant, since the relative error is plotted as well, showing a maximum $\varepsilon_{max} = 3.4\%$ and a mean $\varepsilon_{mean} = 0.5\%$ compared to the measured data.

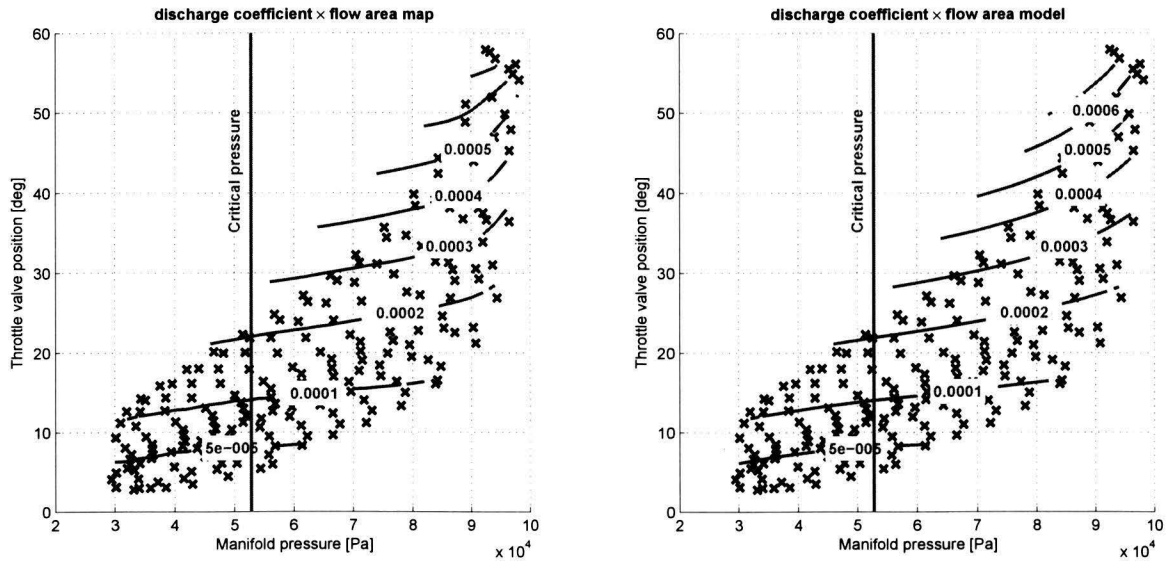

Figure 4.3: Discharge coefficient $\times$ flow area map (left) and model

VGT mass flow and temperature

The turbine air mass flow model as presented with Eq. (4.9) is compared with an obtained map for steady state operating points in Fig. 4.4. Although the model resembles the trends as shown in the map, the absolute relative error of the model is larger. Especially at low loads and small vane opening areas. Compared to the measured values the model error $\varepsilon_{mean} = 9.0\%$ while $\varepsilon_{mean} = 2.5\%$ for the map. The error for both the model and the map is shown in Appendix F.4. The poor approximation performance of the model at low turbine vanes opening positions is probably caused by the modified turbine vanes mechanism. At small opening positions the leakage area becomes significantly large compared to the turbine vanes opening area. Furthermore, the model originates from a VGT research which is validated in a different operating region. Looking at the choking conditions, the model correctly predicts a constant air mass flow level below the critical pressure.

The turbine temperature model parameter fit results are shown in Fig. 4.5. The model is accurate enough to describe the measured temperatures during experiments within a ε_{max} of 2.1% and with a ε_{mean} of 0.3%. Both the map and the model errors with respect to the measured experimental data is shown in Appendix F.4.

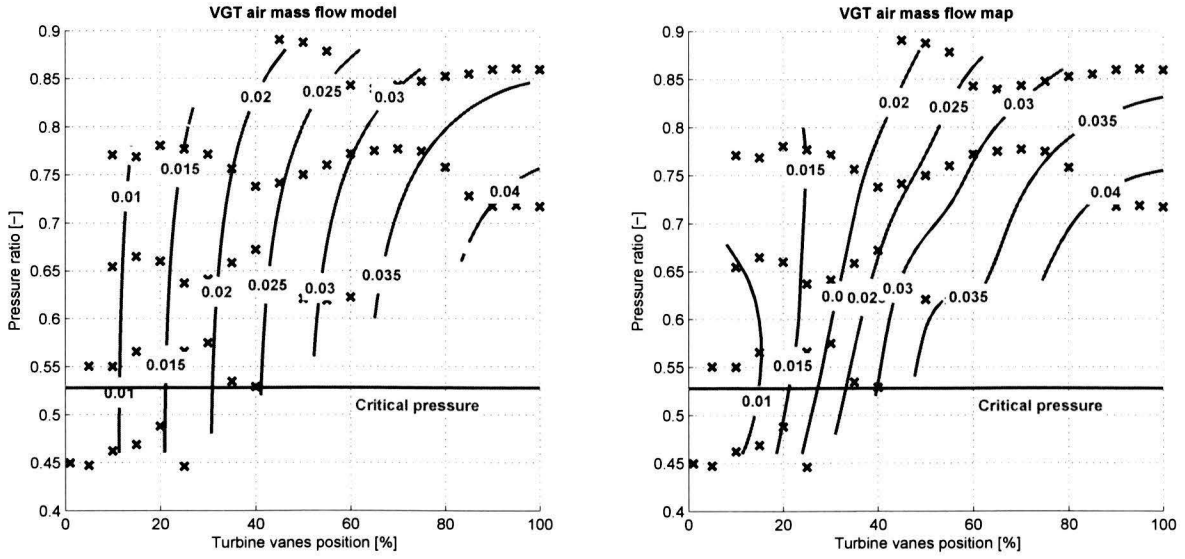

Figure 4.4: Model versus map for the turbine air mass flow under steady state conditions

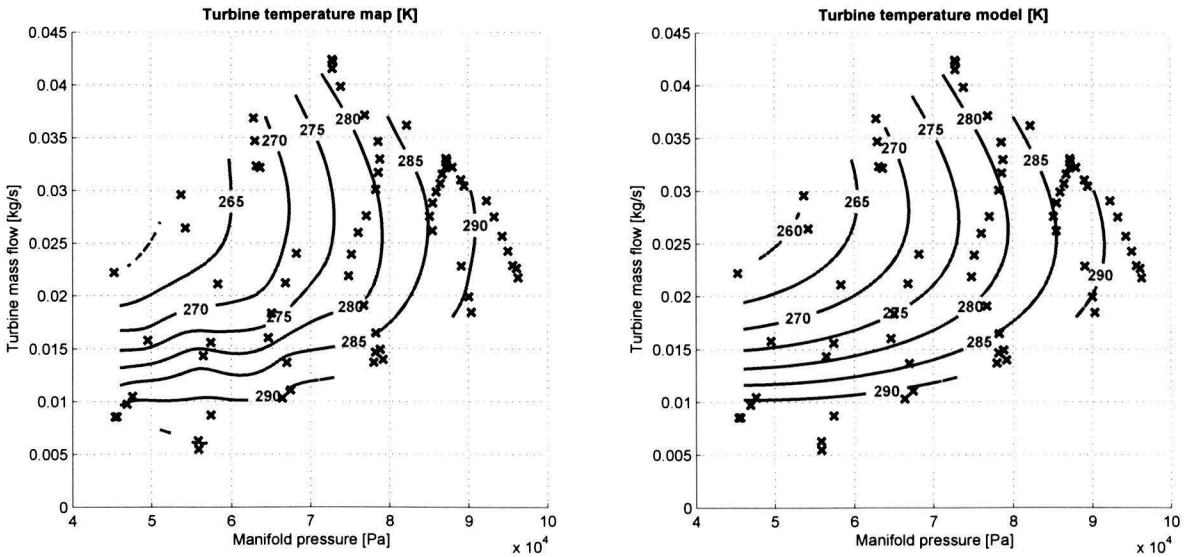

Figure 4.5: Model versus map for the downstream turbine temperature under steady state conditions

Volumetric efficiency

The volumetric efficiency polynomial model in Eq. 4.23 results in a mean absolute relative error ε_{mean} of 3.2% and a maximum absolute relative error ε_{max} of 9.4% as presented in Appendix F.5. When using the map fitting technique as described in Section 4.3.4 however the relative error becomes smaller: $\varepsilon_{mean} = 0.6\%$ and $\varepsilon_{max} = 2.7\%$. See also Fig. 4.6.

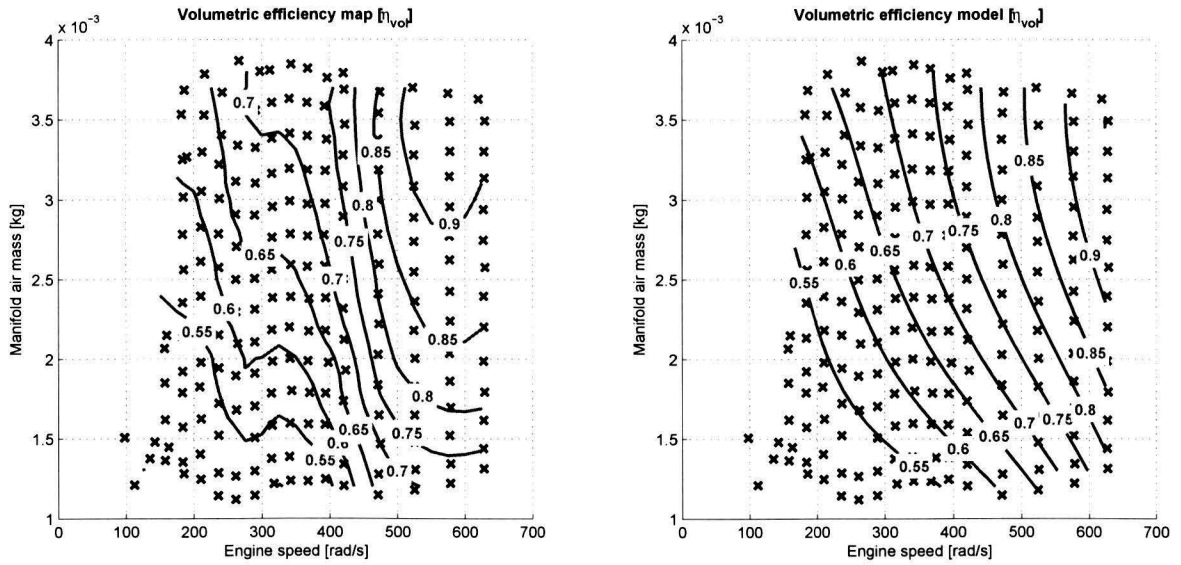

Figure 4.6: Map for the volumetric efficiency under steady state conditions

Manifold volume

The manifold volume $V_{man}[m^3]$ could only be obtained during transients:

$$\frac{d}{dt}p_{man}(t) = \frac{R_{air}T_{man}(t)}{V_{man}}\left(\dot{m}_{in}(t) - \dot{m}_{out}(t)\right) \tag{4.27}$$

In steady state operating points $\dot{m}_{air,in} = \dot{m}_{air,cyl}$ and $\frac{d}{dt}p_{man}(t) = 0$ so the term $\frac{R_{air}T_{man}(t)}{V_{man}}$ cannot be determined. In the experimental setup only $\dot{m}_{air,in}$ is measured. The fitting procedure of the manifold volume therefore needs the previously obtained steady state model for volumetric efficiency in order to be able to calculate $\dot{m}_{air,cyl}$. Two measured transient step responses are used to fit the manifold volume. The fit results are shown in Fig. 4.7. During the transients a mean absolute error of $\varepsilon_{mean} = 2.1\%$ at a low road load and $\varepsilon_{mean} = 1.0\%$ at a high load was found. Simple calculation by hand resulted in a rough estimation of $V_{man} \approx 3 \cdot 10^{-3}[m^3]$, however the fit results in a $V_{man} = 1.09 \cdot 10^{-3}[m^3]$. This significant difference might be caused by the fairly large steady state error of the volumetric efficiency.

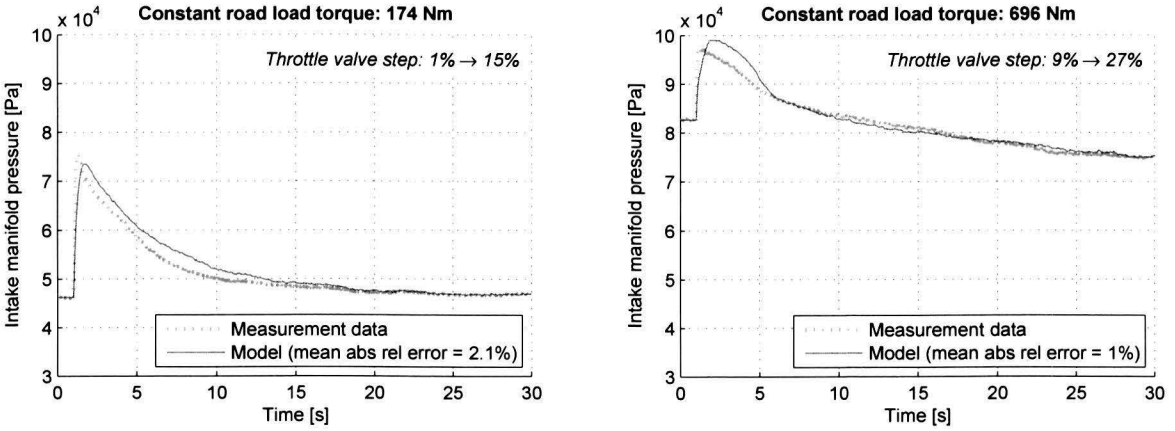

Figure 4.7: Transient experiments manifold

4.4 Fuel system

In modern SI engines the fuel supply is controlled by the ECU. Typically, a fuel pump pressurizes a fuel rail circuit and the ECU controlled valves inside the fuel injectors open for a certain amount of time at a desired crank angle position. A pressure regulator maintains constant fuel rail pressure to ensure a constant fuel mass flow through the opened injectors. Excess fuel is routed back to the fuel tank.

For an indirect multi port injected fuel system, each cylinder has its own port which connects the manifold reservoir to the combustion chamber. The main advantage of fuel injection in the ports is a more homogeneous air/fuel mixture in the cylinders. Due to the high temperature of the port walls and inlet valve, part of the liquid fuel evaporates immediately. Another effect is a liquid fuel film which builds up at the port walls especially when the inlet valve is closed [Moskwa, 1988]. These so called wall wetting effects introduce dynamic transport delays for which different models are proposed. As a result the injected fuel mass flow differs from the aspirated fuel mass flow in transients. However, in steady state conditions the fuel supply is considered constant.
The wall wetting effects can be modeled either using thermodynamic laws or by introducing delays in the fuel supply under transient conditions. Considering the mean value approach the introduction of time delays seems more appropriate here.

The fuel system consists of a fuel supply submodel and an ECU injection control submodel. The ECU controls the fuel injection and the actual fuel mass flow is determined in the fuel supply submodel. In Fig. 4.8 an overview is presented.

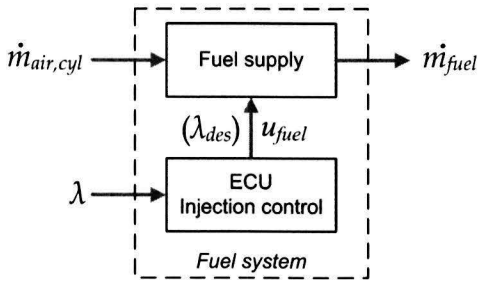

Figure 4.8: Fuel system with the ECU injection control and the fuel supply submodels

4.4.1 ECU injection control submodel

Both the ECU injection signal and the actual fuel mass flow are not measured in the test setup. The ECU controls the fuel injection amount using a feedback loop with λ and feedforward via the throttle valve position sensor signal. The control objective of the ECU is to maintain $\lambda = 1$. Transient experiments have shown no visible peaks in the λ signal during a step input on the throttle valve. The ECU is therefore considered as a optimal controller and assumed to actually maintain $\lambda \approx 1$ at all times. Only at high loads (typically high air mass flows) the ECU will enrich the mixture with an excess in fuel ($\lambda < 1$).

$$\lambda = \lambda_{des} \tag{4.28}$$

$$\lambda_{des} = \begin{cases} a_1 \dot{m}_{air,cyl} + a_2 & \text{if } \dot{m}_{air,cyl} \leq m_{cr} \\ a_3(\dot{m}_{air,cyl} - m_{cr}) + (a_1 M_{cr} + a_2) & \text{if } \dot{m}_{air,cyl} > m_{cr} \end{cases} \tag{4.29}$$

4.4.2 Fuel supply submodel

The fuel mass flow is calculated using the measured air mass flow $\dot{m}_{air,in}[kg/s]$ and the air/fuel ratio $\lambda[-]$. Furthermore, the wall wetting effects are not identified in transient experiments. The effective time scale of the wetting effects appears to be significantly smaller than the time scale at which the influence on engine response is noticeable. Time delays are therefore not incorporated in the fuel delivery model. The fuel delivery model is then reduced to:

$$\dot{m}_{fuel} = \frac{\dot{m}_{air,cyl}}{\lambda_{des} L_{st}} \tag{4.30}$$

with $L_{st}[-]$ the stoichiometric air/fuel ratio and $\lambda_{des}[-]$ the desired air/fuel ratio.

4.4.3 Fuel system parameter fit results

Experiments show that the engine is operating with a slightly rich mixture, since $\lambda < 1$ at all times. It is clearly visible that the mixture is enriched at higher air mass flows. The straight forward λ model is fitted to the data with $\varepsilon_{max} = 23.8\%$ and $\varepsilon_{mean} = 1.7\%$. During transient measurements, no visual delay in fuel supply was discovered. The fuel supply model is therefore only based on static measurement data and assumes a perfect ECU injection control under transients.

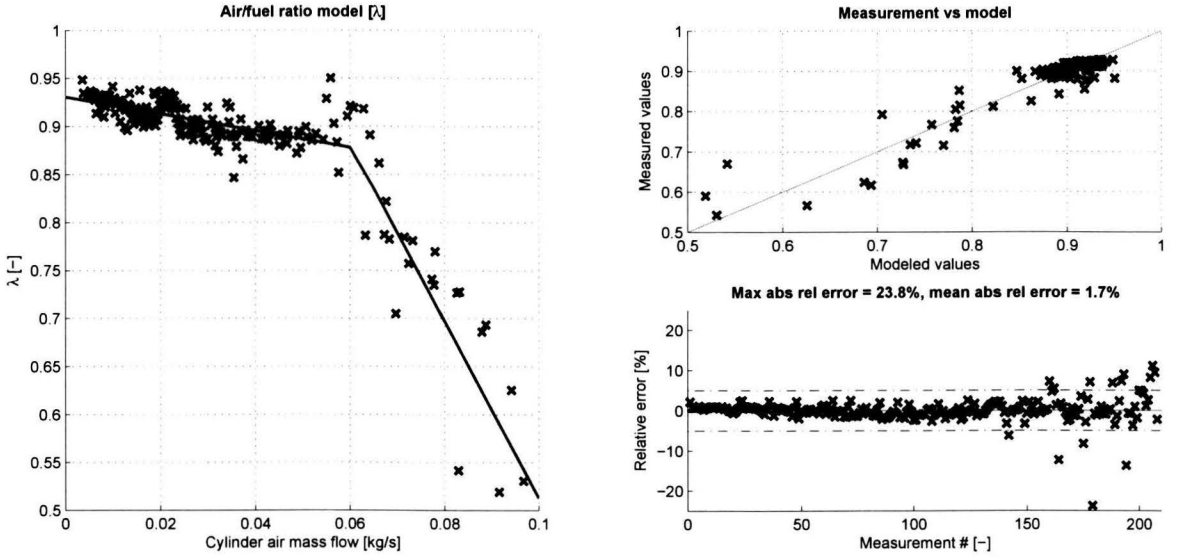

Figure 4.9: Model for air/fuel ratio λ under steady state conditions

4.5 Mechanical system

The engine considered in this report operates in a four stroke cycle and is spark ignited, also known as Otto cycle. In the engine block the chemical energy of the fuel/air mixture is converted via a combustion process into mechanical energy (e.g. torque) at the crankshaft. The torque production is a highly nonlinear result of many variables and efficiencies since several losses occur between the ignition of the fuel/air mixture to the brake torque at the crankshaft. In Fig. 4.10 an overview is given which is build using theory obtained from Johansson [2011]. In combustion studies the term 'mean effective pressure' ($mep[bar]$) is often used to express the cylinder performance. Several defined efficiencies determine the distribution between these effective pressures. The total efficiency from chemical energy from the fuel to mechanical energy at the crankshaft

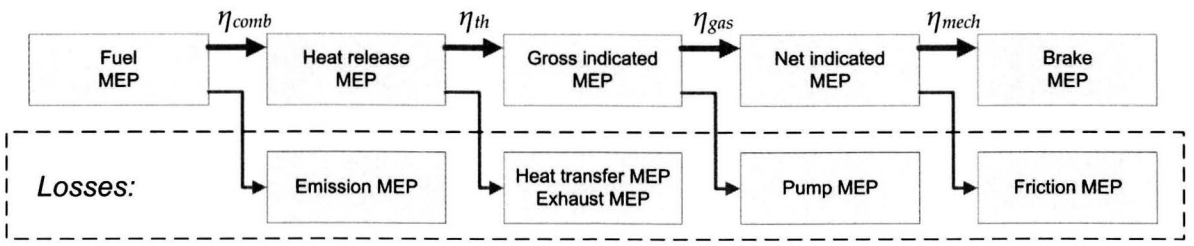

Figure 4.10: Losses in during the combustion process in a SI engine

is then defined as the product of combustion (η_{comb}), thermodynamic (η_{th}), gas exchange (η_{gas}) and mechanical (η_{mech}) efficiencies:

$$\eta_{eng} = \eta_{comb} \cdot \eta_{th} \cdot \eta_{gas} \cdot \eta_{mech} \tag{4.31}$$

In literature, various approaches can be found in order to account for the total engine efficiency. For modeling purposes the separate components as visualized in Fig. 4.10 are not always distin-

guished as such.

The produced torque is acting on the crankshaft via the pistons and piston rods. On the other hand the crankshaft experiences a load from the vehicle drivetrain. A positive difference between the produced torque $M_{eng}[Nm]$ by the cylinders and the drivetrain load torque at the crankshaft $M_{load}[Nm]$ results in a acceleration of the crankshaft. The rate at which the crankshaft accelerates depends on the total inertia. A negative torque difference will decelerate the crankshaft.

The reciprocating motion of the pistons and the four-stroke principle result in a discrete torque production where the number of cylinders and the engine speed determine the sampling period [Guzzella and Onder, 2010]. More cylinders result in a smoother (but never constant) torque production and the flywheel inertia distribute the torque peaks even further. The sampling interval is constant in crank-angle domain, but depends on engine speed. These discrete effects are ignored in the MVM.

The mechanical system is subdivided in a cylinders submodel and a crankshaft submodel, see Fig. 4.11. The combustion process is modeled in the cylinders part, while the engine speed and torque at the crankshaft are modeled in the crankshaft submodel.

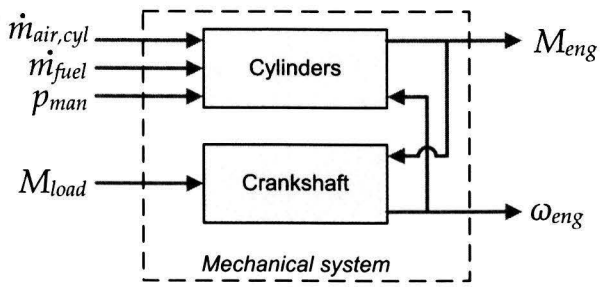

Figure 4.11: Mechanical system with cylinders submodel and crankshaft submodel.

4.5.1 Cylinders subsystem

In the cylinders submodel the torque on the pistons is calculated by multiplying the potential fuel power $P_{chem}[W]$ with efficiencies $\eta_i[-]$ and by subtracting friction and pumping losses $M_{loss}[Nm]$. Here, $M_{loss}[Nm]$ substitutes the gas exchange (η_{gas}) and mechanical (η_{mech}) efficiencies as identified earlier.

$$P_{chem} = \dot{m}_{fuel} Q_{LHV} \tag{4.32}$$

$$P_{ind} = \eta_{comb} \cdot \eta_{th} \cdot P_{chem} \tag{4.33}$$

$$M_{ind} = \frac{P_{ind}}{\omega_{eng}} \tag{4.34}$$

$$M_{eng} = M_{ind} - M_{loss} \tag{4.35}$$

with $P_{ind}[W]$ the gross indicated power. The indicated power is the produced mechanical power due to the combustion process. Below, the efficiencies and losses are described separately.

Combustion efficiency (η_{comb})

The engine is considered to be an open system which exchanges heat and work with its surroundings. Fuel and air are the reactants which flow into the system, while the product is the exhaust gasses flowing out. The exhaust gasses contain incomplete combustion products (e.g. CO, H_2, unburned hydrocarbons and soot) which originate from various reasons. For instance, flame quenching at the cylinder wall and in small crevices between piston and cylinder. Also local irregularities in the air/fuel mixture due to non homogeneous mixing results in an incomplete combustion process. Under lean conditions ($\lambda > 1$) the amount of incomplete combustion products will be small and thus the combustion efficiency will be around $95 - 98\%$. Richer mixtures ($\lambda < 1$) have an increasing negative effect on the combustion efficiency. Heywood [1988] describes the combustion efficiency as the fraction of fuel energy supplied which is released in the combustion process:

$$\eta_{comb} = \frac{H_R(T_{amb}) - H_P(T_{amb})}{m_{fuel} Q_{LHV}} \tag{4.36}$$

with $H_R(T_{amb})$ and $H_P(T_{amb})$ respectively the reactants and product enthalpy at ambient temperature. $Q_{LHV}[J/kg]$ is the lower heating value of fuel.
The combustion efficiency is modeled as function of the air/fuel ratio, since the exact mixture composition and the accompanying enthalpies are unknown:

$$\eta_{comb} = m_1 + m_2(\lambda - 1) \tag{4.37}$$

Thermodynamic efficiency (η_{th})

The thermodynamic efficiency is the lowest efficiency in the combustion process since a significant amount (typically $> 65\%$) of the chemical energy is converted to heat. Heat is lost in exhaust gasses and released through the cylinder walls, engine coolant and engine oil. The thermodynamic efficiency η_{th} is influenced by the engine speed, air/fuel ratio and ignition timing.

The largest influence on the thermodynamic efficiency is determined by the engine speed $\omega_{eng}[rad/s]$ and is significantly smaller than 1 and has a parabolic form due to high losses at both low and high engine speeds [Guzzella and Onder, 2010]. At low engine speeds relatively large heat transfer occurs with the cylinder walls due to a slower expansion stroke. At very high engine speeds the combustion duration becomes larger compared to the time of the expansion stroke which has a negative effect on the thermal efficiency.

The air/fuel ratio λ indicates whether the burnt mass is lean or rich. Slightly lean mixtures (roughly for $\lambda < 1.3$) have a surplus in air but this will not affect the efficiency. For leaner mixtures, misfires start to occur. Effects that decrease the thermal efficiency due to a rich mixture are the incomplete combustion and water/gas shift reactions. Since the ECU fuel control is assumed to operate optimal, the air/fuel ratio effect on thermal efficiency is considered a constant value.

The ignition of the mixture is dependent on the spark timing in an SI engine. This timing is referred to a spark advance. At the optimal spark advance $\theta_{opt}[^oCA$ TDC] there exists a maximum torque for each engine operating point. The minimum best torque spark advance ($\theta_{MBT}[^oCA$ TDC]) is defined as the spark advance at which the $98 - 99\%$ of maximum torque is

reached with a spark advance smaller than the optimal spark advance [White, 2008]. This is done in order to prevent knocking, a phenomenon which causes abnormal combustion due to auto ignition the gas mixture in the cylinders. Knocking can cause serious engine failure [Heywood, 1988]. Moskwa [1988] assumes that a parabolic relation exists between MBT and brake torque. An experimental sequence is described from which the data is obtained to prove this assumption. He found that the spark advance influence increased at lower brake torque loads.
The ECU ignition control signals are assumed to be optimal at all times. The influence on the thermodynamic efficiency is then considered insignificant with respect to the engine speed influence as described earlier. Therefore the ECU ignition control signal is discarded from the model as presented earlier in Fig. 5.1.
As a result, the total thermodynamic efficiency is modeled as function of engine speed only:

$$\eta_{th} = w_1 - w_2(\omega_{eng} - w_3)^2 \tag{4.38}$$

Gas exchange and mechanical efficiency (η_{gas} and η_{mech})

To determine the total pumping and friction losses Sandoval and Heywood [2003] presented an improved friction model based on an earlier model by K.J. Patton and Heywood [1989]. The model computes the total friction mean effective pressure *tfmep*$[bar]$ which is the sum of the crankshaft bearings friction *cfmep*$[bar]$, reciprocating friction of the pistons/cylinder walls with and without gas pressure loading *rfmep*$[bar]$, valve train friction *vfmep*$[bar]$, auxiliary losses *afmep*$[bar]$, intake pumping losses $pmep_i[bar]$ and exhaust pumping losses $pmep_e[bar]$.

$$M_{loss} = \frac{tfmep \cdot N \cdot V_d}{60 \cdot 2 \cdot 10^5 \cdot \omega_{eng}} \tag{4.39}$$

$$tfmep = \underbrace{cfmep + rfmep + vfmep + afmep}_{\text{friction mep}} + \underbrace{pmep_i + pmep_e}_{\text{pumping mep}} \tag{4.40}$$

The equations describing the losses of (4.40) are given in App. D.3 and are mainly based on engine parts geometry and material and lubricant properties. Although these various submodels have been validated with actual measurement data on several engine types, there is no hard evidence to presume that this specific model applies to any given SI engine. Also most geometrical parameters are unknown.
In Karmiggelt [1999] a simplified approximation for engine loss torque $M_{loss}[Nm]$ due to friction and pumping losses is given as function of engine speed $\omega_{eng}[rad/s]$ and manifold pressure $p_{man}[Pa]$:

$$M_{loss} = z_1 + z_2\omega_{eng} + z_3\omega_{eng}^2 + (z_4 + z_5\omega_{eng})\, p_{man} \tag{4.41}$$

This approximation includes the engine auxiliaries as well and is used in the model. Now Eq. (4.35) is used to determine the produced engine torque $M_{eng}[Nm]$:

$$\eta_{comb} = m_1 + m_2(\lambda - 1) \tag{4.42}$$

$$\eta_{th} = w_1 - w_2(\omega_{eng} - w_3)^2 \tag{4.43}$$

$$M_{ind} = \eta_{th}\eta_{comb}\frac{\dot{m}_{fuel}Q_{LHV}}{\omega_{eng}} \tag{4.44}$$

$$M_{loss} = z_1 + z_2\omega_{eng} + z_3\omega_{eng}^2 + (z_4 + z_5\omega_{eng})\, p_{man} \tag{4.45}$$

$$M_{eng} = M_{ind} - M_{loss} \tag{4.46}$$

4.5.2 Crankshaft submodel

The crankshaft submodel is used to determine the engine speed as a function of the produced torque and the load torque at the crankshaft. The engine crankshaft acceleration $\dot{\omega}_{eng}[rad/s^2]$ is described using the following differential equation:

$$J_{eng}\dot{\omega}_{eng} = M_{eng} - M_{load} \tag{4.47}$$

with $J_{eng}[kg \cdot m^2]$ the engine inertia.

The load torque $M_{load}[Nm]$ must be a known input and is equal to the engine torque $M_{eng}[Nm]$ under steady state driving conditions (e.g. $\frac{d\omega_{eng}}{dt} = 0$ and $\frac{dM_{load}}{dt} = 0$). When the produced engine torque exceeds the load torque the surplus torque will accelerate the engine inertia. As a result of increased engine speed the load torque will also increase, leading to a new equilibrium. This holds not only for the experimental setup, but also for a vehicle on the road.
The engine inertia is assumed to be constant since all friction phenomena are included in the engine torque. Furthermore, the total vehicle inertia and friction is included in de load torque.
The load torque at the crankshaft is an input, because the experiments are conducted on a test bench with a dynamometer. However, the efficiency of the CVT is only determined in steady state conditions and transient effects are unknown. Therefore the load torque at the crankshaft becomes an uncontrolled input:

$$M_{load} = d_1 + d_2 \cdot M_{road} + d_3 \cdot \omega_{eng} + d_4 \cdot \omega_{eng}^2 + d_5 \cdot \omega_{eng}^3 + d_6 \cdot \omega_{eng}^4 + d_7 \cdot \omega_{eng}^5 \tag{4.48}$$

4.5.3 Mechanical system parameter fit results

Combustion and thermodynamic efficiency

Since the combustion efficiency $\eta_{comb}[-]$ and the thermodynamic efficiency $\eta_{th}[-]$ could not be measured directly on the test setup, both models could not be validated separately. However, both efficiencies together determine the indicated power as fraction of the chemical power of the fuel/air mixture.

$$\eta_{comb}\eta_{th} = \frac{P_{ind}}{P_{chem}} \tag{4.49}$$

The in-cylinder pressure sensor data was used to determine the indicated pressure at various steady state engine operating points. Integrating this pressure over the compression and power stroke results in the indicated work for one cylinder $W_{ind,cyl}[J]$. The total indicated power for the engine is then determined using:

$$W_{ind,cyl} = \int_{-180^oCA}^{180^oCA} p_{cyl}\frac{\mathrm{d}V_{cyl}}{\mathrm{d}\theta}\mathrm{d}\theta \tag{4.50}$$

$$P_{ind,eng} = 4W_{ind,cyl}\frac{N_{eng}}{60 \cdot 2} \tag{4.51}$$

Next the two models for the combustion and thermodynamic efficiency are combined to one equation:

$$\eta_{comb}\eta_{th} = (s_1 + s_2\lambda)\left(s_3 + s_4(\omega_{eng} - s_5)^2\right) \tag{4.52}$$

Again, the mapped values are compared with the fitted model values in Fig. 4.12. The map predicts the values within $\varepsilon_{max} = 3.3\%$ with an average $\varepsilon_{mean} = 1.5\%$. The model has a maximum absolute relative error of $\varepsilon_{max} = 6.0\%$ and a mean absolute relative error of $\varepsilon_{mean} = 2.1\%$ and is therefore accurate enough to predict the indicated engine power. The detailed parameter fit are found in Appendix F.6.

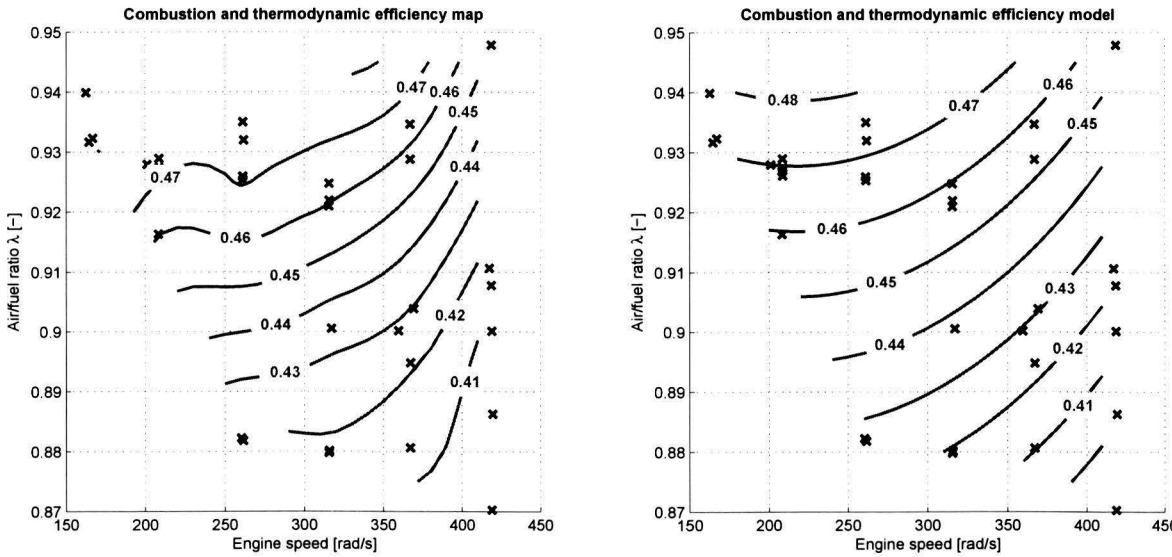

Figure 4.12: Model versus map for the term $\eta_{comb}\eta_{th}[-]$ under steady state conditions.

Friction and pumping torque loss

A model for total friction and pumping losses in terms of torque loss ($M_{loss}[Nm]$) is proposed before. In Fig. 4.13 this model is fitted to experimental steady state data and compared with a map which is fitted to the same dataset. It appears that the model could predict the trends in the losses but is not able to provide accurate results. Where the map gives results in $\varepsilon_{max} = 1.4\%$ and $\varepsilon_{mean} = 0.1\%$ the maximum relative absolute error of the model increases rapidly to $\varepsilon_{max} = 134.2\%$ at higher speed/load points. The mean absolute relative error of the model is $\varepsilon_{mean} = 20.3\%$, which is not accurate enough. More details about the relative errors for each operating points is given in Appendix F.7.

Engine inertia

The engine inertia $J_{eng}[kg \cdot m^2]$ could only be fitted on transients such that $\dot{\omega}_{eng} \neq 0$:

$$J_{eng}\dot{\omega}_{eng} = M_{eng} - M_{load} \tag{4.53}$$

An experiment is conducted where the road torque was kept constant and a step in throttle valve position was performed. By increasing the air mass flow and inherent the fuel mass flow (ECU control) the produced engine torque becomes larger then the load torque. As a result the $\dot{\omega}_{eng} > 0$

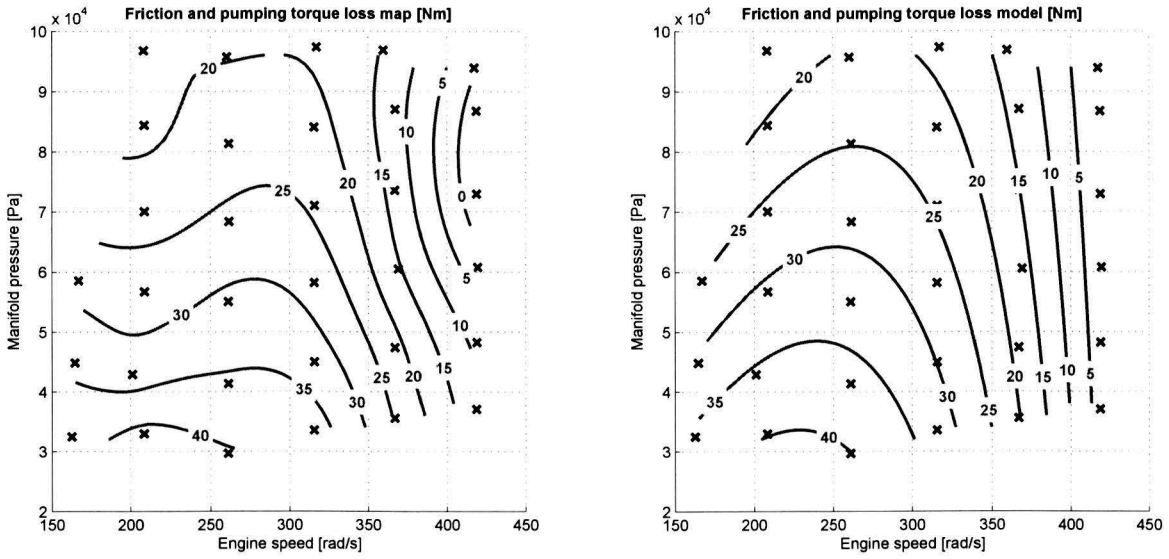

Figure 4.13: Model versus map for the friction and pumping torque loss under steady state conditions.

and then engine accelerates. The rate at which the engine accelerates is dependent on the inertia. The load also has an inertia but that is incorporated with the load torque at the crankshaft. Consequently, the load torque is also increasing resulting in a new engine operating point equilibrium. To provide stability in the model, the engine acceleration is damped at small torque differences. Since the exact produced engine torque is unknown, the inertia fit procedure also requires the model for engine torque. The fit results are shown in Fig. 4.14, where a value of $J_{eng} = 0.43[kg \cdot m^2]$ was found, which is lower then expected. This could be explained by the poor reliability of the transient load torque data due to neglected dynamic effects (i.e. CVT, torque converter, dyno torque control). Also dynamic engine friction and pumping loss and efficiencies are not considered, since there is too little transient experimental data available.

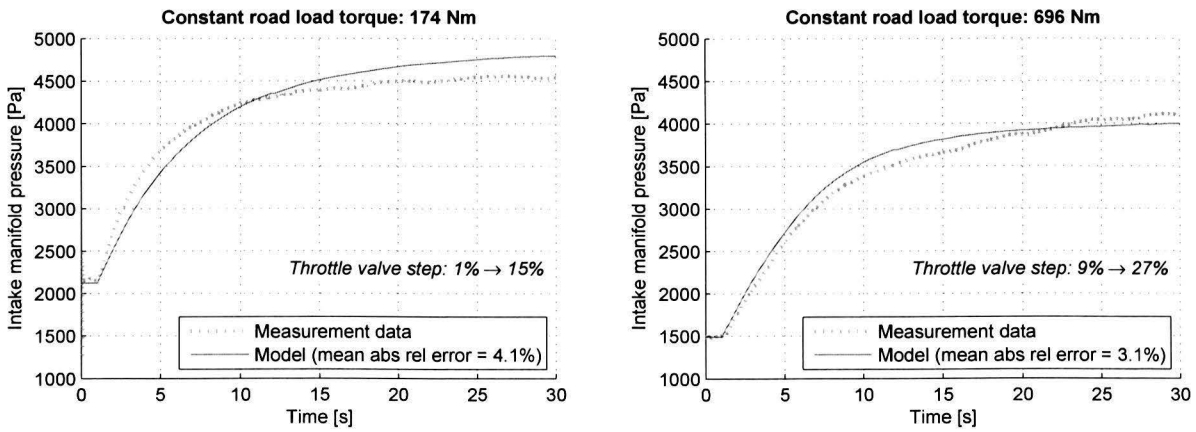

Figure 4.14: The fitted engine inertia on transient experiments

4.6 Model validation

The fitted submodels are now combined into one model as schematically presented earlier in Fig. 4.1. In Appendix E, a complete model overview is given in terms of the defined air system, fuel system and mechanical system.

An effective method to value the model accuracy is to validate the engine speed and manifold pressure transients. Therefore, the experimental results of two throttle valve step response transients and two turbine vanes step response transients are used to validate the constructed model. During those measurements the dynamometer load was kept constant. However, since the CVT efficiency is not constant, the actual engine torque output is not constant during the step response experiments. A combination of a simultaneous throttle valve and turbine vane step is not measured.

In Fig. 4.15 and Fig. 4.16 the transient experimental data is compared with the modeled transient response to a step in throttle valve position and a step in turbine vanes position respectively. The data set consist of two step responses at medium-high torque loads, which differ from the data set as used for parameter fitting. The model accuracy in terms of absolute relative errors with respect to the measured data is depicted in Table 4.2.

Although the values of the mean absolute relative errors suggest a fairly proper result concerning the model accuracy, a steady state error at the end of the transient is noticed. Especially the manifold pressure seems to deviate significantly at higher loads ($M_{road} = 522[Nm]$), where the modeled engine speed is lower than the experimentally obtained results. The manifold pressure is calculated using the static volumetric efficiency model, which already has a mean absolute relative error of $9.4[\%]$.
The model should be extended with respect to dynamic effects during combustion-to-torque (e.g. friction, efficiencies, CVT dynamics) and the air system (e.g. dynamic air flow characteristics), in order to further reduce the error during the transients.

The model needs initial conditions for the manifold pressure and engine speed. Ideally these states are found in maps as function of the input variables. However, it is difficult to predict the initial engine speed and manifold pressure both as function of throttle valve position, turbine vane position, torque load and ambient conditions. To further complicate the initial state estimation, the CVT efficiency is also speed dependent and therefore the initial brake torque load transfer through the CVT is very hard to predict.

Table 4.2: Transient step response model results: throttle valve versus turbine vanes steps

Step	**Road load**	**Engine speed**		**Manifold pressure**	
	$M_{road}[Nm]$	$\epsilon_{mean}[\%]$	$\epsilon_{max}[\%]$	$\epsilon_{mean}[\%]$	$\epsilon_{max}[\%]$
Throttle	$348[Nm]$	4.5	15.6	6.8	10.7
valve	$522[Nm]$	7.5	10.4	9.7	12.4
Turbine	$348[Nm]$	3.1	31.2	6.8	14.5
vanes	$522[Nm]$	7.5	10.3	15.7	19.9

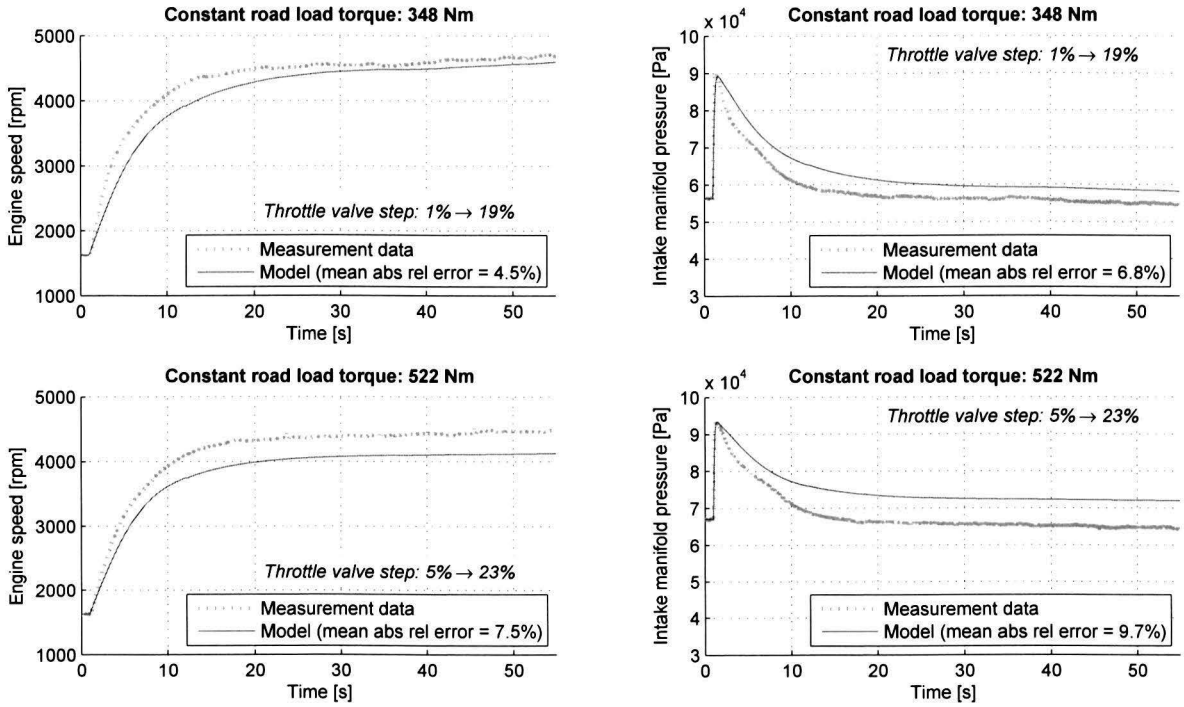

Figure 4.15: Transient throttle valve step response: model versus measured data for engine speed and intake manifold pressure. The turbine vanes are fully closed.

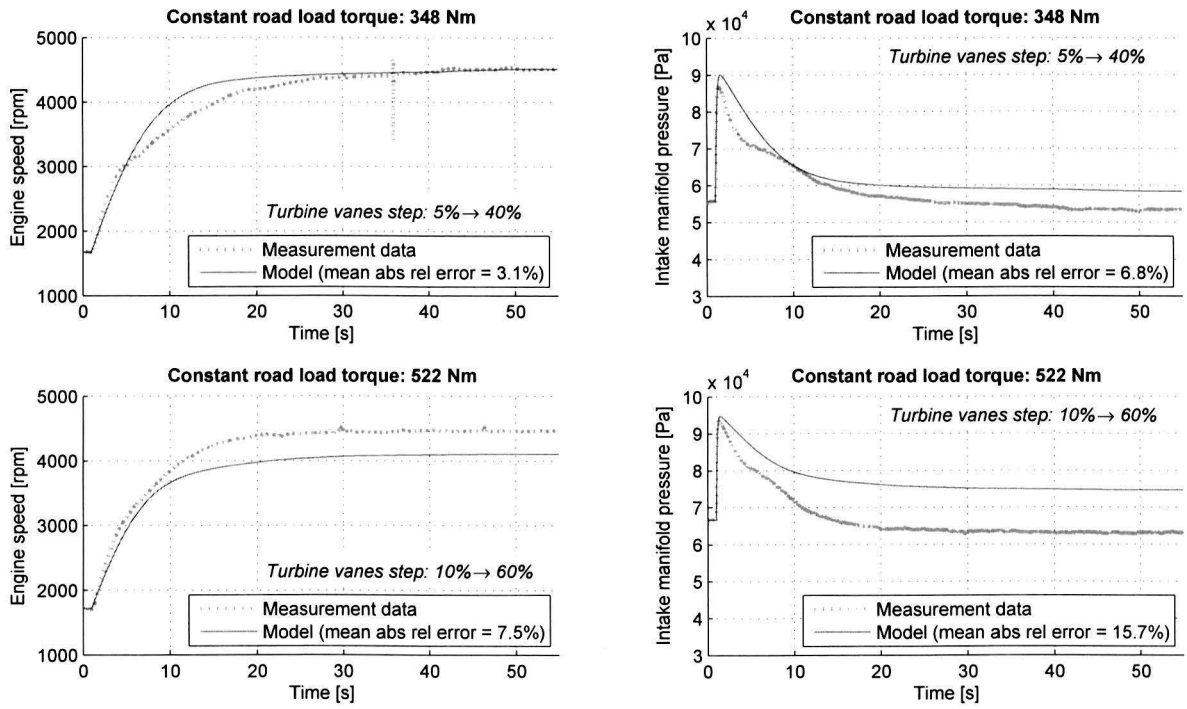

Figure 4.16: Transient turbine vanes step response: model versus measured data for engine speed and intake manifold pressure. The throttle valve is fully closed.

The model also predicts the fuel mass flow during transients. The model results are compared with the experimental data in Fig. 4.17 for both throttle valve and VGT transients. In the tested situations $\epsilon_{mean} < 10[\%]$, which means the model complies with the objective as stated in the beginning of this chapter.

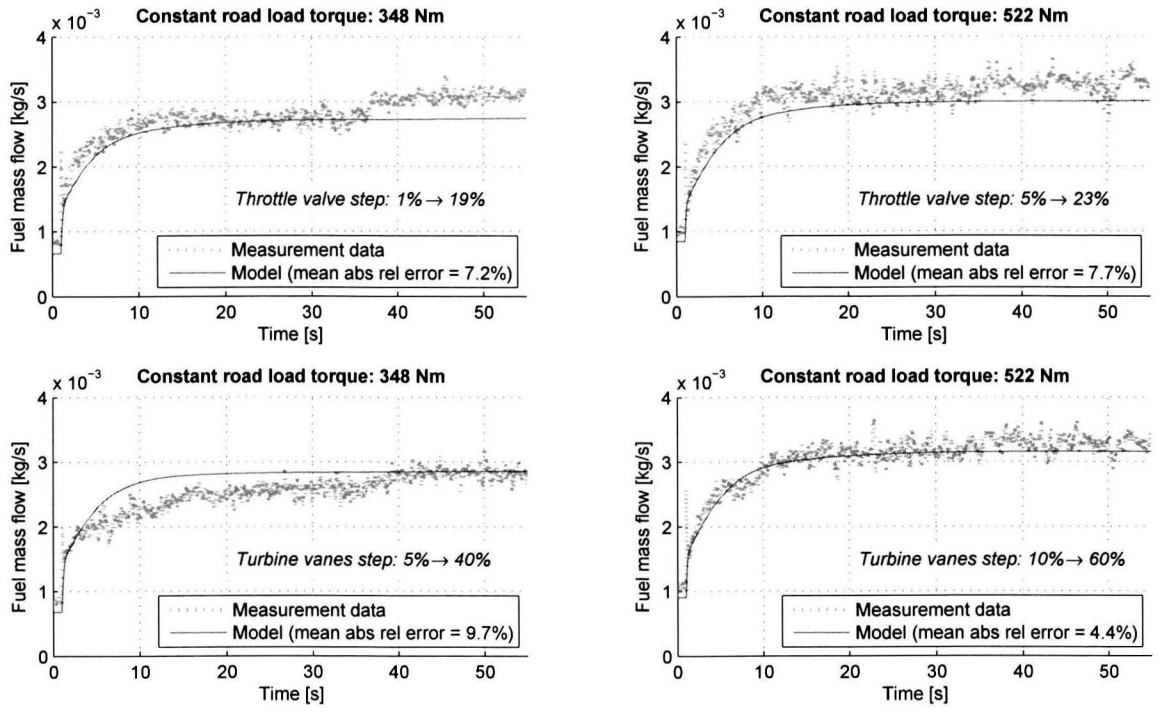

Figure 4.17: Transient throttle valve and turbine vanes step responses for the fuel mass flow

The computed potential turbine power from the experiments with the VGT is compared with the modeled potential turbine power in Fig. 4.18. The figure shows a significant mean absolute error for the lowest road load situation of $\epsilon_{mean} = 23.8[\%]$. The model does not meet the requirements regarding the turbine power during transients. A plausible cause for the fairly large deviation is found in the manifold submodel, since the computation of the turbine power is dependent on both temperature and pressure. In fact, the experimental data is computed the same way, only with the measured temperature and pressure.

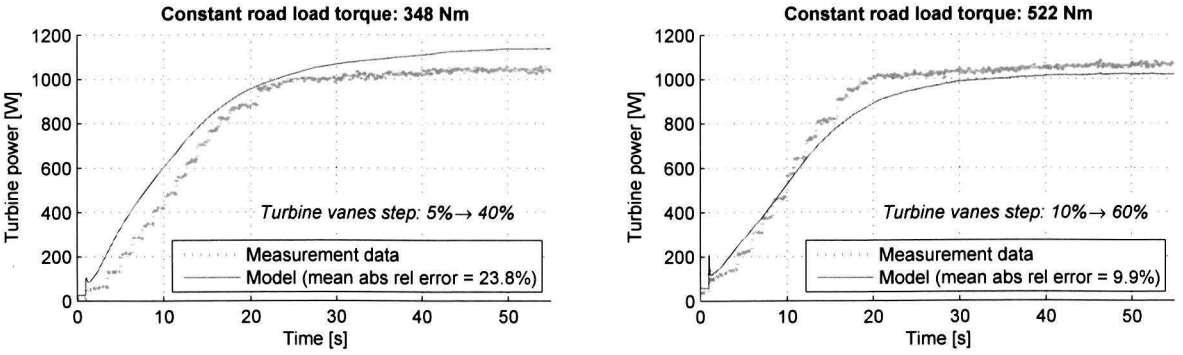

Figure 4.18: Transient turbine vanes step responses for potential turbine power

4.7 Modeling chapter summary & discussion

The model is proposed, fitted and validated in this Chapter. The model consists of seven submodels which are all fitted separately before being merged into one model. Steady state experimental data was used to fit various parameters to account for the VGT temperature, the VGT air mass flow, the throttle valve discharge coefficient and effective opening area, the ECU λ control signal, the friction and pumping torque loss and the volumetric, thermodynamic and combustion efficiencies. The manifold volume and the engine inertia parameters were fitted using two transient measurements. The fuel delivery delay and the ECU ignition influence on the combustion process where discarded for simplicity.

The model parameters where fitted by minimizing the objective function. A performance criterium for the model was set by demanding $\epsilon_{mean} < 10[\%]$. This criterium was met when evaluating the model output in terms of engine speed and manifold pressure on a different set of transient experiments. The turbine power exceeded this criterium with a maximum ϵ_{mean} of $23.8[\%]$. This is likely to be caused by the relatively poor volumetric efficiency model.

It is recommended to further extend the model with an initial condition estimator for $p_{man}[Pa]$ and $\omega_{eng}[rad/s]$. Also the effects of using the throttle valve and the turbine vanes simultaneously during transients is an interesting topic for further research.

Chapter 5

Control strategy

5.1 Control objective

The main objective of this research is twofold since fuel consumption reduction is often contradictory to performance. Therefore, the control objective is split in two parts in order to develop a proper control strategy. First, the control strategy of the fuel consumption reduction of WEDACS during steady state operation is discussed. Next, the dynamic engine response with WEDACS is investigated.

Fig. 5.1 shows an overview of the engine model and the engine control situation with respect to the throttle pedal input by the driver. The engine control is subdivided into WEDACS control and ECU control. The ECU control signals for fuel injection u^*_{inj} and spark timing u^*_{ign} are not externally controlled or bypassed in the test setup and therefore the ECU functions are already included in the MVM.

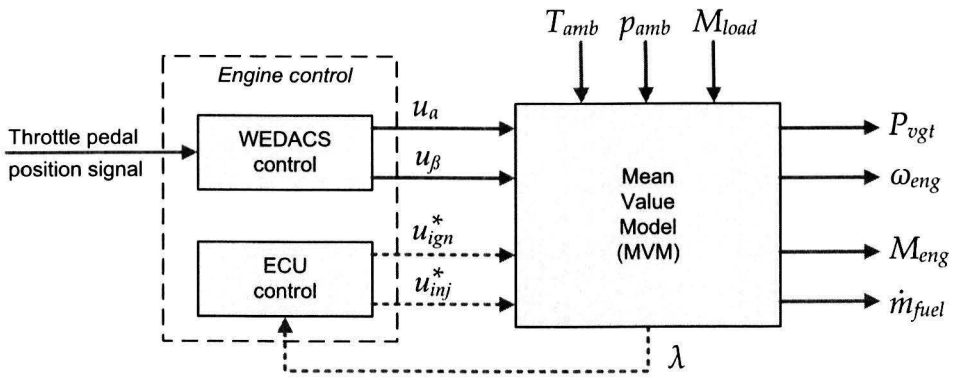

Figure 5.1: Engine control with respect to the mean value model. The ECU control functions are included in the MVM.

5.2 Control strategy

5.2.1 Steady state WEDACS control strategy

A steady state WEDACS operating map is built to relate the reference throttle valve position $\phi[\%]$ to the control signals u_i for both the turbine vanes β and throttle valve α position. In Fig. 5.2 the relation between original throttle valve position and WEDACS positions is shown for various engine speeds. It appears that the position is independent of engine speed. This map is based on maximum usage of the turbine, i.e. the throttle valve remains closed until the turbine vanes are fully opened. The solid green line relates the reference position to the turbine vanes position. Up to a reference position of $\phi = 39[\%]$, the turbine is able to control the engine without assistance of the throttle valve. From $\phi > 39[\%]$ the throttle valve opens for assistance since the vanes are fully opened ($\beta = 100[\%]$). The original cable operated throttle valve position is correlated with the throttle pedal position, so the horizontal axis of the figure could also be interpreted as throttle pedal position. However, regarding aftermarket WEDACS adaptation it is more convenient to control the WEDACS using existing throttle valve inputs from for instance the ECU.

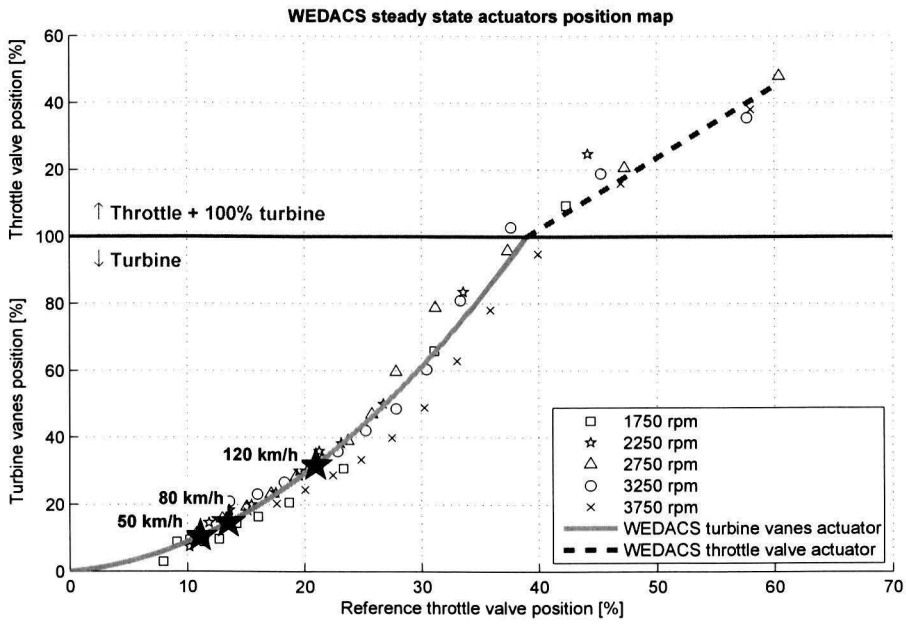

Figure 5.2: Steady state WEDACS control map dependent on reference throttle valve position

A WEDACS power map is constructed in Fig. 5.3, where the power is dependent on turbine vanes position and engine speed. In general, the power increases for increasing engine speeds. For each engine speed isoline there exists a maximum potential WEDACS power, indicated by the thick dotted line. As already mentioned by J.R. Serrano [2008], the VGT is most efficient when the vanes are opened near halfway. The maximum value occurs roughly between $\beta = 30 - 50[\%]$, which suggests to assist with the throttle valve from that point on. However, one should take the influence of the pressure drop into account here. In general, the engine speed isolines represent an increasing pressure ratio when following the line from left to right. This is also shown in Fig. 5.4 where a map for pressure ratio under the same conditions is given. Here, the same

maximum potential WEDACS power line is given. It is concluded that for every engine speed there exists an optimal pressure ratio at which the potential power is at maximum.

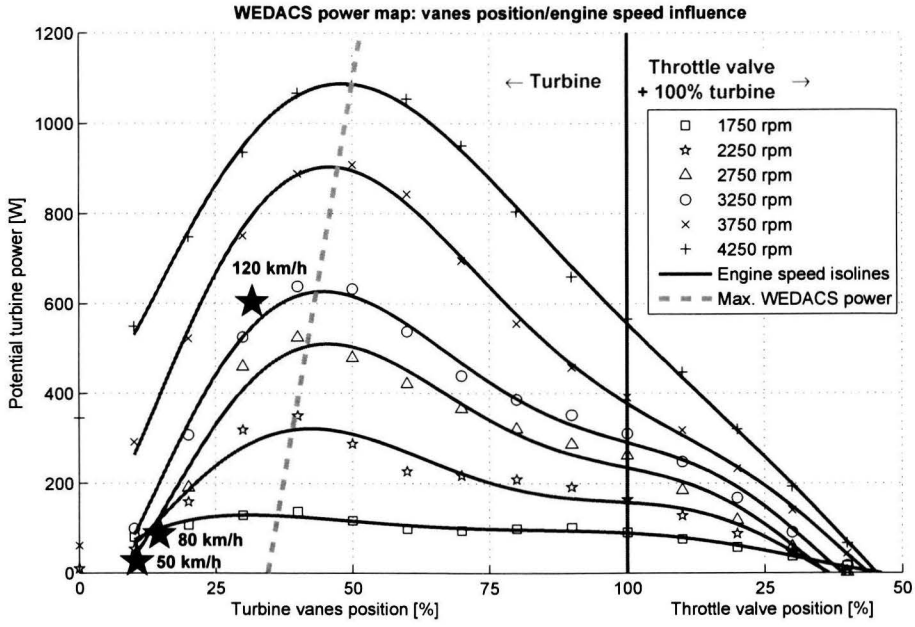

Figure 5.3: Steady state power map dependent on WEDACS position and engine speed

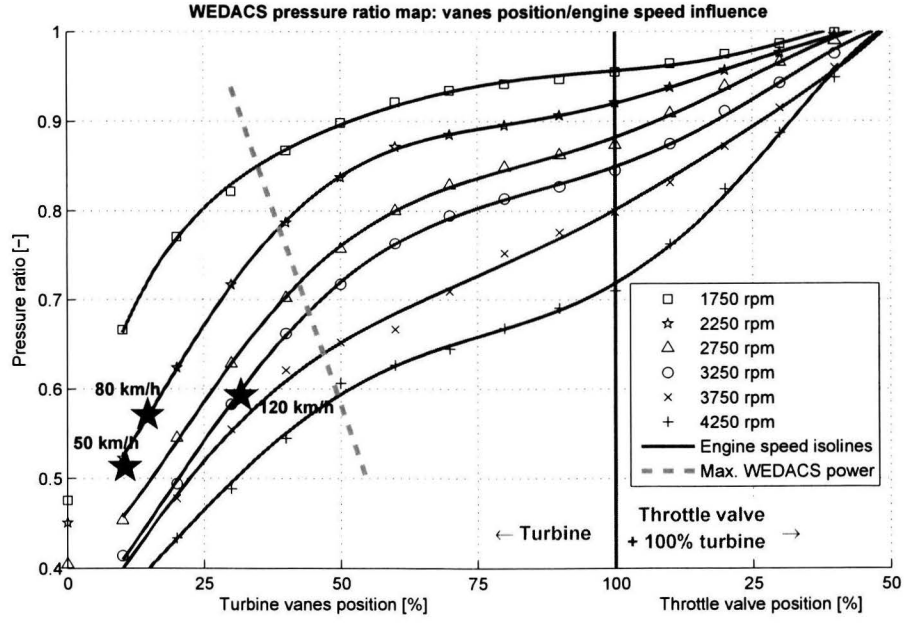

Figure 5.4: Steady state pressure ratio map dependent on WEDACS position and engine speed

In both Fig. 5.3 and Fig. 5.4 the constant vehicle speeds of $50 - 80 - 120[km/h]$ are indicated. It appears that the maximum power at the corresponding engine speeds is not reached yet. Investigating downsizing of the turbine geometry is an interesting topic here. Although it might

reduce the absolute maximum turbine power, the potential could be utilized more efficiently. This was also the case in the research described in Lino Guzzella and Auckenthaler [2004], who investigated a similar turbine concept as used in WEDACS.

The maximum potential WEDACS power line is plotted in an engine speed/torque map in Fig. 5.5. Here, the poor VGT efficiency at $50 - 80[km/h]$ is again clearly visible. The squared markers in the figure are obtained from Fig. 5.3.

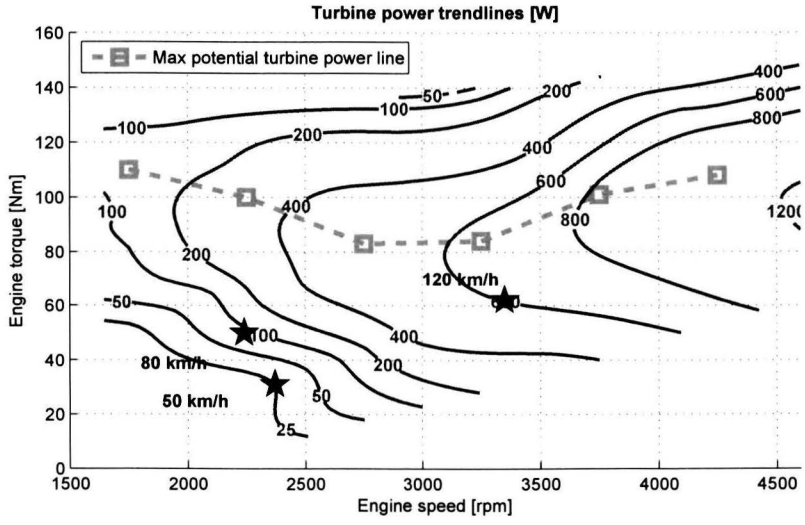

Figure 5.5: WEDACS maximum potential power line

5.2.2 Steady state results

The commonly used New European Driving Cycle (NEDC) trajectory is now plotted in the WEDACS power map in Fig. 5.6. The trajectory concentrates around $50-80-120[km/h]$ in lower speed/load part of the engine operating area. In fact, the throttle valve is not necessary at all since the turbine vanes opening will not exceed $50[\%]$ as shown in the same graph.

During the NEDC cycle the cumulative fuel mass is calculated. Therefore the NEDC vehicle speed trajectory is converted to a engine torque and speed trajectory (resp. $M_{eng,NEDC}(t)$ and $N_{eng,NEDC}(t)$). These trajectories are then projected on a fuel mass flow map obtained from experimental data.

The fuel saving when using WEDACS is estimated by extracting the turbine power from the engine power. This results in a lower torque demand from the engine $M_{eng,NEDCw}(t)$:

$$N_{eng,NEDCw}(t) = N_{eng,NEDC}(t) \tag{5.1}$$

$$M_{eng,NEDCw}(t) = M_{eng,NEDC}(t) - \frac{P_{vgt,NEDC}}{N_{eng,NEDCw}(t)} \tag{5.2}$$

As a result $2[g]$ of fuel mass is saved during the $20[min]$ drive cycle, which equals $0.33[\%]$. However, one should consider the inaccuracies of the engine torque calculation and the steady state fuel map which influence the fuel consumption calculation. In Appendix C.2 the fuel mass flow

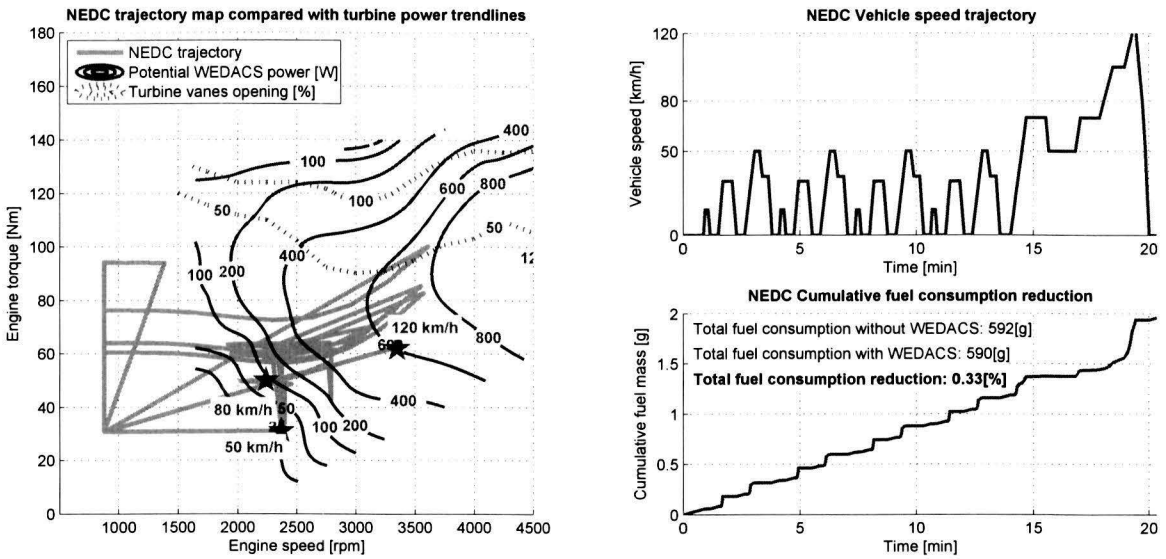

Figure 5.6: Expected NEDC drive cycle results

map is given with an average mean absolute error of $0.6[\%]$.

During the cycle a distance of approximately $11[km]$ is traveled and €0.005 is saved when assuming a fuel consumer price of €1.75. This results in a total saving of €8.90 per year when driving $20000[km]$ annually.

If a significant part of the annually driven kilometers was performed on a highway, then the savings would increase rapidly. As indicated earlier the potential turbine power at $120[km/h]$ will be $605[W]$. The financial benefit is estimated to be €0.0022 per km. Then $20000[km]$ on a highway would result in a saving of €44 in total.

5.2.3 Dynamic WEDACS control strategy

The main goal of transient engine response is not to maximize turbine power since an average drive cycle remains in steady state points more often. What is important, is to maintain the reference comfort/performance level in terms of engine speed/torque response. The driver should not notice the presence of WEDACS during transients.
Both WEDACS actuators are positioned to the desired setpoint using the PID controlled Woodward rotational actuators with friction compensation. By assuming a perfect position control of the actuator position to any setpoint, the control strategy is now focussed on feedforward control as function of throttle pedal position.
To compare transient engine response between throttle valve and turbine vanes various step responses have been performed. For both situations similar engine operating points are chosen for the comparison. The accompanying WEDACS actuator setpoints for both the throttle valve and turbine vanes are obtained from the steady state actuator position map in Fig. 5.2.

5.2.4 Dynamic results

Effective variables to compare the engine performance between throttle valve and VGT, are the engine speed and manifold pressure profiles during transients. Four sets of equal transient experiments have been performed. Each set consists of one throttle valve step transient and one comparable VGT step transient under fixed road load torque conditions. The experimental results of the engine speed and manifold pressure transients are shown in Fig. 5.7 and Fig. 5.8.

To analyse the engine performance, the difference between measured variables x_i for both the throttle valve and the turbine transients is specified in terms of mean absolute relative difference $\Delta_{mean}[\%]$. The mean absolute relative difference is defined as:

$$\Delta_{mean} = \frac{1}{n}\sum_{i=1}^{n} \left| \frac{[x_i]_{vgt} - [x_i]_{valve}}{[x_i]_{valve}} \right| \tag{5.3}$$

where the $[.]_{valve}$ brackets indicate the throttle valve step experiments and $[.]_{vgt}$ are the VGT measurements. The results for engine speed and manifold pressure are shown in Table 5.1.

Table 5.1: Transient response experiments results: throttle valve versus turbine vanes steps

Road load	**Engine speed**		**Manifold pressure**	
$M_{road}[Nm]$	$\Delta_{mean}[\%]$	$\Delta_{max}[\%]$	$\Delta_{mean}[\%]$	$\Delta_{max}[\%]$
$174[Nm]$	4.2	68.3	1.7	30.2
$348[Nm]$	6.1	14.2	2.5	14.9
$522[Nm]$	1.4	7.1	2.2	4.6
$696[Nm]$	1.7	7.8	1.4	4.0

The experimental results show that a change in performance will not be noticed by the driver during transients, since the mean relative difference is small. The engine response to a step input on the turbine vanes equals a throttle valve step response. The limited airflow through the turbine results in a limited engine operating range. Only at higher engine speeds/loads the throttle valve is necessary.

The WEDACS potential electric power during the transient experiments was not measured directly. Instead thermodynamic relation Eq. (3.12) was used. This relation is based on the temperature drop over the turbine and does not incorporate dynamics of the turbine shaft. $P_{vgt}[W]$ is therefore an indication of the maximum potential power for this turbine. The cumulative potential recovered energy at the end of the transient is calculated using:

$$Q_{vgt} = \int_{t_{start}}^{t_{end}} P_{vgt} \mathrm{d}t \tag{5.4}$$

During the four transients of $50[s]$ between $22.9[kJ]$ and $43.2[kJ]$ could be recovered depending on the road load. The turbine power transient results are shown in Fig. 5.9.

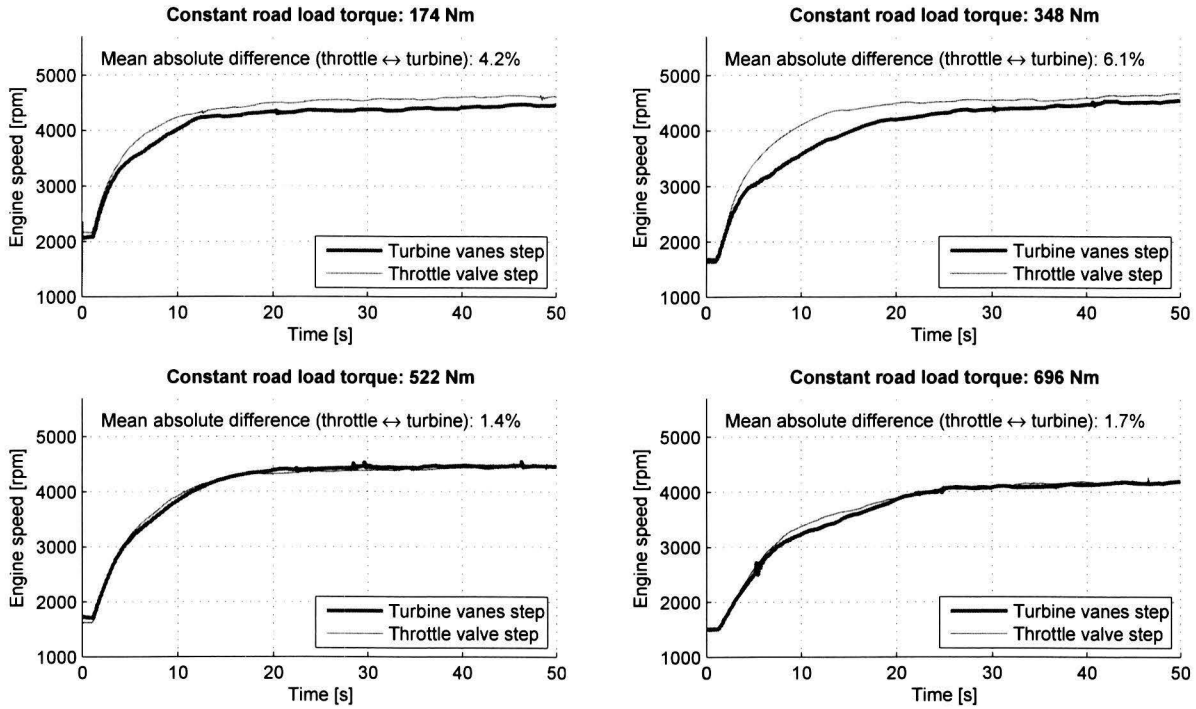

Figure 5.7: Dynamic step response WEDACS vs throttle valve: engine speed

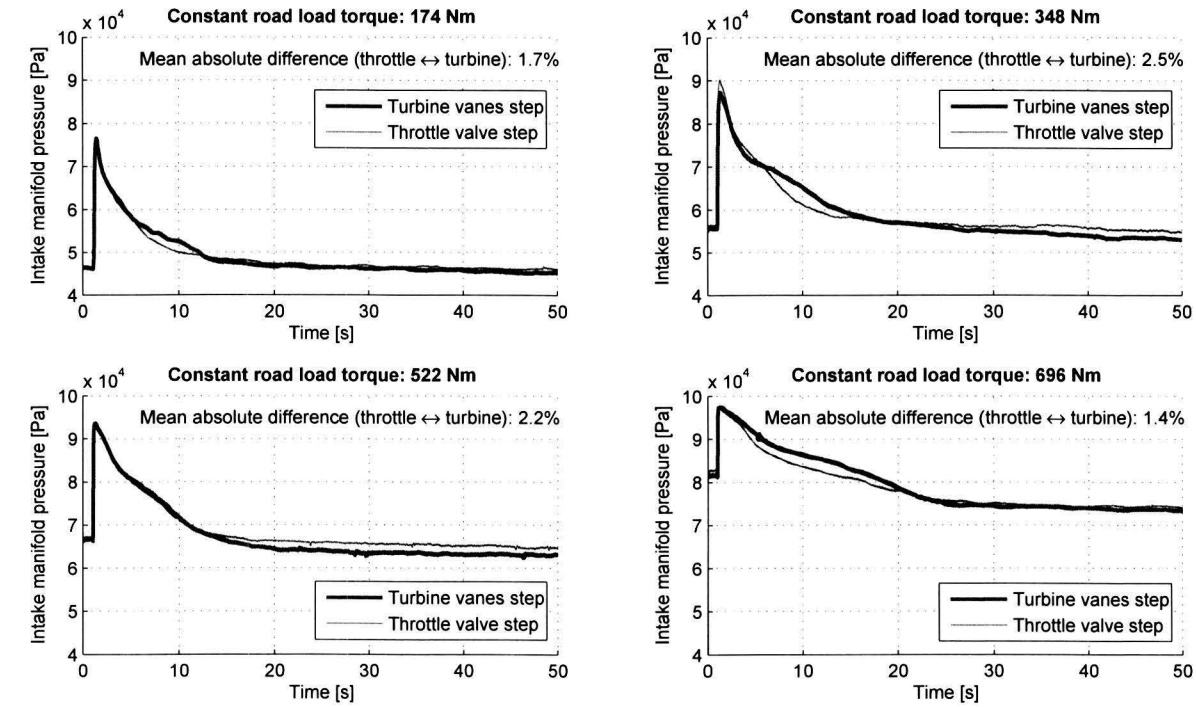

Figure 5.8: Dynamic step response WEDACS vs throttle valve: manifold pressure

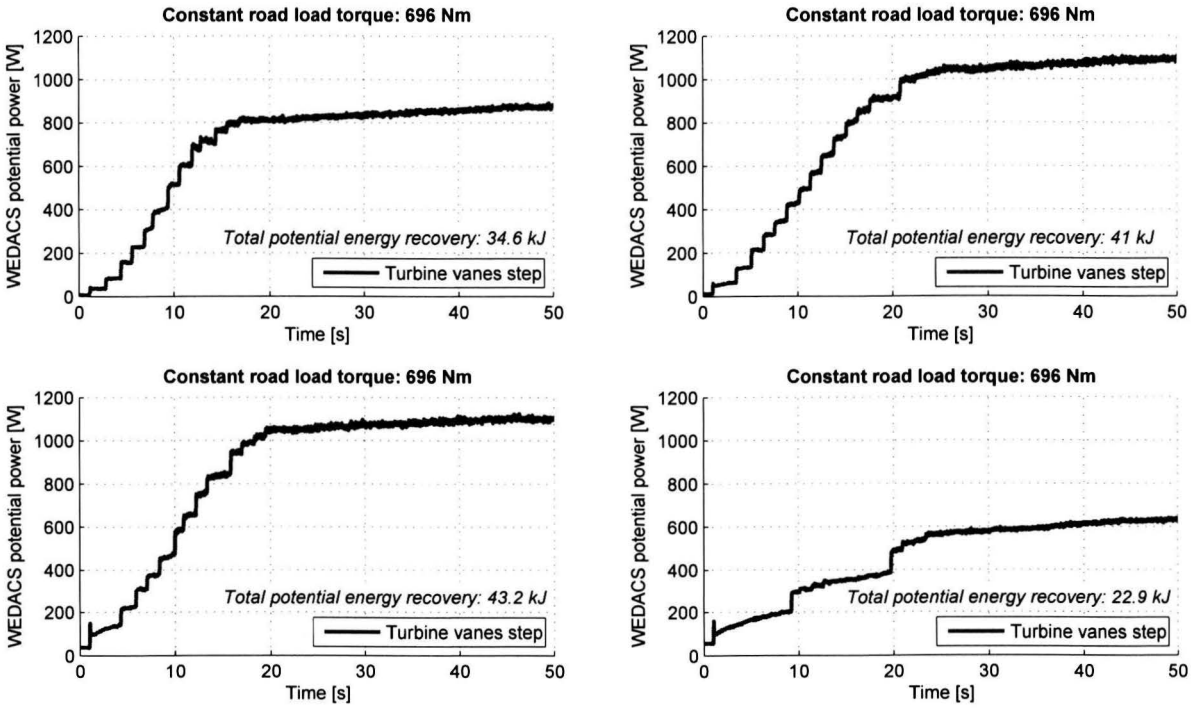

Figure 5.9: Dynamic step response WEDACS: recovered power by turbine

5.3 Control strategy chapter summary & discussion

In the introduction of this research the control objective was formulated to optimize the fuel consumption reduction while retaining the engine performance and throttle pedal response. Therefore the control strategy was split in a steady state control and a dynamic control strategy. Experiments have shown that WEDACS is capable of providing an equal engine step response when the steady state obtained operating map is used in during transients.

Steady state operating maps show that the turbine vanes position is independent of engine speed. The reference throttle valve position is used to define setpoints for the WEDACS actuator positions for throttle valve and turbine vanes. The WEDACS throttle valve assists the turbine at higher air mass flows. However, it appears that for common steady state driving situations ($50 - 80 - 120[km/h]$) the turbine vanes position will not exceed $32[\%]$.

Experimental data has shown that the maximum turbine power occurs when the vanes are opened halfway, at a certain pressure ratio. Since the vanes are opened only $10 - 15[\%]$ at $50 - 80[km/h]$ the efficiency of generating power rapidly decreases. For this reason, WEDACS produces most power at $120[km/h]$. It is highly recommended to investigate downsizing of the turbine. Although downsizing would decrease the maximum potential turbine power the turbine might operate more efficiently. This might have a greater fuel saving effect, since the WEDACS control strategy options are limited in the present situation.

A NEDC drive cycle trajectory has been projected on the steady state fuel consumption map. When utilizing the turbine alone, the vanes position will not exceed $50[\%]$ during the cycle. The resulting fuel consumption reduction is minor, with an estimated $0.33[\%]$. At $20000[km]$ per year only €8.90 is saved on fuel based on the NEDC drive cycle pattern. When driving $20000[km]$ on highways up to €44 could be saved, which equals a fuel reduction of $1.63[\%]$. In order to be financially economic the WEDACS system must be cheap in both manufacturing and installation. Due to the fairly low fuel consumption reduction, WEDACS will not be suitable as an aftermarket product when using the presented turbine. However, further research may increase the effective power generation making WEDACS a throttling system worth investigating for usage by car manufacturers.

In the expected results the potential power is presented. The actual generated power will be lower due to energy conversion efficiencies from turbine to ready-to-use electrical power. Although the expected generator efficiency will be high in the order of $80 - 90[\%]$ variations will occur between power supply and power demand. To overcome the differences the car battery is to be used as a buffer, introducing additional losses in energy transfer and storage. The electric power generation as function of time could be another control parameter in future research.

Transient experiments show little to no lag when using the turbine instead of the throttle valve. The main goal of transient engine response is not to maximize turbine power but to maintain the reference comfort/performance level in terms of speed/torque response. Therefore the engine speed trajectory during a step from under similar road load and ambient conditions is compared between throttle valve and turbine vanes steps. The measured average relative difference between the two trajectories was found between $1.4[\%]$ and $6.1[\%]$.

Chapter 6

Conclusions and recommendations

6.1 Conclusions

The research objective in this report was to develop a transient engine model in order to simulate the WEDACS performance with respect to the reference situation without WEDACS. Furthermore a control strategy was to be found to optimize the implementation of WEDACS in terms of maximizing the fuel consumption reduction while retaining engine performance and throttle pedal responses. To finish this report the following is concluded:

- The greatest challenge in order to reduce the fuel consumption in an SI engine is to recuperate the throttling losses. WEDACS consists of a variable geometry turbine (VGT) which combines the throttling action (adjustable vanes) with electric power generation using an alternator. For high engine speed/load points a throttle valve bypass completes the WEDACS system.

- The complete engine is modeled using the Mean Value Model approach on the different engine submodels. Experiments have been performed to fit the submodels and validate the complete engine model. The model could be improved with a suitable initial conditions estimator for manifold pressure and engine speed. The model is able to predict transient engine speed and manifold pressure below a mean relative deviation of $15.7[\%]$ compared to the validation experiments.

- The experimental setup was calibrated prior to the experiments in order to provide reliable results. Due to a malfunctioning torque sensor an uncertainty of at least $7[\%]$ is introduced in the engine torque results. The experiments show a potential throttle loss recovery between 3 and $50[\%]$ under steady state driving conditions at 50 and $120[km/h]$ respectively. Under steady state driving at $50 - 80 - 120[km/h]$ the vanes are only opened at $10 - 15 - 32[\%]$ respectively. The relatively low throttling loss recovery at low engine speed/loads is due to the low efficiency of the turbine when the vanes are almost closed or fully opened. Therefore, most fuel is saved on highways. At $120[km/h]$ $2.8[\%]$ of engine power could be obtained from WEDACS, when the turbine power generation efficiency is $100[\%]$. The turbine in this research is not used at its full potential and is therefore not optimal for this case.

- The influence on the dynamic engine response using WEDACS is negligible compared to the reference situation. Therefore the control objective is focussed towards steady state

fuel consumption reduction. Feedforward control is used to define the WEDACS actuator setpoints as function of the throttle valve position of the reference situation. This strategy projected on a NEDC drive cycle and $0.33[\%]$ fuel consumption reduction is expected.

- The WEDACS system in the present situation is therefore not suitable for the aftermarket. Only when the effective power generation is increased together with low manufacturing costs WEDACS might be interesting for car manufacturers. To obtain a higher fuel consumption reduction the VGT needs to be optimized by matching the turbine efficiency to commonly used engine operating points. Downsizing the turbine should be considered here.

6.2 Recommendations for future work

During the research several interesting topics for further research were born.

- It is wise to investigate downsizing of the turbine. The vanes positions should be around $50[\%]$ near the turbine peak potential power location when driving under steady state conditions. Another possible improvement would be the VGT vane geometry in terms of flattening the turbine power curve to a more equal power range with respect to the turbine vanes position. Otherwise, shifting the maximum potential turbine power peak more towards a smaller vane opening is an interesting topic. One could also think of two turbines in parallel: a small turbine optimized at the $50 - 80[km/h]$ range and one for $120[km/h]$ with a higher power output.

- The VGT used in this research was modified in order to reduce the air leakages under fully closed conditions. The design of the vanes mechanisme should be revised to further reduce the leakage. In the present conditions it is not possible to run the engine below $1700[rpm]$ at little to no load at the crankshaft. Tests with the WEDACS prototype also showed a considerable oil leakage caused by the VGT bearings oil circuit. The influence of oil spill in the intake manifold was not investigated but should obviously be avoided and taken into account for further development of WEDACS. The VGT used here was designed to withstand the extremely high exhaust temperatures ($> 850^oC$) which occur in a normal passenger car. For the purpose in this research the temperatures will be below ambient temperature. This yields opportunities in using low cost, light materials to manufacture a customized and cheaper VGT.

- The IACV/AAC valve air mass flow should be minimized in the setup. This would result in a larger turbine air mass flow and consequently more potential turbine power. When the ECU control with respect to the IACV/AAC valve cooperates with WEDACS, the IACV/AAC valve might be eliminated.

- The cold air could be utilized to cool the intake manifold. This (isolated) intake manifold could act as an intercooler, cooling down the air mass flow into the cylinders. Since cold air has a higher density, the volumetric efficiency increases which enables a higher maximum engine power. One could think of engine downsizing possibilities. However, the effect on engine emissions using WEDACS is not investigated in this research. One could imagine that the cold air might reduce the burning speeds in the combustion chambers creating more hydrocarbon emissions. Slower burning speeds also lower the thermodynamic efficiency since most contribution to piston work occurs just after top dead center.

- The proposed control strategy could be extended with simultaneous throttle valve and turbine vanes actuation. This becomes necessary when downsizing the turbine. Furthermore, the pedal velocity could be taken into account to further extend the control strategy in terms of driver comfort. Therefore the implementation of the mean value engine model becomes important. The proposed control strategy in this research should be extended in terms of disturbance rejection and stability. It is interesting to investigate cooperation with the standard ECU to expand the control strategy with combustion control.
- The model could be examined in terms of parameter sensitivity. This could eventually result in a more stable model by adding weighting factors in the optimization algorithm during the parameter fitting.
- The concept of using a turbine to generate power using existing pressure drops could be extended to the exhaust manifold or might even coexist with the mentioned alternatives such as direct injection.
- The turbine speed influence was not taken into account in this research. The effects when using a generator to extract power from the rotating turbine shaft are therefore unknown at this point. The power generation by the alternator could also be a control input. The effect of the turbine shaft inertia on energy recovery and transient engine response is also unknown.

Bibliography

AutoWeek. Carbase. `http://www.autoweek.nl/carbase.php`, July 2011.

Alberto A. Boretti. Use of variable valve actuation to control the load in a direct injection, turbocharged, spark-ignition engine. *SAE Powertrains Fuels & Lubricants Meeting*, (2010-01-2225), October 2010.

Yunus A. Çengel and Michael A. Boles. *Thermodynamics, an engineering approach.* McGraw-Hill, fourth edition edition, 2002.

Michael Grimmer Darrell Robinette and Randall Beikmann. Dynamic torque characteristics of the hydrodynamic torque converter. *SAE Int. J. of Passeng. Cars Ű Mech. Syst.*, (2011-01-1540): 1023–1032, 2011.

DynamometerWorld. Eddy Current Performance Specifications. `http://www.dynamometer-world.com/index.php?option=com_content&view=article&id=67&Itemid=74`, July 2011.

M.-C. Lai F. Zhao and D.L. Harrington. Automotive spark-ignited direct-injection gasoline engines. *Progress in Energy and Combustion Sience*, pages 437–562, 1999.

Lino Guzzella and Christopher H. Onder. *Introduction to Modeling and Control of Internal Combustion Engine Systems.* Springer, 2010.

E. Hendricks. Isothermal vs. adiabatic SI engine mean value engine models. *3rd IFAC Advances in Automative Control, Karlsruhe, Germany*, pages 363–368, 2001.

John B. Heywood. *Internal Combustion Engine Fundamentals.* McGraw-Hill, 1988.

H. Cohen P.V. Straznicky H.I.H. Saravanamuttoo, G.F.C. Rogers. *Gas Turbine Theory.* Pearson Prentice Hall, sixt edition edition, 2009.

Prof. Bengt Johansson. Lecture: The path to high fuel efficiency and low emission with partially premixed combustion, ppc. 2011.

V. Dolz A. Tiseira C. Cervello J.R. Serrano, F.J. Arnau. A model of turbocharger radial turbines appropiate to be used in zero- and one-dimensional gas dynamics codes for interal combustion engines modelling. *Energy Conversion and Management*, pages 3729–3745, 2008.

José Carlos Zavala Jurado. *Engine modeling and control for minimization of hydrocarbon coldstart emissions in SI engine.* University of California, Berkeley, 2007.

Rob Karmiggelt. Mean value modelling of a MB A-class S.I. Engine. Master's thesis, Eindhoven University of Technology, March 1999.

R.G. Nitschke K.J. Patton and J.B. Heywood. Development and evaluation of a performance and efficiency model for spark-ignition engines. 89:1441–1461, 1989.

T. Fickenscher L.A. Smith and R.P. Osborne. Engine breathing - steady speed columetric efficiency and its validity under transient engine operation. *Internal Congress and Exposition, Detroit, Michigan*, March 1999.

David Bouquain Daniel Hissel Marie-Cècile Pèra Jean-Marie Kauffmann Laurent Bertoni, Hamid Gualous. Hybrid auxiliary power unit (apu) for automotive applications. *Vehicular Technology Conference*, pages 1840–1845, 2002.

Thomas Fluri Roberto De Santis-Christopher Onder Lino Guzzella, Michael Betschart and Theophil Auckenthaler. Recuperative Throttling of SI Engines for Improved Fuel Economy. *SAE World Congress & Exhibition*, (2004-01-0514), March 2004.

Helen Liu. Fuel component effects on hydrocarbon emissions from a spark-ignition engine. Master's thesis, Massachusetts Institute of Technology, June 1998.

Lars Malcolm Pedersen Bo Bernhardsson Magnus Gäfvert, Karl-Erik Årzén. Control of GDI engines using torque feedback exemplified by simulations. *Control Engineering Practice*, pages 165–180, 2004.

Keith Glover Nick Collings Urs Christen Merten Jung, Richard G. Ford and Michael J. Watts. Parameterization and Transient Validation of a Variable Geometry Turbocharger for Mean-Value Modeling at Low and Medium Speed-Load Points. *SAE Powertrain & Fluid Systems Conference & Exhibition*, (2002-01-2729), October 2002.

John J. Moskwa. *Automotive Engine Modeling for Real Time Control.* PhD thesis, Massachusetts Institute of Technology, May 1988.

NissanMotorCoporation. *Nissan Manual EC-SR.*

Alper Tolga Calik Osman Akin Kutlar, hikmet Arslan. Methods to improve efficienncy of four stroke, spark ignition engines at part load. *Energy conversion and Management*, pages 3202–3220, 2005.

C.C.M. Luijten R.H.L. Eichhorn, M.D. Boot. Waste Energy Driven Air Conditioning System (WEDACS). *SAE Int. J. Engines*, 2:477–492, 2009.

Daniel Sandoval and John B. Heywood. An improved friction model for spark-ignition engines. March 2003.

K. Iida M. Murakami K. Akishino T. Kume, Y. Iwamoto and H. Ando. Combustion control technologies for direct injection SI engine. *SAE Technical paper*, (960600), 1996.

Paul Tan. How does Variable Turbine Geometry work? `http://paultan.org/2006/08/16/how-does-variable-turbine-geometry-work/`, August 2006.

Johan Wahlström and Lars Eriksson. Modeling of a diesel engine with VGT and EGR including oxygen mass fraction. Master's thesis, Linkopings Universiteit, Sweden, September 2006.

Tim White. Knock, knock - part 1. *AutoSpeed*, November 2008.

A. van Scherpenzeel W.J. Gorter, H. Mulder. Motorproefstand TR3 TU/e. Master's thesis, Hogeschool Drenthe/Technische Universiteit Eindhoven, 2003.

Appendix A

Nomenclature

Table A.1: List of used symbols

Symbol	**Definition** [*unit*]
α	Throttle valve angle [%]
β	VGT vane position [%]
Δ	Relative absolute deviation [%]
ε	Relative absolute error [%]
κ	Ratio of specific heat for air [−]
λ	Ratio of actual air fuel ratio to stoichiometry [−]
η	Efficiency [−]
Π	Pressure ratio [−]
ϕ	Reference throttle valve position [%]
ω	Angular velocity $[rad/s]$
$\dot{\omega}$	Angular acceleration $[rad/s^2]$
θ	Crankshaft angle position $[^oCATDC]$
μ/μ_0	Engine oil viscosity ratio [−]
ζ	Humidity $[mg/l]$
A	Area $[m^2]$
B	Cylinder bore $[mm]$
c_d	Throttle valve discharge coefficient [−]
c_p	Specific heating value of air $[J/(kg \cdot K)]$
C_{ff}	Valvetrain cam follower constant [−]
C_{rf}	Valvetrain cam flat roller constant [−]
C_{oh}	Valvetrain cam oscillating hydrodynamic constant [−]
C_{om}	Valvetrain cam oscillating mixed constant [−]
D_b	Bearing diameter $[mm]$
h	Heat transfer coefficient $[W/(m^2 \cdot K)]$
i	Ratio [−]
J	Inertia $[kg \cdot m^2]$

Symbol	Definition [*unit*] (***cont'd***)
K_{vgt}	VGT choke exponent [−]
L_b	Bearing length $[mm]$
L_{st}	Stoichiometric air/fuel ratio [−]
L_v	Latent heat of condensation $[kJ/kg]$
$\dot{m}$	Mass flow $[kg/s]$
m	Mass$[kg]$
M	Torque $[Nm]$
N	Angular speed $[rpm]$
n_{cyl}	Number of cylinders [−]
n_b	Number of bearings [−]
n_v	Number of valves [−]
P	Power $[W]$
p	Absolute pressure $[Pa]$
Q_{LHV}	Lower heating value $[J/kg]$
R_{air}	Air gas constant $[J/(kg \cdot K)]$
r_c	Cylinder compression ratio [−]
r_e	Exhaust valve diameter/bore ratio [−]
r_i	Intake valve diameter/bore ratio [−]
S	Cylinder stroke $[mm]$
S_p	Mean piston speed $[m/s]$
T	Temperature $[K]$
u	Control input $[V]$
V	Volume $[m^3]$
V_d	Total engine displacement volume $[m^3]$
W	Work $[J]$

Table A.2: List of used abbreviations

Abbreviation	Definition
air,cyl	Total cylinder air flow
air,in	Total air flow to manifold
air,tot	Total air flow to manifold
air,valve	Throttle valve air flow
air,vgt	VGT air flow
afmep	Auxiliary losses MEP
amb	Ambient
cfemp	Crankshaft bearings friction MEP
chem	Chemical (fuel/air mixture)
comb	Combustion
cvt	CVT

Abbreviation	Definition (*cont'd*)
dyno	Dynamometer
ECU	Engine Control Unit
eng	Engine
EVC	Exhaust valve closure
EVO	Exhaust valve opening
exh	Exhaust
fd	Final drive
fuel	Fuel
gas	Gas exchange
ind	Indicated
IVC	Intake valve closure
IVO	Intake valve opening
load	Engine crankshaft load
man	Intake manifold
MEP	Mean Effective Pressure
loss	Pumping and friction loss
max	Maximum
MBT	Minimum best torque
mean	Mean
meas	Measured
mech	Mechanical
min	Minimum
model	Modeled
NEDC	New European Drive Cycle
opt	Optimal
$pmep_i$	Intake pumping losses MEP
$pmep_e$	Exhaust pumping losses MEP
rel	Relative
rfmep	Reciprocating friction MEP
road	Road load
SI	Spark ignition
SOI	Start of injection
TDC	Top Dead Center (of piston in cylinder)
tfmep	Total friction MEP
th	Thermodynamic
throtl	Throttling
vfmep	Valve train friction MEP
vgt	Variable Geometry Turbine

Appendix B

Experimental setup

B.1 Nissan ECU functions

Input (sensors)	ECU functions	Output (actuators)
-Camshaft position -Mass air flow -Engine coolant temperature -Front heated oxygen -Ignition switch -Throttle position -PNP switch -Air conditioner switch -Knock sensor -EGR temperature [1] -Crankshaft position (OBD)[1] -Tank fuel temperature [1] -Battery voltage -Power steering oil pressure switch -Vehicle speed -Intake air temperature -Rear heated oxygen[2] -TCM (Transmission control module)[3] -Closed throttle position switch -Electrical load -Refrigerant pressure	Fuel injection and mixture ratio control	Injectors
	Distributor ignition system	Power transistor
	Idle air control system	IACV-AAC valve
	Fuel pump control	Fuel pump relay
	Front heated oxygen sensor monitor, OBD	Malfunction indicator (On the instrument panel)
	EGR control	EGR volume control valve
	Front and rear heated oxygen sensor heater control	Heated oxygen sensor heater
	EVAP canister purge flow control	EVAP canister purge volume control solenoid valve
	Cooling fan control	Cooling fan relay
	Air conditioning cut control	Air conditioner relay

1 : These sensors are not used to control the engine system. They are used only for the on board diagnosis.
2 : Under normal conditions, this sensor is not for engine control operation.
3 : The DTC related to CVT will be sent to ECM.

B.2 Nissan Multiport Fuel Injection (MFI) control

Table B.1: MFI specifications [NissanMotorCoporation]

State	Timing	Static map compensation	λ-control	Fuel trim
Engine start	Simultaneous	Increase	Open-loop	No
Warm up	Sequential	Increase	Open-loop	No
Gear change N $\rightarrow$ D	Sequential	Increase	Closed-loop	Yes
Acceleration	Sequential	Increase	Open-loop	No
Deceleration	Sequential	Decrease	Open-loop	No
Hot engine	Sequential	Increase	Closed-loop	Yes
High speed, high load	Sequential	Increase	Open-loop	No
High engine speed	Sequential	Decrease	Closed-loop	Yes
High coolant temperature	Sequential	Decrease	Open-loop	No
λ-sensor malfunctioning	Sequential	-	-	No
Engine safe mode	Simultaneous	-	-	No

B.3 Schenck dynamometer power curves

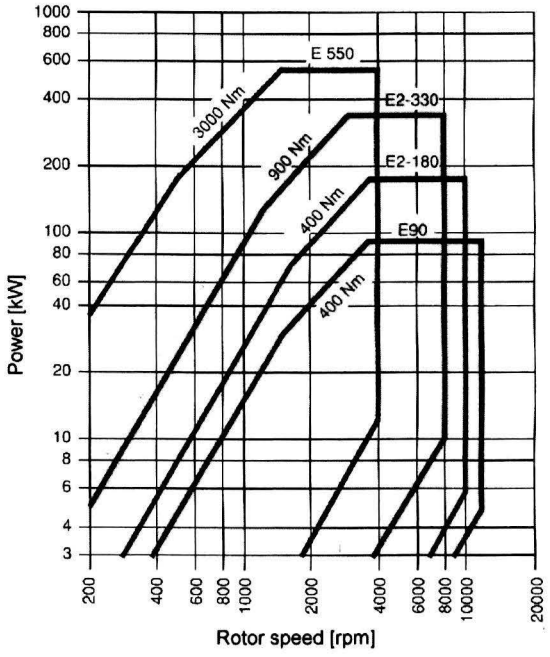

Figure B.1: Various Schenck dynamometer power curves. The E550 is used in this research. [W.J. Gorter, 2003]

B.4 Signal conditioning

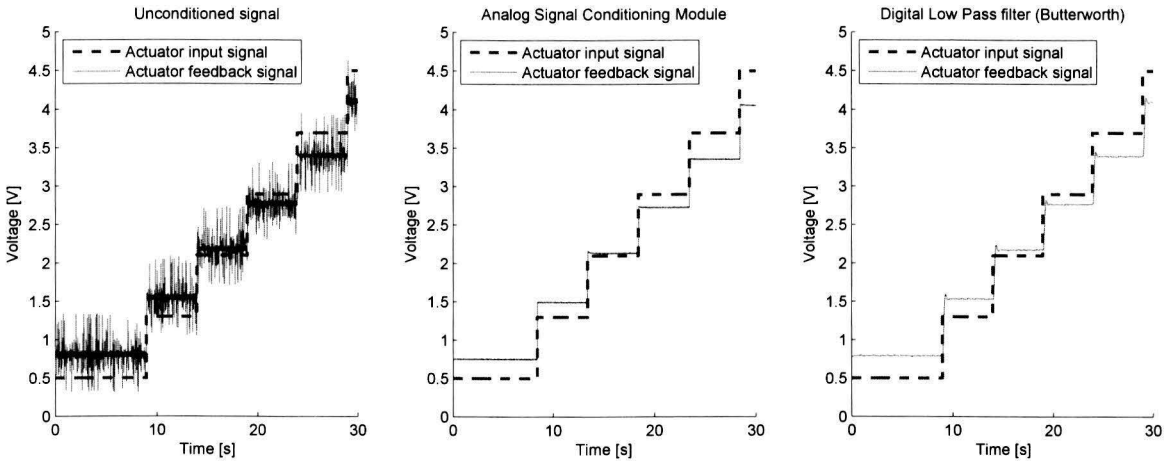

Figure B.2: Compare different signal processing methods

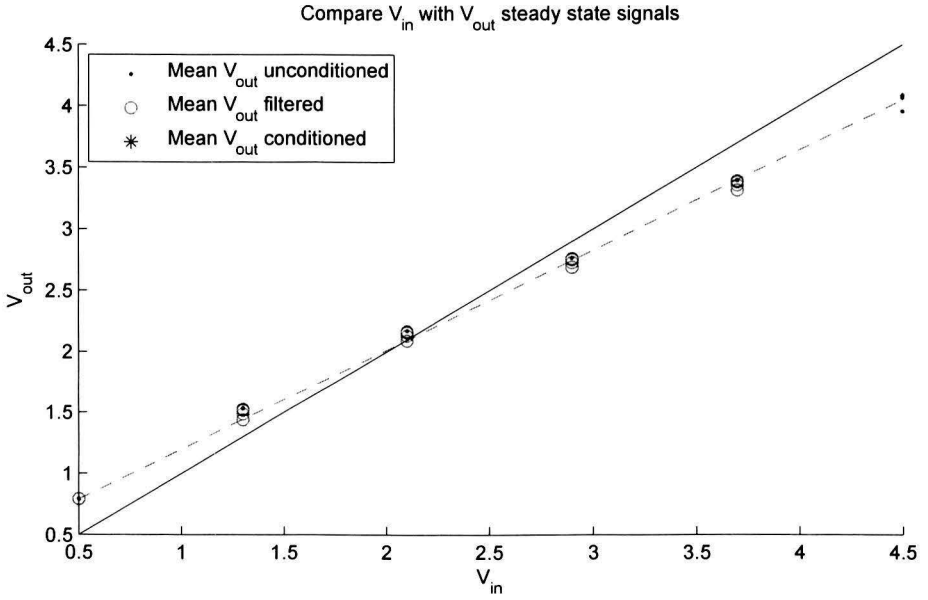

Figure B.3: Woodward control vs feedback signal. Feedback signal unfiltered vs analog filter vs digital filter

B.5 Calibration results

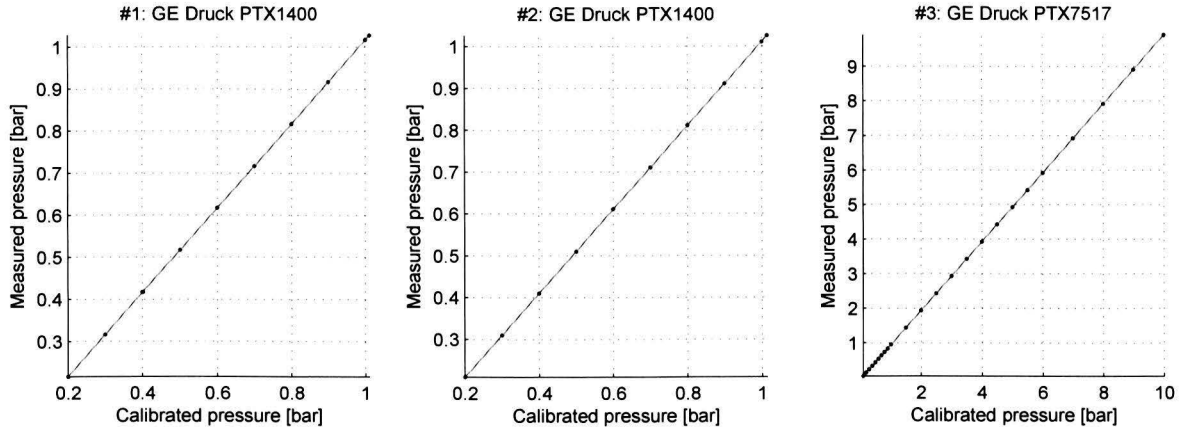

Figure B.4: Pressure sensors calibration with Druck DPI620

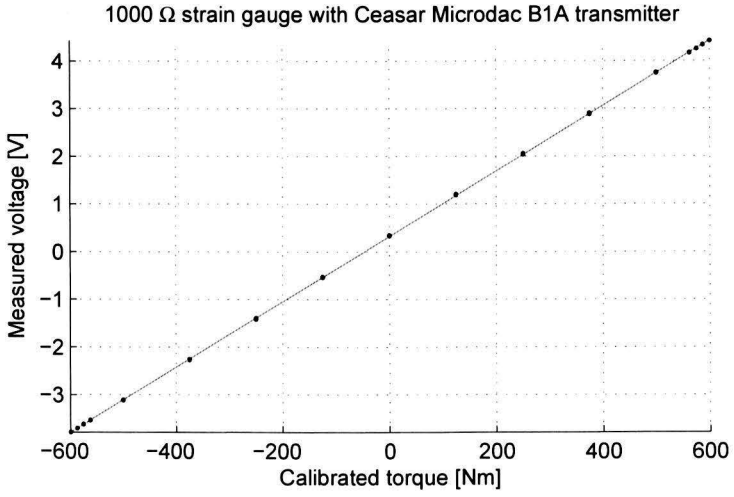

Figure B.5: Torque strain gauge calibration results

Appendix C

Experimental results

C.1 Statistical analysis

The box-and-whisker diagrams for steady state normalized experimental data are shown below. The central marks (red line) is the median, the top and bottom edges of the box are the 25th and 75th percentiles, while the whiskers are the extreme data points not considered outliers. The outliers are plotted individually. The horizontal axis show the experiment number, which indicated an engine operating point as shown in Fig. C.1.

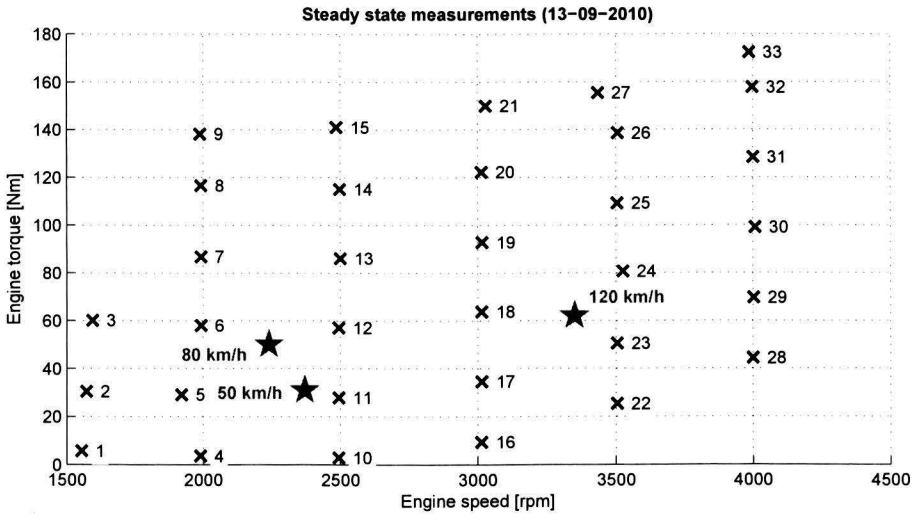

Figure C.1: Engine operating points per experiment

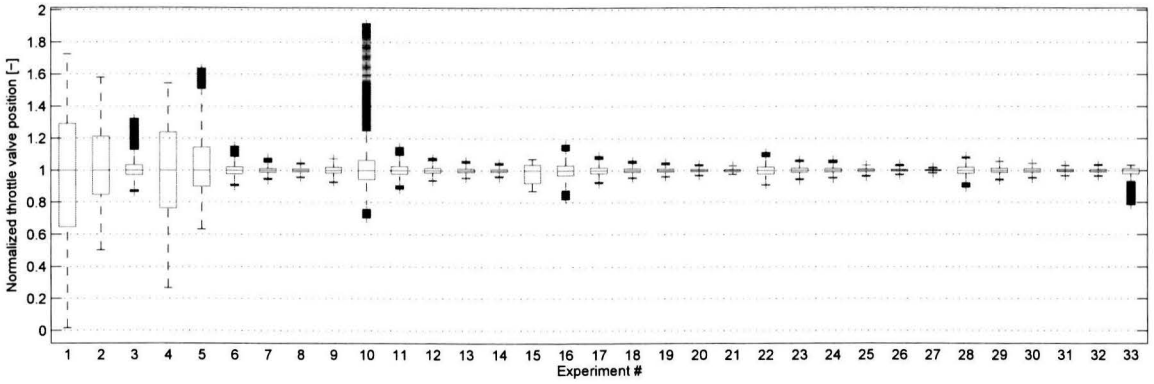

Figure C.2: Normalized throttle position box-and-whisker diagram

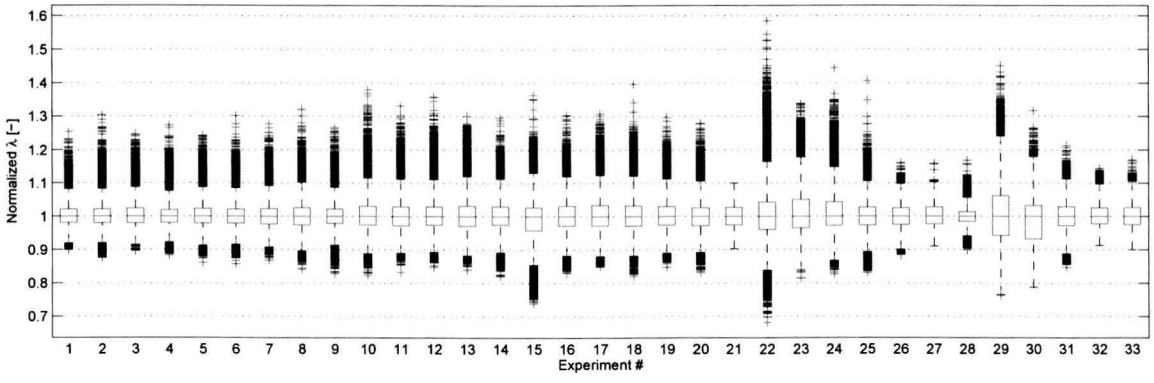

Figure C.3: Normalized λ box-and-whisker diagram

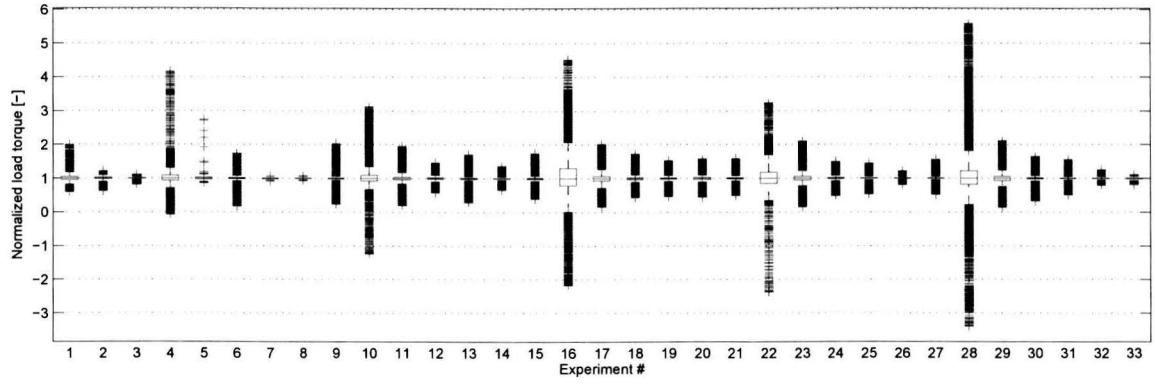

Figure C.4: Normalized load torque box-and-whisker diagram

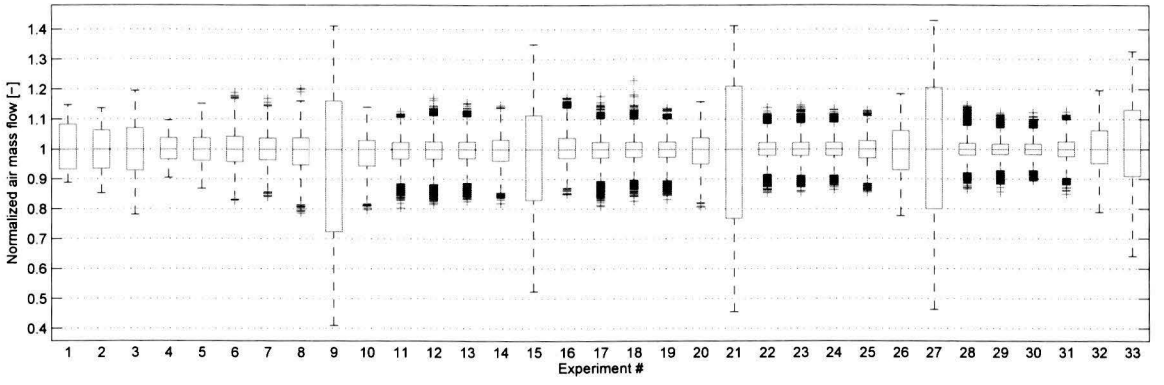

Figure C.5: Normalized throttle valve air flow box-and-whisker diagram

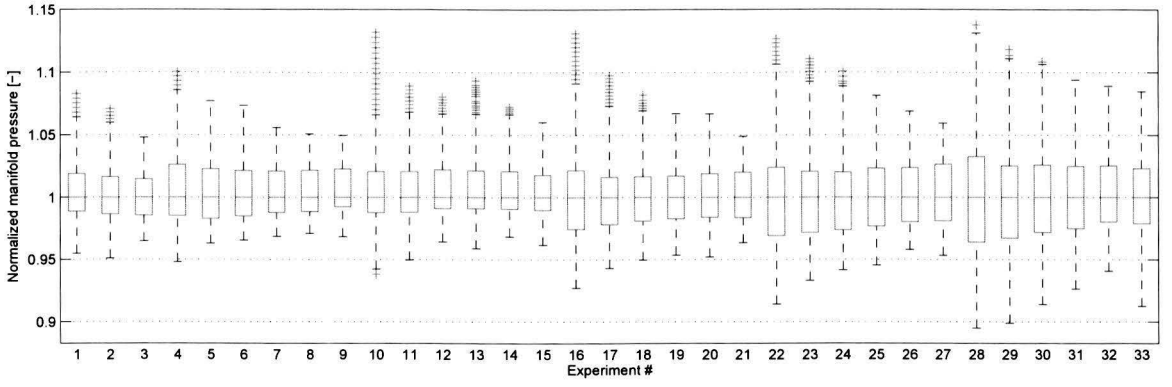

Figure C.6: Normalized manifold pressure box-and-whisker diagram

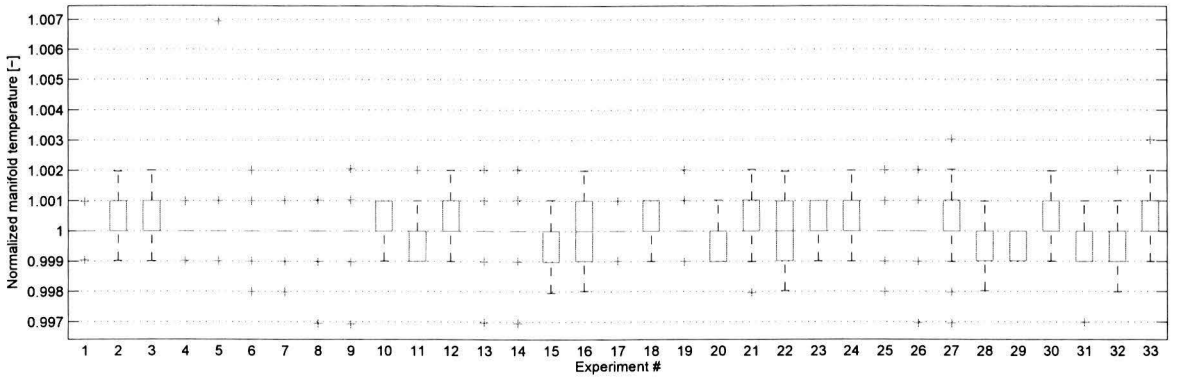

Figure C.7: Normalized manifold temperature box-and-whisker diagram

C.2 Steady state reference measurements

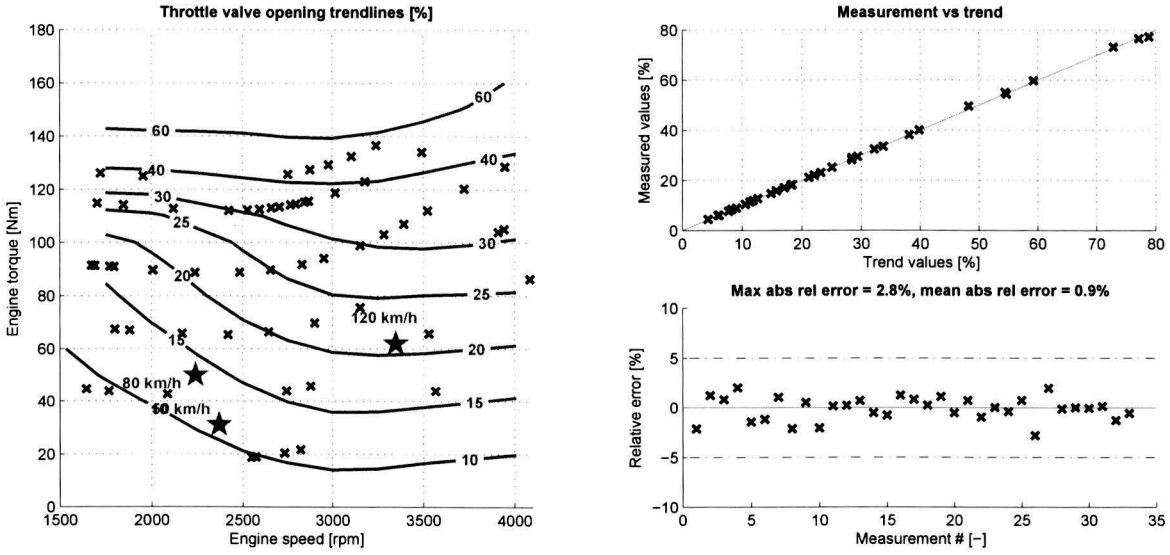

Figure C.8: Throttle valve opening position trendlines

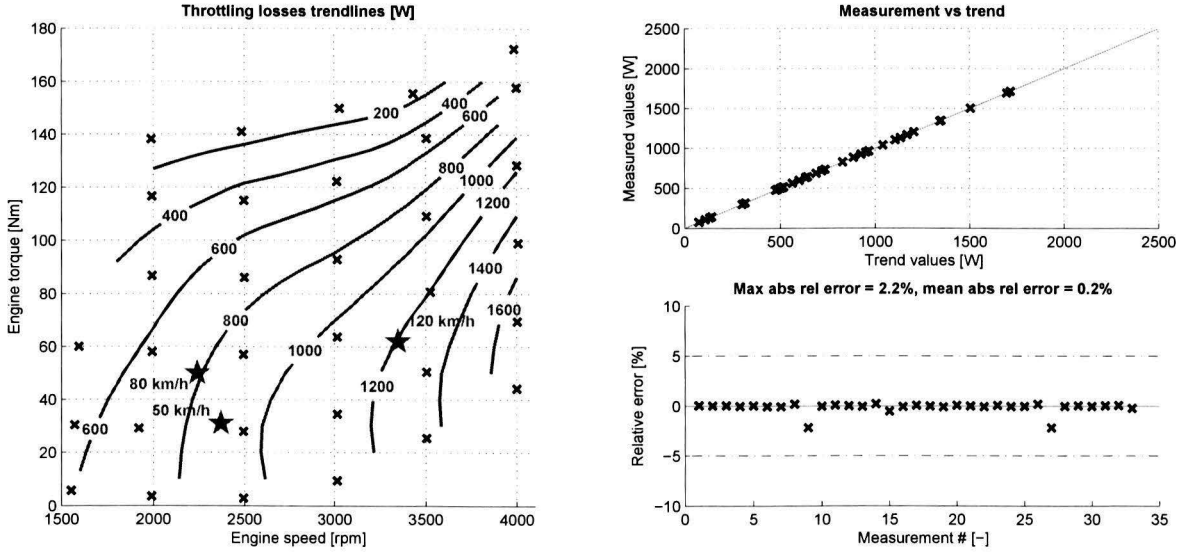

Figure C.9: Engine throttling loss trendlines

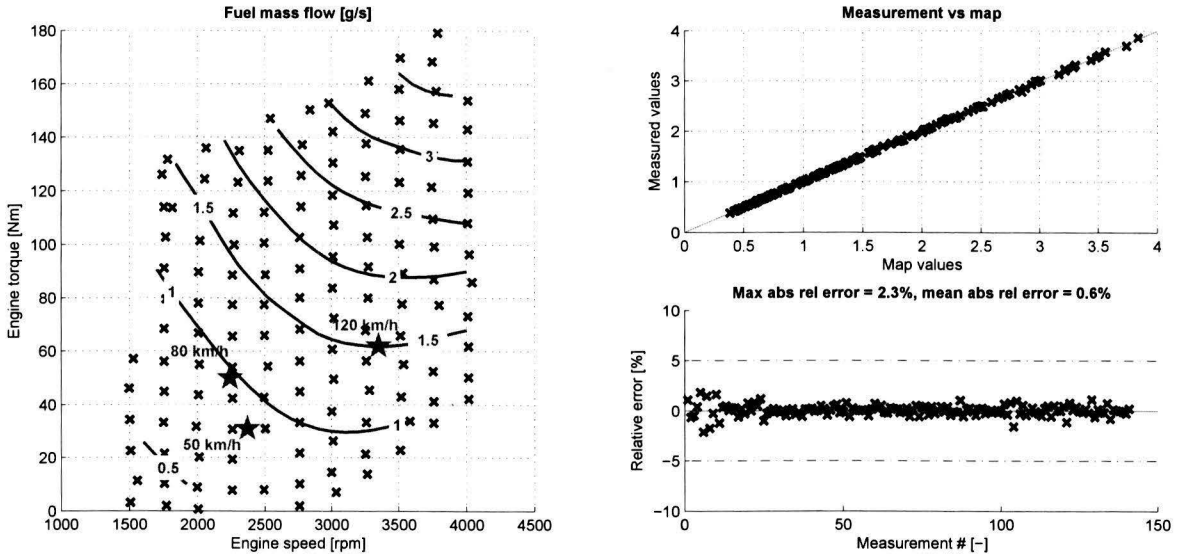

Figure C.10: Fuel mass flow trendlines

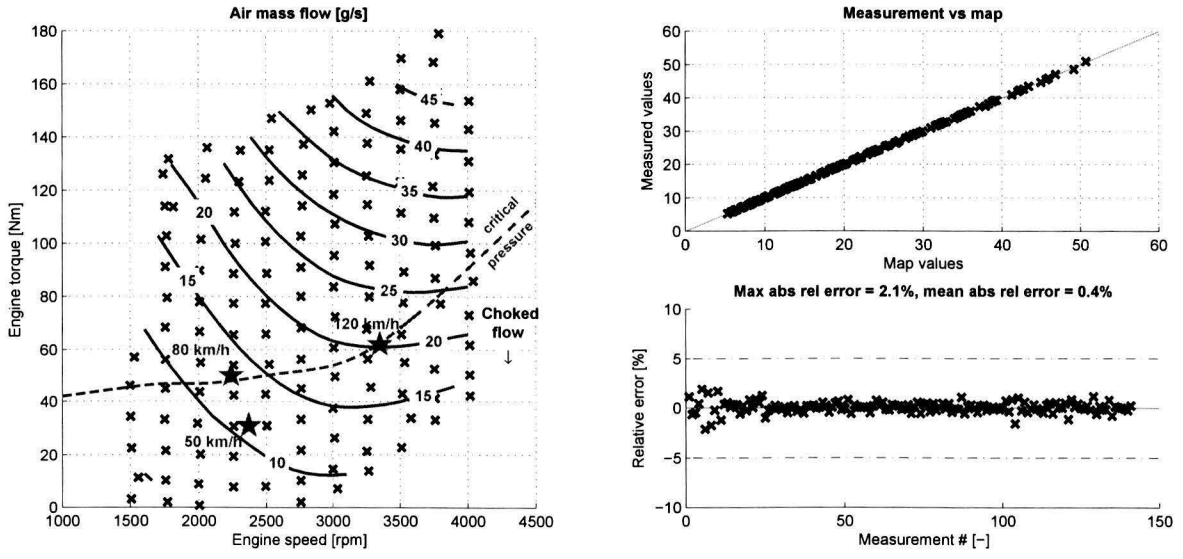

Figure C.11: Air mass flow trendlines

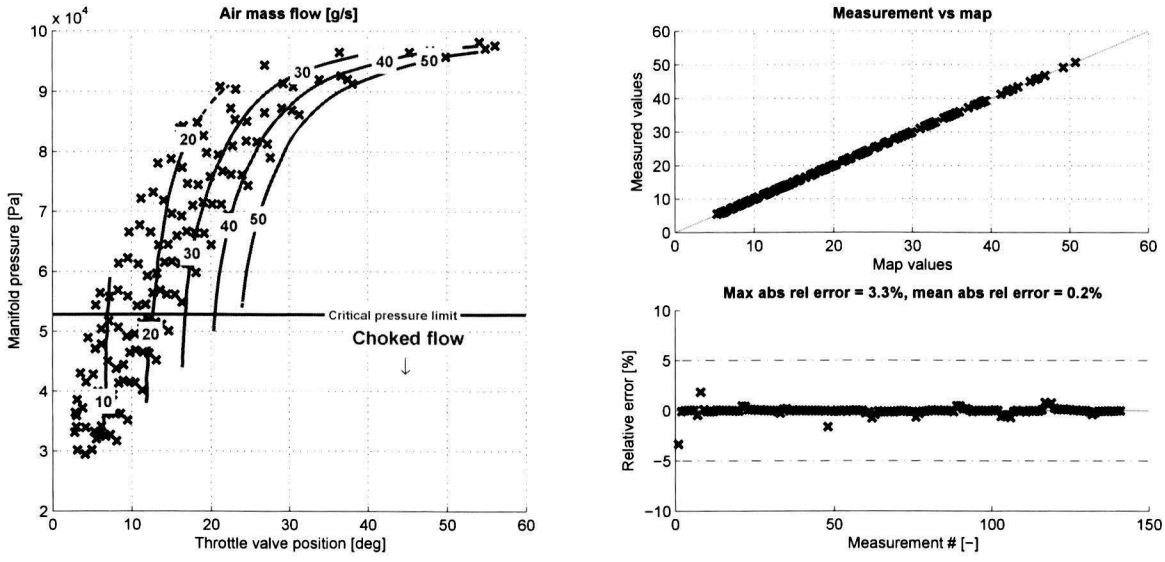

Figure C.12: Air mass flow trendlines: choked flow at critical manifold pressure

C.3 Steady state measurements with WEDACS

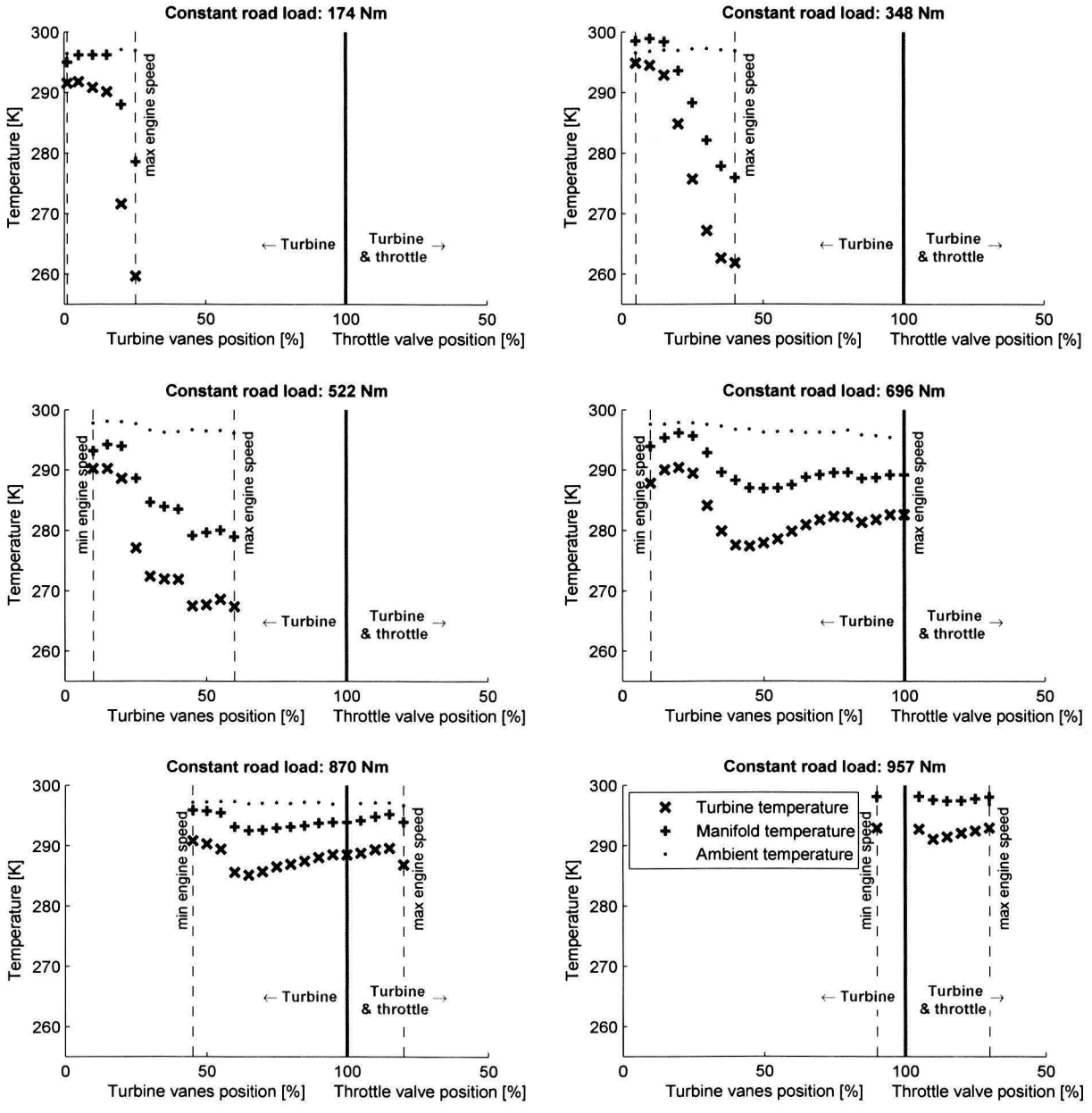

Figure C.13: Temperature curves as function of vane positions ($0 - 100\%$) and additional throttle positions ($> 100\%$) for different brake loads

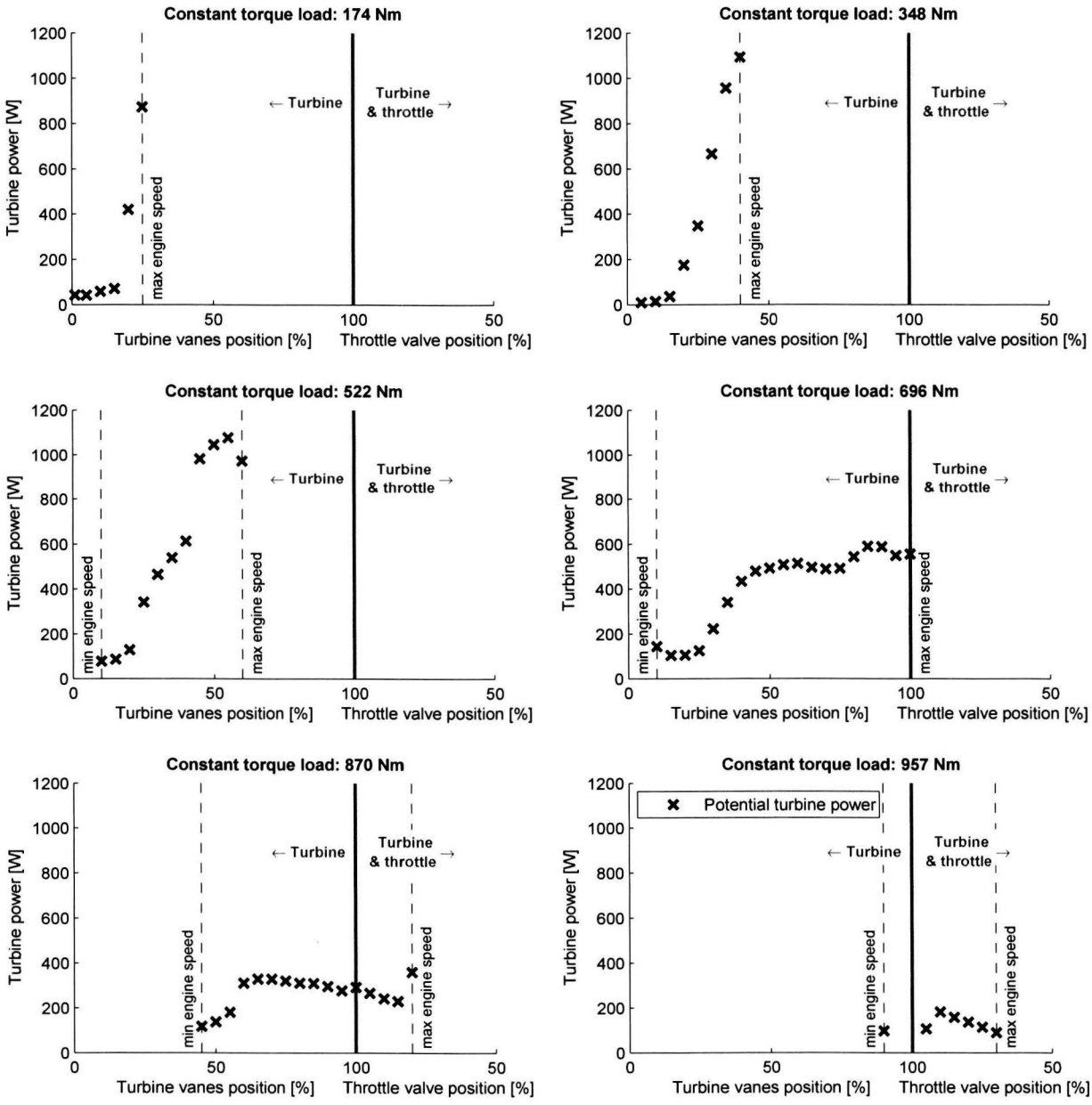

Figure C.14: WEDACS power recovery curves

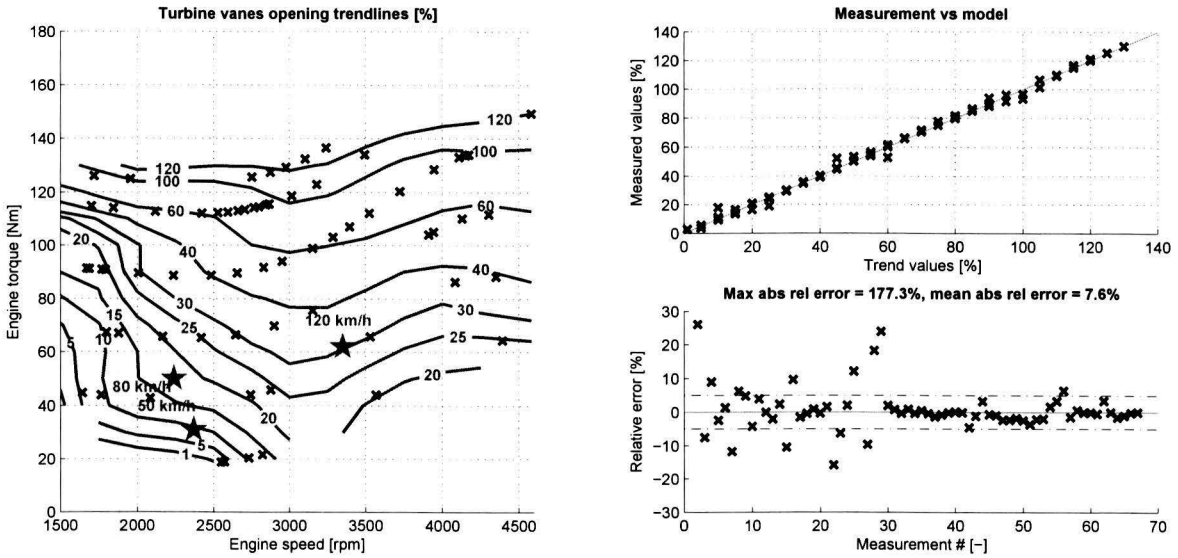

Figure C.15: Turbine vanes position trendlines

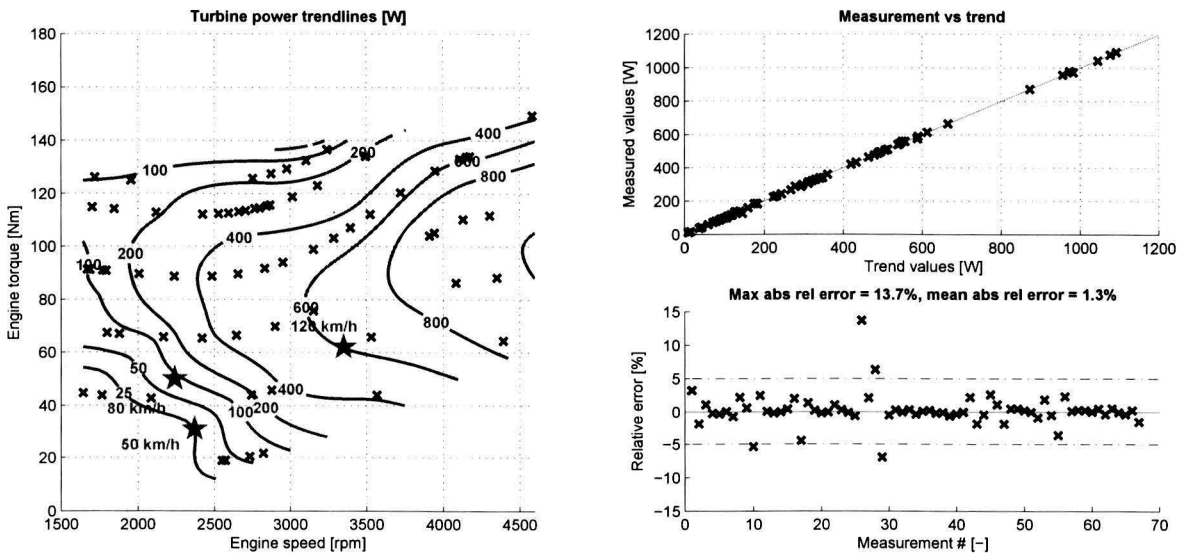

Figure C.16: WEDACS power recovery trendlines

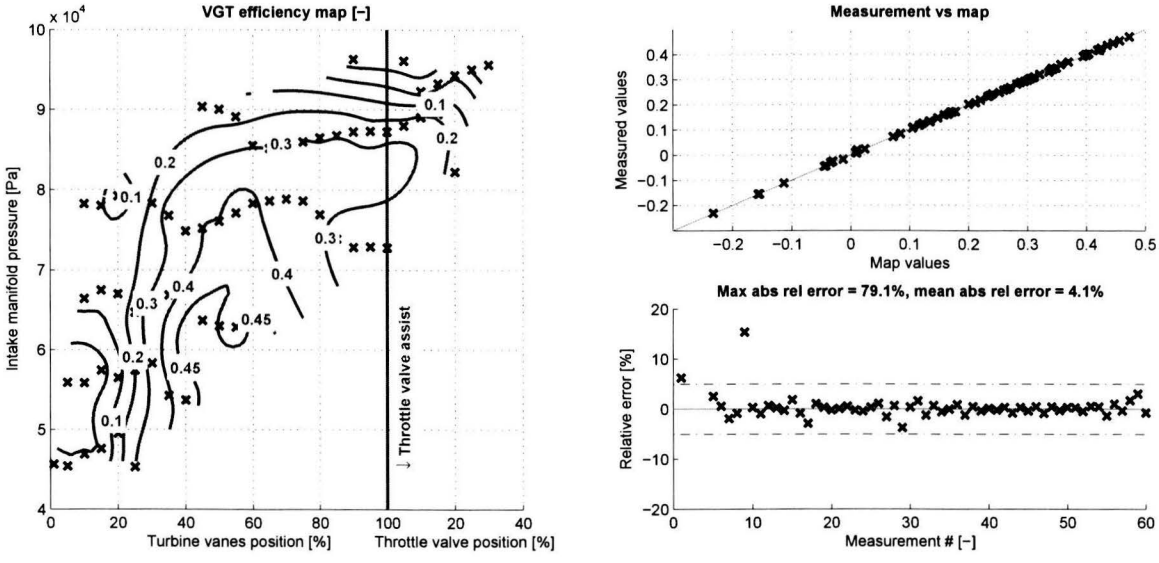

Figure C.17: Turbine efficiency trendlines

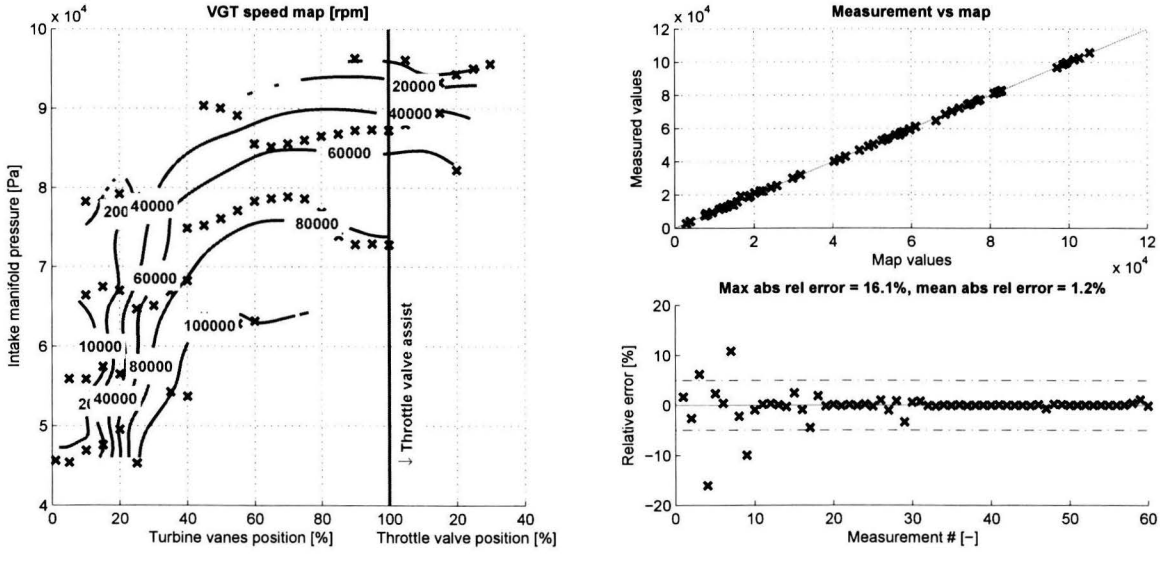

Figure C.18: Turbine speed trendlines

Appendix D

Mathematical equations

D.1 Receiver equations

Mass and energy balance:

$$\frac{d}{dt}m(t) = \dot{m}_{in}(t) - \dot{m}_{out}(t) \tag{D.1}$$

$$\frac{d}{dt}U(t) = \dot{H}_{in}(t) - \dot{H}_{out}(t) + \dot{Q}(t) - \dot{W}(t) \tag{D.2}$$

Ideal gas law:

$$p(t) \cdot V = m(t) \cdot R \cdot T(t) \tag{D.3}$$

Caloric relations, assume $T_{out}(t) = T(t)$:

$$\begin{aligned} U(t) = c_v \cdot T(t) \cdot m(t) \quad &= \frac{1}{\kappa - 1} \cdot p(t) \cdot V \\ \dot{H}_{in} &= c_p \cdot T_{in}(t) \cdot \dot{m}_{in}(t) \\ \dot{H}_{out} &= c_p \cdot T(t) \cdot \dot{m}_{out}(t) \\ \kappa &= c_p / c_v \\ R &= c_p - c_v \end{aligned} \tag{D.4}$$

Substitute D.3 and D.4 in D.1 and D.2:

$$\frac{d}{dt}p(t) = \frac{\kappa \cdot R}{V}\left(\dot{m}_{in}(t) \cdot T_{in}(t) - \dot{m}_{out}(t) \cdot T(t)\right) \tag{D.5}$$

$$\begin{aligned} \frac{d}{dt}T(t) = \frac{T(t) \cdot R}{p(t) \cdot V \cdot c_v} \cdot \ldots \\ \ldots \left(c_p \cdot \dot{m}_{in}(t) \cdot T_{in}(t) - c_p \cdot \dot{m}_{out}(t) \cdot T(t) - c_v(\dot{m}_{in}(t) - \dot{m}_{out}(t))T(t)\right) \end{aligned} \tag{D.6}$$

Assume large dwell time and large surface-to-volume ratio, then:

$$T(t) = T_{in}(t) \quad (= T_{out}(T)) \tag{D.7}$$

(D.8)

Now, (D.5) and (D.6) are simplified to:

$$\frac{d}{dt}p(t) = \frac{R \cdot T(t)}{V}\left(\dot{m}_{in}(t) - \dot{m}_{out}(t)\right) \tag{D.9}$$

$$\frac{d}{dt}T(t) = T_{in}(t) \tag{D.10}$$

D.2 Throttle valve opening area equations

The throttle valve opening area $A_{valve}[m^2]$ is a function of the throttle valve position $\alpha[^o]$:

$$\begin{aligned} A_{valve}(\alpha) = &-\frac{d \cdot D}{2}\left[1-\left(\frac{d}{D}\right)^2\right]^{\frac{1}{2}} + \frac{d \cdot D}{2}\left[1-\left(\frac{d}{D}\cdot\frac{\cos(\alpha_0)}{\cos(\alpha_0+\alpha)}\right)^2\right]^{\frac{1}{2}} \ldots \\ &\ldots + \frac{D^2}{2}\sin^{-1}\left(\left[1-\left(\frac{d}{D}\right)^2\right]^{\frac{1}{2}}\right) \ldots \\ &\ldots - \frac{D^2}{2}\cdot\frac{\cos(\alpha_0+\alpha)}{\cos(\alpha_0)}\sin^{-1}\left(\left[1-\left(\frac{d}{D}\cdot\frac{\cos(\alpha_0)}{\cos(\alpha_0+\alpha)}\right)^2\right]^{\frac{1}{2}}\right) \end{aligned} \tag{D.11}$$

with $D[m]$ the throttle canal internal diameter, $d[m]$ the throttle plate shaft diameter and $\alpha_0[^o]$ the fully closed throttle valve position. Due to the geometry of the throttle valve plate there exists a maximum flow area before $\alpha = 90^o$, which is dependent on the throttle valve shaft diameter. The flow area is then constant and given in Eq. (D.12).

$$\begin{aligned} A_{valve}(\alpha) = &\frac{D^2}{2}\sin^{-1}\left(\left[1-\left(\frac{d}{D}\right)^2\right]^{\frac{1}{2}}\right) - \frac{d \cdot D}{2}\left[1-\left(\frac{d}{D}\right)^2\right]^{\frac{1}{2}} \\ &\forall\alpha \geq \cos^{-1}\left[\frac{d}{D}\cdot\cos(\alpha_0)\right] - \alpha_0 \end{aligned} \tag{D.12}$$

D.3 Improved friction model equations

$$M_{loss,tot} = \frac{tfmep \cdot N \cdot V_d}{60 \cdot 2 \cdot 10^5 \cdot \omega_e} \tag{D.13}$$

$$tfmep = cfmep + rfmep + vfmep + afmep + pmep_i + pmep_e \tag{D.14}$$

with,

$$cfmep = 1.22e^3\left(\frac{D_b}{B^2 S n_c}\right) + 3.03e^{-6}\sqrt{\frac{\mu}{\mu_0}}\left(\frac{N D_b^3 L_b n_b}{B^2 S n_c}\right) + 1.35e^{-12}\left(\frac{D_b^2 N^2 n_b}{n_c}\right) \tag{D.15a}$$

$$\begin{aligned} rfmep = &2.94\sqrt{\frac{\mu}{\mu_0}}\left(\frac{S_p}{B}\right) + 4.06e^2\left(1+\frac{1000}{N}\right)\frac{1}{B^2} + 3.03e{-}6\sqrt{\frac{\mu}{\mu_0}}\left(\frac{N D_b^3 L_b n_b}{B^2 S n_c}\right) \\ &+ 6.89e^{-2}\left(\sqrt{\frac{\mu}{\mu_0}}8.8e^{-2} r_c + 1.82e^{-3} r_c^{(1.33-K S_p)}\right)\Pi \end{aligned} \tag{D.15b}$$

$$\begin{aligned} vfmep = &2.44\sqrt{\frac{\mu}{\mu_0}}\left(\frac{N n_b}{B^2 S n_c}\right) + C_{ff}\cdot 1e^{-2}\left(1+\frac{500}{N}\right)\frac{n_v}{S n_c} + C_{rf}\cdot 1e^{-2}\left(\frac{N n_v}{S n_c}\right) \\ &+ C_{oh}\cdot 1e^{-2}\sqrt{\frac{\mu}{\mu_0}}\left(\frac{L_v^{1.5} N^{0.5} n_v}{B S n_c}\right) + C_{om}\cdot 1e^{-2}\left(1+\frac{500}{N}\right)\frac{L_v n_v}{S n_c} \end{aligned} \tag{D.15c}$$

$$afmep = 8.3155e^{-2} + 1.86e^{-5} N + 7.45e^{-9} N^2 \tag{D.15d}$$

$$pmep_i = (p_{amb} - p_{man})\, e^{-5} + 3e^{-5}\left(\frac{S_p^2}{n_v^2 r_i^4}\right)\Pi^2 \tag{D.15e}$$

$$pmep_e = 1.78e^{-3} S_p^2 \cdot \Pi^2 + 3e^{-5}\left(\frac{S_p^2}{n_v^2 r_e^4}\right)\Pi^2 \tag{D.15f}$$

Appendix E

Model equations

Air system model

Throttle valve air mass flow:

$$\dot{m}_{air,valve}(t) = c_d A_{valve}(p_{man}, \alpha) \frac{p_{amb}(t)}{\sqrt{R T_{amb}(t)}} \cdot \Psi\left(\Pi(t)\right)$$

$$\Psi(\Pi(t)) = \begin{cases} \sqrt{\kappa \left[\frac{2}{\kappa+1}\right]^{\frac{\kappa+1}{\kappa-1}}} & \text{for } p_{out} < p_{cr} \\ \Pi(t)^{\frac{1}{\kappa}} \sqrt{\frac{2\kappa}{\kappa-1}\left[1 - \Pi(t)^{\frac{\kappa-1}{\kappa}}\right]} & \text{for } p_{out} \geq p_{cr} \end{cases}$$

$$\Pi(t) = \frac{p_{out}(t)}{p_{in}(t)}$$

$$p_{cr} = \left[\frac{2}{\kappa+1}\right]^{\frac{\kappa}{\kappa-1}} \cdot p_{in}$$

$$c_d A_{valve} = a_1 p_{man}^4 + a_2 p_{man}^3 + a_3 p_{man}^2 + a_4 p_{man} + a_5 \alpha^4 + a_6 \alpha^3 + a_7 \alpha^2 ... \\ ... + a_8 (p_{man} \cdot \alpha)^4 + a_9 (p_{man} \cdot \alpha)^3 + a_{10} (p_{man} \cdot \alpha)^2 + a_{12} (p_{man} \cdot \alpha) + a_{13}$$

$$\alpha(t) = u_\alpha(t)$$

VGT air mass flow:

$$\dot{m}_{air,vgt}(t) = A_{vgt,max} \frac{p_{amb}(t)}{\sqrt{T_{amb}(t)}} f_\Pi(\Pi(t)) f_{vanes}(u_\beta(t))$$

$$f_\Pi(\Pi(t)) = \sqrt{1 - \Pi(t)^\kappa}$$

$$f_{vanes}(u_\beta(t)) = c_1 + c_2 \sqrt{1 - \left(\frac{u_\beta(t) - c_3}{c_4}\right)^2}$$

$$u_\beta(t) = b_1 \beta^2(t) + b_2 \beta(t)$$

VGT downstream temperature:

$$f_{vgt}(p_{man}, \dot{m}_{vgt}) = g_1 p_{man}^3 + g_2 p_{man}^2 + g_3 p_{man} + g_4 \dot{m}_{vgt}^3 + g_5 \dot{m}_{vgt}^2 + g_6 \dot{m}_{vgt} ... \\ ... + g_7 (p_{man} \dot{m}_{vgt})^2 + g_8 (p_{man} \dot{m}_{vgt}) + g_9$$

$$T_{vgt} = \begin{cases} f_{vgt}(p_{man}, \dot{m}_{vgt}) & \text{if } f_{vgt}(p_{man}, \dot{m}_{vgt}) < (T_{amb} - g_{10}) \\ T_{amb} - g_{10} & \text{if } f_{vgt}(p_{man}, \dot{m}_{vgt}) \geq (T_{amb} - g_{10}) \end{cases}$$

VGT power:

$$P_{vgt}(t) = \dot{m}_{air}(t)c_p(T_{amb}(t) - T_{vgt}(t))$$

Manifold pressure:

$$\frac{d}{dt}p_{man}(t) = \frac{R \cdot T_{man}(t)}{V_{man}}\left(\dot{m}_{in}(t) - \dot{m}_{out}(t)\right)$$

Manifold temperature:

$$T_{man} = T_{amb} - j_1(T_{amb} - T_{vgt}) + j_2$$

Cylinders air mass flow:

$$\begin{aligned}\dot{m}_{air,cyl} &= \frac{p_{man}}{R_{air}T_{man}}\eta_{vol}\frac{V_d}{2}\frac{\omega_{eng}}{2\pi}\\ \eta_{vol} &= \left(b_1\omega_{eng}^2 + b_2\omega_{eng} + b_3\right)m_{air,man}^2 + \left(b_4\omega_{eng}^2 + b_5\omega_{eng} + b_6\right)m_{air,man} + ...\\ &\quad ... \left(b_7\omega_{eng}^2 + b_8\omega_{eng} + b_9\right)\\ m_{air,man} &= \frac{p_{man}V_{man}}{R_{air}T_{man}}\end{aligned}$$

Fuel system model

Desired air/fuel ratio:

$$\lambda_{des} = \begin{cases} a_1\dot{m}_{air,cyl} + a_2 & \text{if } \dot{m}_{air,cyl} \leq m_{cr} \\ a_3(\dot{m}_{air,cyl} - m_{cr}) + (a_1M_{cr} + a_2) & \text{if } \dot{m}_{air,cyl} > m_{cr} \end{cases} \tag{E.1}$$

Fuel mass flow:

$$\dot{m}_{fuel} = \frac{\dot{m}_{air,cyl}}{\lambda_{des}L_{st}} \tag{E.2}$$

Mechanical system model

Combustion and thermodynamic efficiencies:

$$\eta_{comb}\eta_{th} = (s_1 + s_2\lambda)\left(s_3 + s_4(\omega_{eng} - s_5)^2\right)$$

Pumping and friction torque loss:

$$M_{loss} = z_1 + z_2\omega_{eng} + z_3\omega_{eng}^2 + (z_4 + z_5\omega_{eng})\,p_{man}$$

Torque load:

$$M_{load} = d_1 + d_2 \cdot M_{road} + d_3 \cdot \omega_{eng} + d_4 \cdot \omega_{eng}^2 + d_5 \cdot \omega_{eng}^3 + d_6 \cdot \omega_{eng}^4 + d_7 \cdot \omega_{eng}^5$$

Engine torque:

$$M_{ind} = \eta_{th}\eta_{comb}\frac{\dot{m}_{fuel}Q_{LHV}}{\omega_{eng}}$$

$$M_{eng} = M_{ind} - M_{loss}$$

Engine speed:

$$J_{eng}\dot{\omega}_{eng} = M_{eng} - M_{load}$$

Appendix F

Model parameter fit results

F.1 Model parameters

$$c_d A_{valve} = a_1 p_{man}^4 + a_2 p_{man}^3 + a_3 p_{man}^2 + a_4 p_{man} + a_5 \alpha^4 + a_6 \alpha^3 + a_7 \alpha^2 ... \quad \text{(F.1)}$$
$$... + a_8 (p_{man} \cdot \alpha)^4 + a_9 (p_{man} \cdot \alpha)^3 + a_{10} (p_{man} \cdot \alpha)^2 + a_{12} (p_{man} \cdot \alpha) + a_{13}$$
$$\alpha(t) = u_\alpha(t)$$

Table F.1: Throttle valve discharge coefficient and opening area parameters

Submodel (variable)	Parameter	Value	Parameter	Value
Throttle valve ($c_d A_{valve}$)	a_1	$3.28 \cdot 10^{-24}$	a_8	$5.32 \cdot 10^{-6}$
	a_2	$-9.44 \cdot 10^{-19}$	a_9	$-4.03 \cdot 10^{-31}$
	a_3	$1.06 \cdot 10^{-13}$	a_{10}	$-2.39 \cdot 10^{-24}$
	a_4	$-4.68 \cdot 10^{-9}$	a_{11}	$8.52 \cdot 10^{-18}$
	a_5	$1.32 \cdot 10^{-10}$	a_{12}	$-1.08 \cdot 10^{-10}$
	a_6	$-8.87 \cdot 10^{-9}$	a_{13}	$2.92 \cdot 10^{-5}$
	a_7	$5.06 \cdot 10^{-7}$		

$$\eta_{vol} = \left(b_1 \omega_{eng}^2 + b_2 \omega_{eng} + b_3\right) m_{air,man}^2 + \left(b_4 \omega_{eng}^2 + b_5 \omega_{eng} + b_6\right) m_{air,man} + ...$$
$$... \left(b_7 \omega_{eng}^2 + b_8 \omega_{eng} + b_9\right) \quad \text{(F.2)}$$

Table F.2: Volumetric efficiency parameters

Submodel (variable)	Parameter	Value	Parameter	Value
Intake manifold (η_{vol})	b_1	$4.55 \cdot 10^{-1}$	b_6	$-4.41 \cdot 10^{2}$
	b_2	$-4.68 \cdot 10^{2}$	b_7	$4.31 \cdot 10^{-6}$
	b_3	$8.42 \cdot 10^{4}$	b_8	$-3.44 \cdot 10^{-3}$
	b_4	$-2.76 \cdot 10^{-3}$	b_9	1.01
	b_5	2.78		

$$u_\beta(t) = b_1\beta^2(t) + b_2\beta(t) \tag{F.3}$$

$$\dot{m}_{air,vgt}(t) = A_{vgt,max}\frac{p_{amb}(t)}{\sqrt{T_{amb}(t)}}f_\Pi(\Pi(t))f_{vanes}(u_\beta(t)) \tag{F.4}$$

$$f_\Pi(\Pi(t)) = \sqrt{1-\Pi(t)^\kappa} \tag{F.5}$$

$$f_{vanes}(u_\beta(t)) = c_1 + c_2\sqrt{1-\left(\frac{u_\beta(t)-c_3}{c_4}\right)^2} \tag{F.6}$$

Table F.3: Turbine air mass flow parameters

Submodel (variable)	Parameter	Value	Parameter	Value
VGT ($\dot{m}_{air,vgt}$)	c_1	$1.08 \cdot 10^1$	b_1	$-1.07 \cdot 10^{-3}$
	c_2	$-2.66 \cdot 10^1$	b_2	$2.28 \cdot 10^{-1}$
	c_3	$-1.80 \cdot 10^2$	$A_{vgt,max}$	$1.24 \cdot 10^{-6}$
	c_4	$1.95 \cdot 10^2$		

$$f_{vgt}(p_{man},\dot{m}_{vgt}) = g_1p_{man}^3 + g_2p_{man}^2 + g_3p_{man} + g_4\dot{m}_{vgt}^3 + g_5\dot{m}_{vgt}^2 + g_6\dot{m}_{vgt}... \\ ... + g_7(p_{man}\dot{m}_{vgt})^2 + g_8(p_{man}\dot{m}_{vgt}) + g_9 \tag{F.7}$$

$$T_{vgt} = \begin{cases} f_{vgt}(p_{man},\dot{m}_{vgt}) & \text{if } f_{vgt}(p_{man},\dot{m}_{vgt}) < (T_{amb}-g_{10}) \\ T_{amb}-g_{10} & \text{if } f_{vgt}(p_{man},\dot{m}_{vgt}) \geq (T_{amb}-g_{10}) \end{cases} \tag{F.8}$$

Table F.4: Turbine downstream temperature parameters

Submodel (variable)	Parameter	Value	Parameter	Value
VGT (T_{vgt})	g_1	$-5.71 \cdot 10^{-14}$	g_6	$1.66 \cdot 10^5$
	g_2	$1.78 \cdot 10^{-8}$	g_7	$-8.73 \cdot 10^3$
	g_3	$-1.74 \cdot 10^{-3}$	g_8	$-3.85 \cdot 10^{-6}$
	g_4	$-1.14 \cdot 10^6$	g_9	$4.61 \cdot 10^{-2}$
	g_5	$1.66 \cdot 10^5$	g_{10}	4.21

$$\lambda = \lambda_{des} \tag{F.9}$$

$$\lambda_{des} = \begin{cases} a_1\dot{m}_{air,cyl} + a_2 & \text{if } \dot{m}_{air,cyl} \leq m_{cr} \\ a_3(\dot{m}_{air,cyl} - m_{cr}) + (a_1M_{cr} + a_2) & \text{if } \dot{m}_{air,cyl} > m_{cr} \end{cases} \tag{F.10}$$

Table F.5: ECU injection control parameters

Submodel (variable)	Parameter	Value	Parameter	Value
ECU injection control (λ_{des})	a_1	$-8.76 \cdot 10^{-1}$	a_3	-9.23
	a_2	$9.31 \cdot 10^{-1}$	m_{cr}	$6.05 \cdot 10^{-2}$

$$\eta_{comb}\eta_{th} = (s_1 + s_2\lambda)\left(s_3 + s_4(\omega_{eng} - s_5)^2\right) \tag{F.11}$$

Table F.6: Combustion and thermodynamic efficiencies parameters

Submodel (variable)	Parameter	Value	Parameter	Value
Cylinders ($\eta_{comb} \cdot \eta_{th}$)	s_1	-2.75	s_4	$-2.38 \cdot 10^{-7}$
	s_2	6.63	s_5	$2.18 \cdot 10^{2}$
	s_3	$1.38 \cdot 10^{-1}$		

$$M_{loss} = z_1 + z_2\omega_{eng} + z_3\omega_{eng}^2 + (z_4 + z_5\omega_{eng})\, p_{man} \tag{F.12}$$

Table F.7: Pumping and friction loss parameters

Submodel (variable)	Parameter	Value	Parameter	Value
Crankshaft (M_{loss})	z_1	9.96	z_4	$-6.94 \cdot 10^{-4}$
	z_2	$4.15 \cdot 10^{-1}$	z_5	$1.53 \cdot 10^{-6}$
	z_3	$-1.02 \cdot 10^{-3}$		

F.2 Throttle valve discharge coefficient and opening area parameter fit

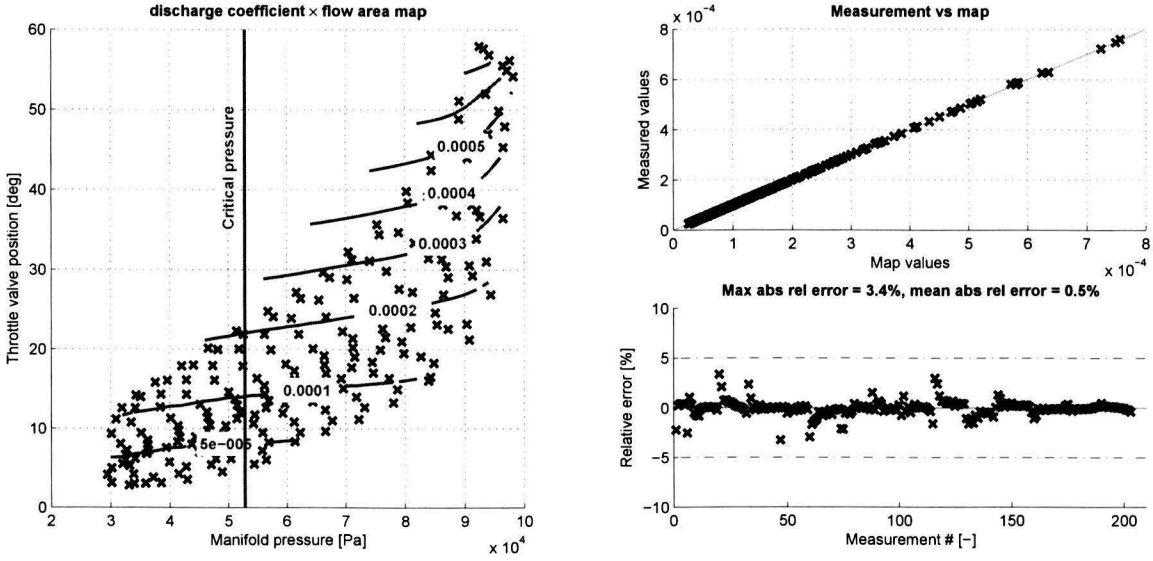

Figure F.1: Map for the throttle valve discharge coefficient and opening area under steady state conditions

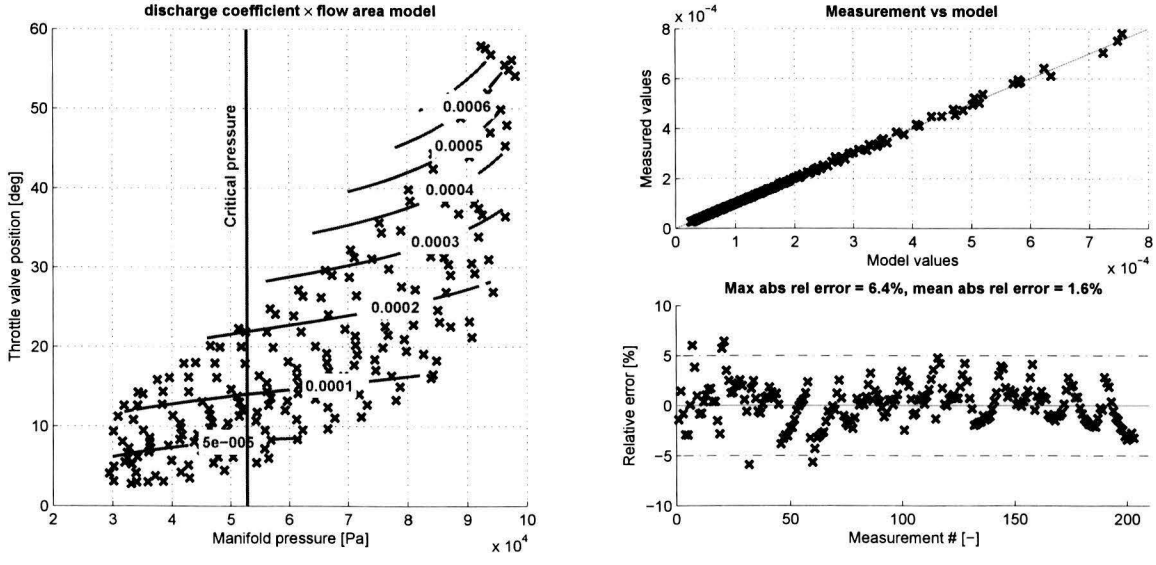

Figure F.2: Model for the throttle valve discharge coefficient and opening area under steady state conditions

F.3 Turbine air mass flow model parameter fit

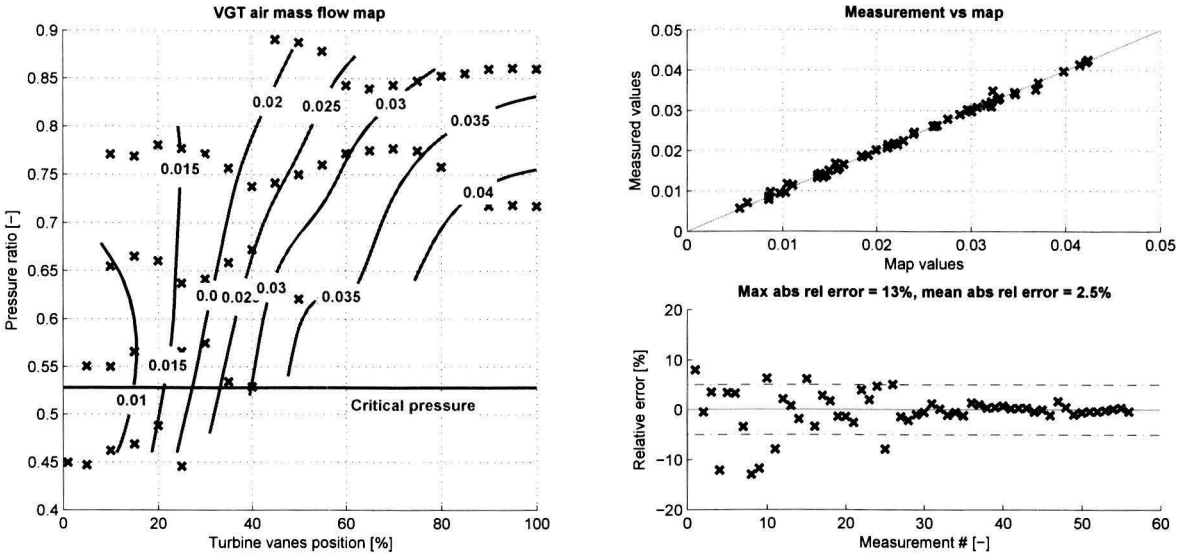

Figure F.3: Map for the turbine air mass flow under steady state conditions

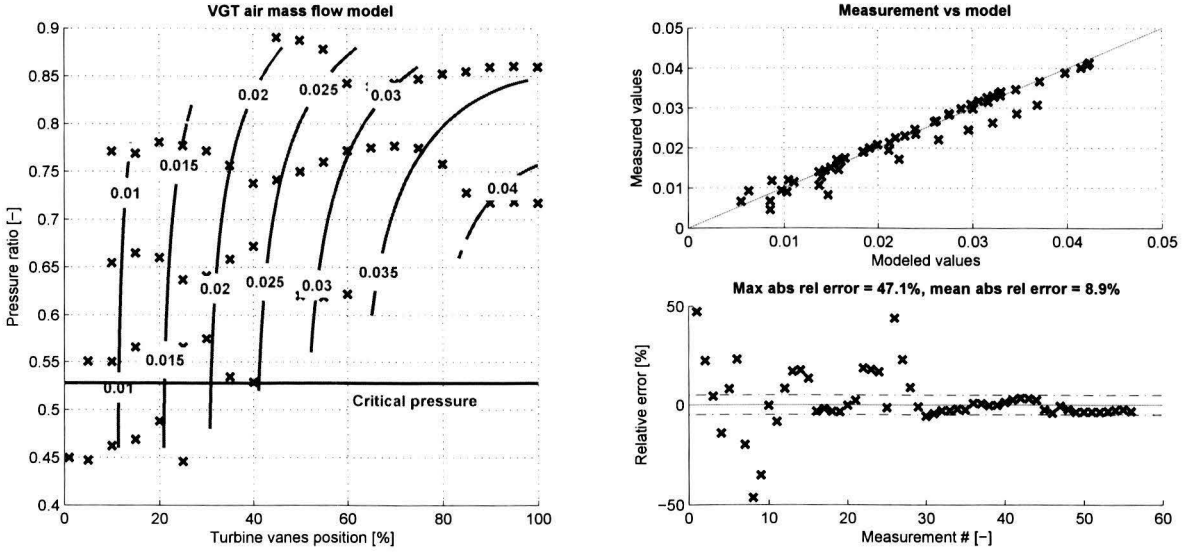

Figure F.4: Model for the turbine air mass flow under steady state conditions

F.4 Turbine downstream temperature model parameter fit

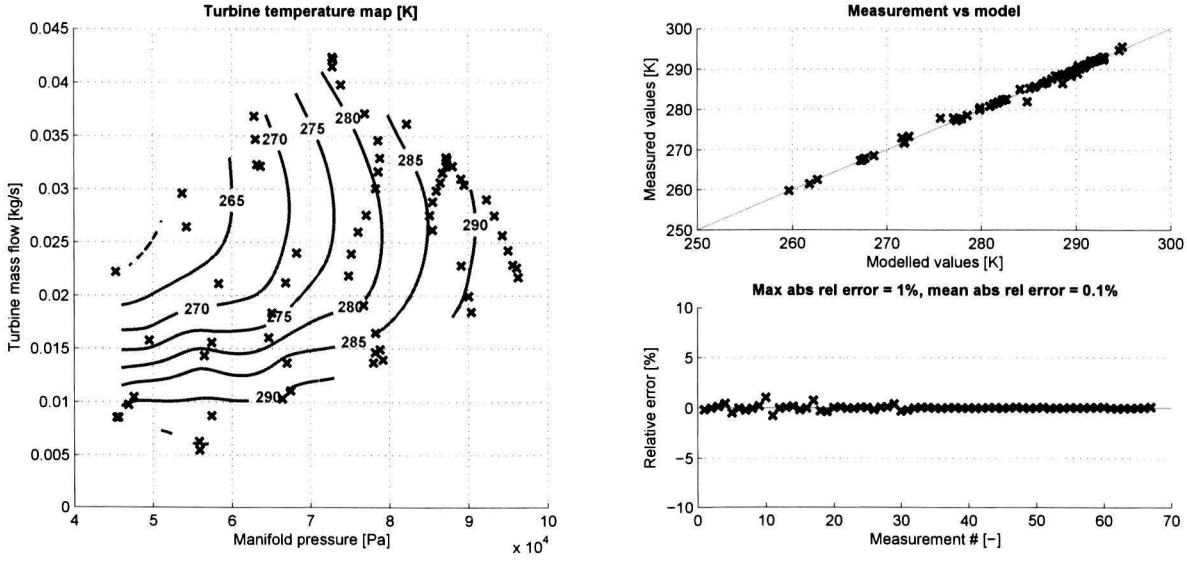

Figure F.5: Map for the downstream turbine temperature under steady state conditions

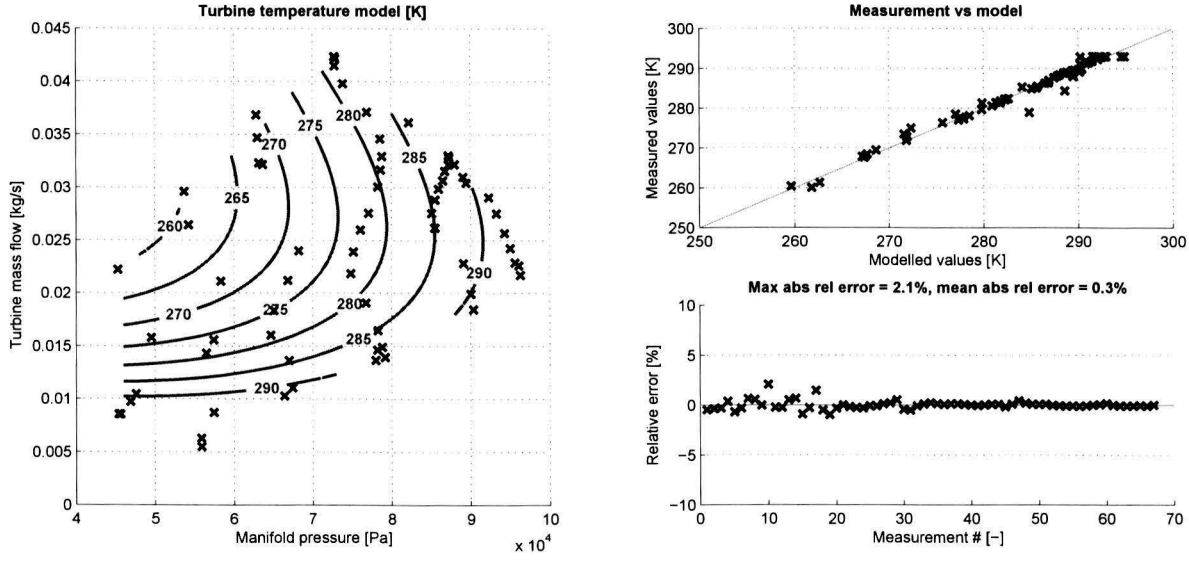

Figure F.6: Model for the downstream turbine temperature under steady state conditions

F.5 Volumetric efficiency model parameter fit

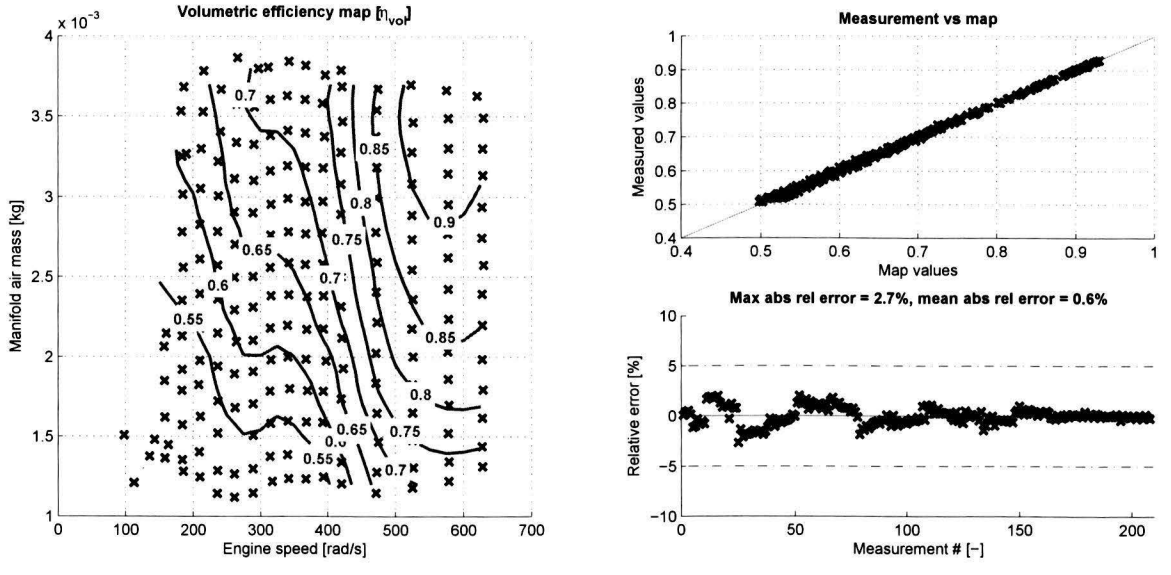

Figure F.7: Map for the volumetric efficiency under steady state conditions

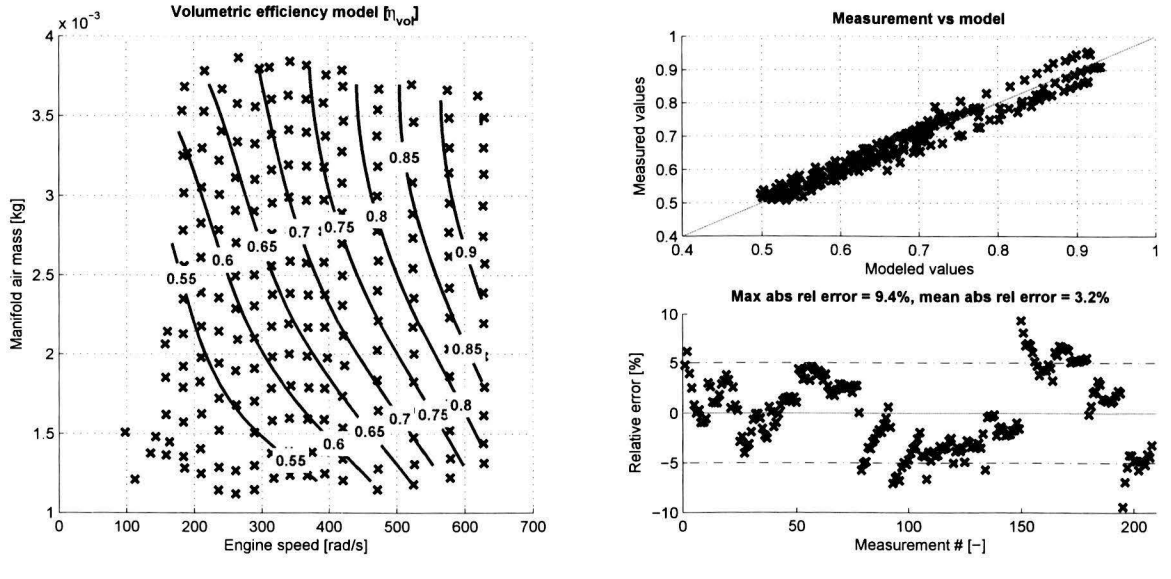

Figure F.8: Model for the volumetric efficiency under steady state conditions as presented in Eq. F.2

F.6 Combustion and thermodynamic efficiency model parameter fit

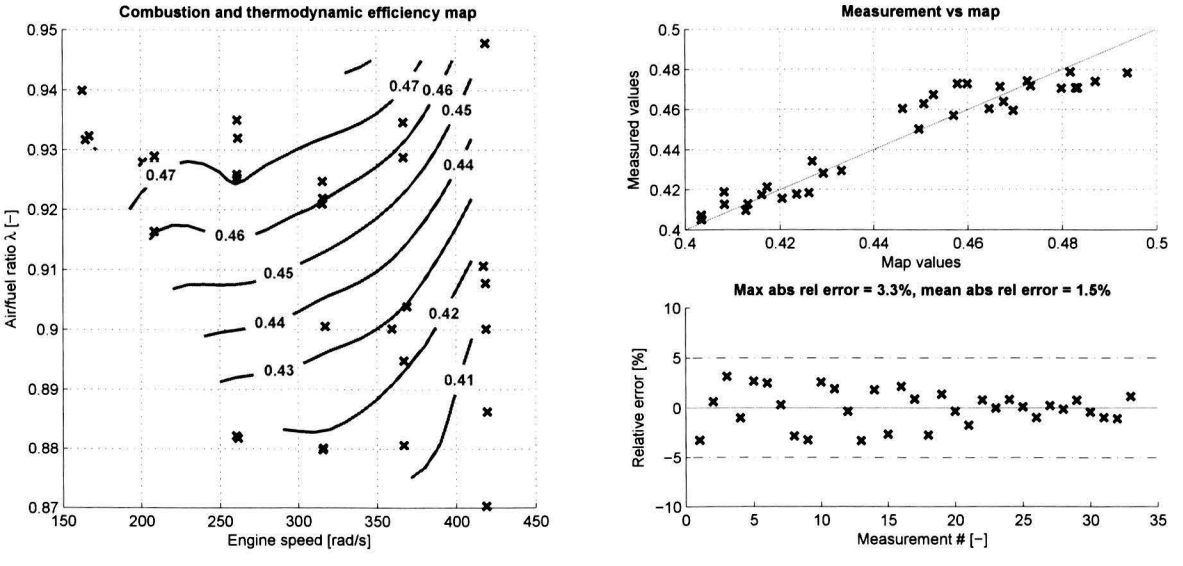

Figure F.9: Map for the term $\eta_{comb}\eta_{th}[-]$ under steady state conditions

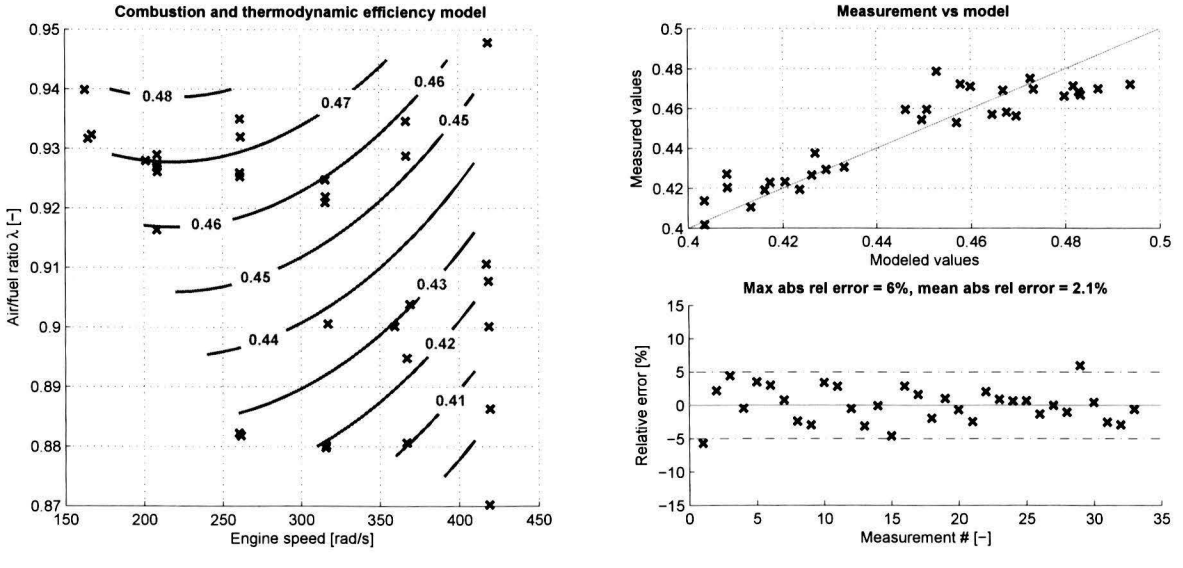

Figure F.10: Model for the term $\eta_{comb}\eta_{th}[-]$ under steady state conditions

F.7 Friction and pumping torque loss model parameter fit

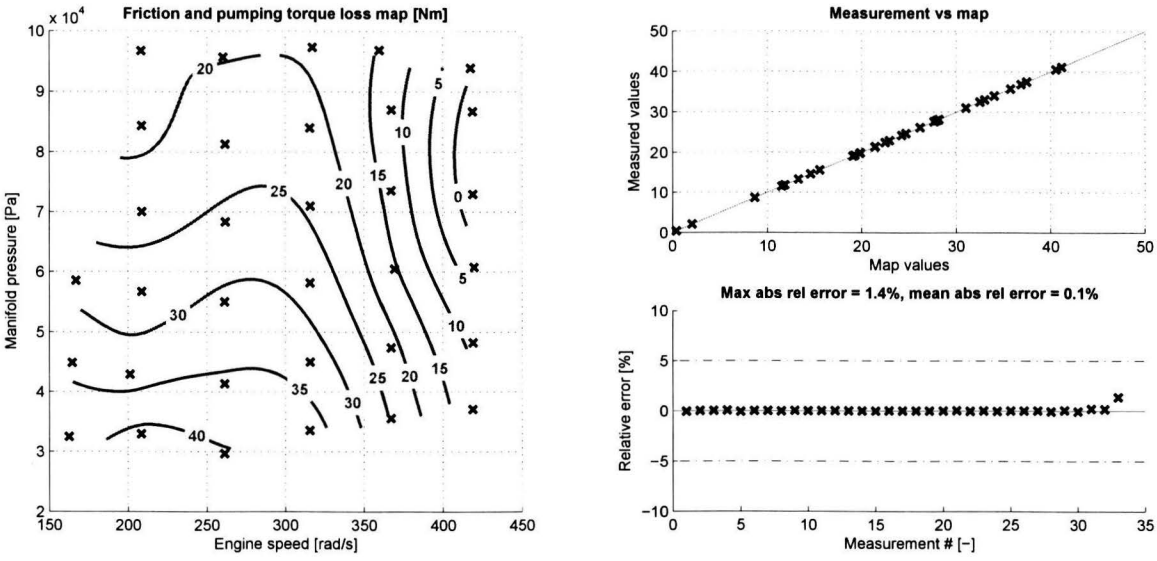

Figure F.11: Map for the friction and pumping torque loss under steady state conditions

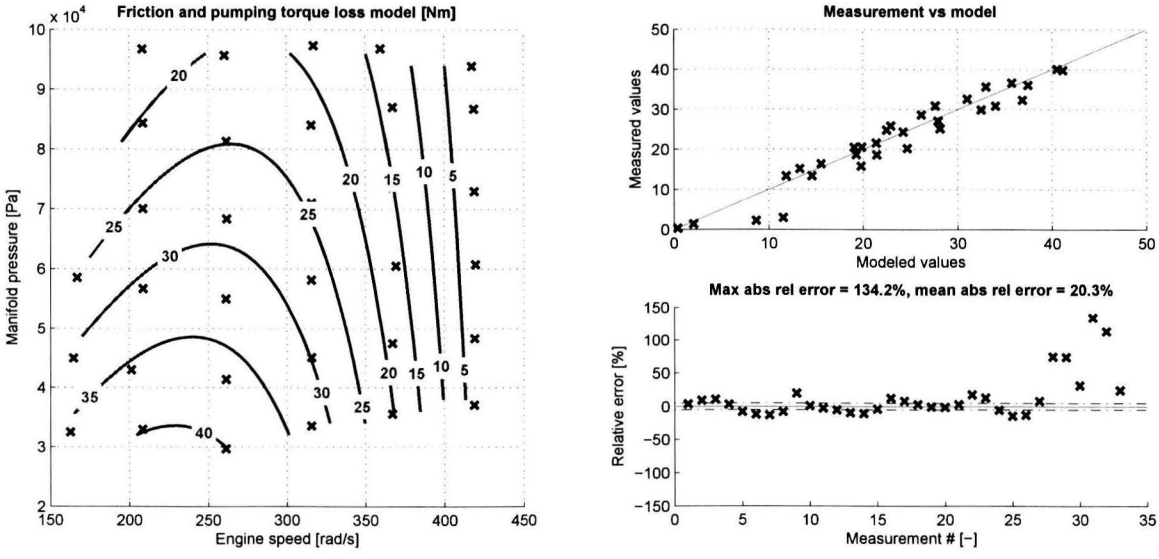

Figure F.12: Model for the friction and pumping torque loss under steady state conditions